Biomass Gasification for the Production of Methane

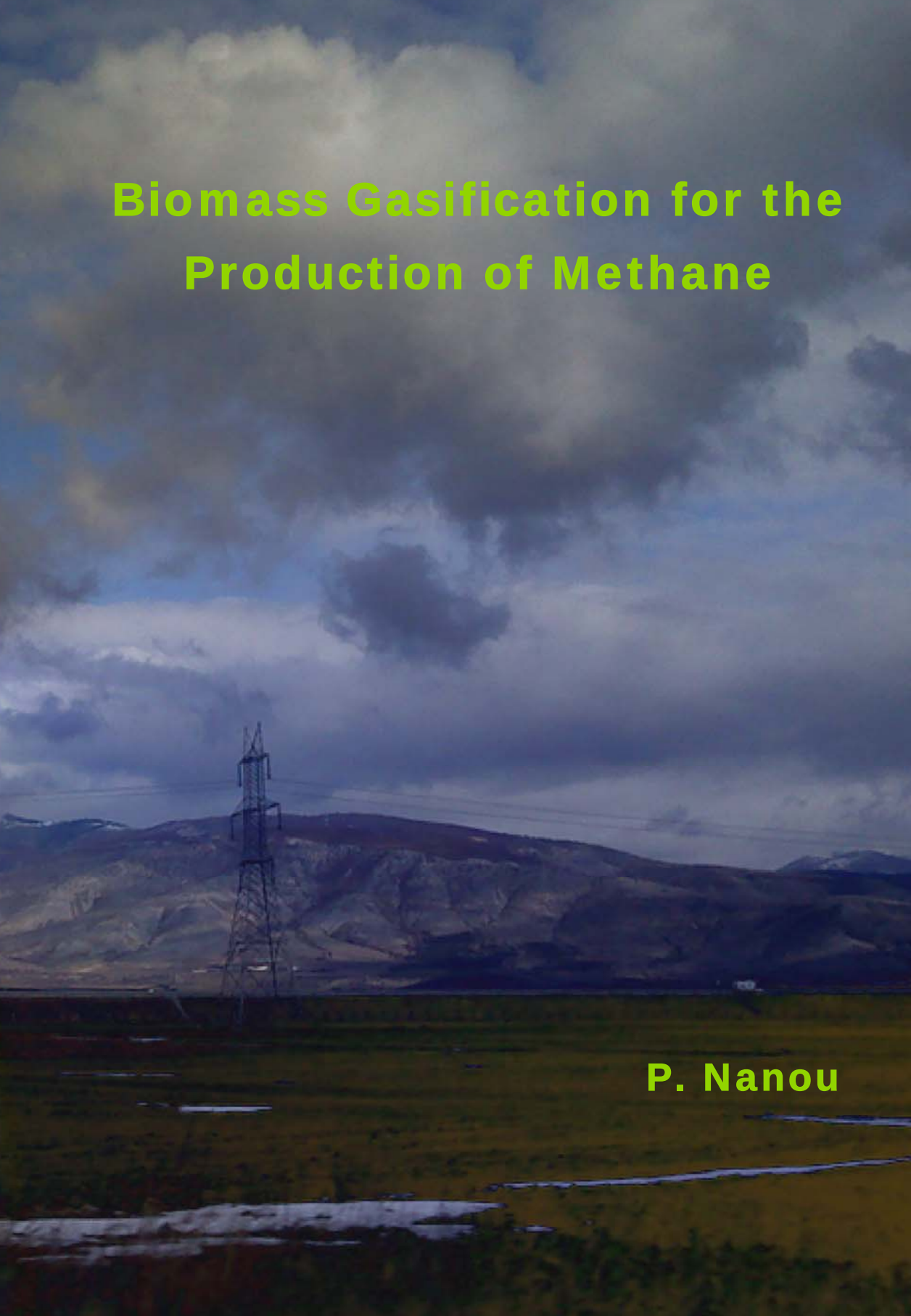

P. Nanou

BIOMASS GASIFICATION FOR THE PRODUCTION OF METHANE

P. Nanou

The research presented in this thesis was financially supported by the Dutch Ministry of Economic Affairs, Agriculture and Innovation, in the framework of EOS-LT (Energie Onderzoek Subsidie-Lange Termijn) subsidy program, managed by Agentschap NL, under Project EOSLT06007, EOSLT07007, EOSLT08007 and EOSLT09002.

Committee Members

Prof. dr. G. van der Steenhoven (Chairman/Secretary)	University of Twente
Prof. dr. S.R.A. Kersten (Promoter)	University of Twente
Prof. dr. ir. W.P.M. van Swaaij (Promoter)	University of Twente
Dr. ir. G. van Rossum (Assistant Promoter)	University of Twente
Prof. dr. K. Seshan	University of Twente
Prof. dr. G. Mul	University of Twente
Prof. dr. ir. W. Prins	Ghent University
Dr. A.A. Lappas	Center for Research and Technology Hellas (CERTH)

Cover design

"The Cloud Factory"

Ptolemaida Power Plant, Greece (© Pavlina Nanou, 2012)

The work described in this thesis was performed at the Sustainable Process Technology (SPT) research group, Faculty of Science and Technology, University of Twente, P.O. Box 217, 7500 AE Enschede, The Netherlands.

Biomass Gasification for the Production of Methane
DOI: 10.3990/1.9789036535434
URL: http://dx.doi.org/10.3990/1.9789036535434

Printed by Ipskamp Drukkers, Enschede, The Netherlands

ISBN: 978-90-365-3543-4

BIOMASS GASIFICATION FOR THE PRODUCTION OF METHANE

DISSERTATION

to obtain
the degree of doctor at the University of Twente,
on the authority of the rector magnificus,
prof. dr. H. Brinksma,
on account of the decision of the graduation committee,
to be publicly defended
on Friday the 17th of May, 2013 at 14:45

by

Pavlina Nanou

born on May 7th, 1981
in Groningen, The Netherlands

This dissertation has been approved by:

Promoter:	Prof. dr. S.R.A. Kersten
Promoter:	Prof. dr. ir. W.P.M. van Swaaij
Assistant promoter:	Dr. ir. G. van Rossum

To the memory of my beloved uncle,
Dr. G.A. Tijssen

Contents

Summary

Biomass is very promising as a sustainable alternative to fossil resources because it is a renewable source that contains carbon, an essential building block for gaseous and liquid fuels. Methane is the main component of natural gas, which is a fuel used for heating, power generation and transportation. In The Netherlands, the contribution of natural gas to the primary energy consumption is almost 50% (*Source: Energy Research Centre of The Netherlands [ECN]*) and it is a fuel with a well-developed pipeline distribution network and infrastructure.

There are different biomass conversion routes to methane depending on the water content of the biomass feed. The thermochemical conversion route to convert relatively dry biomass into methane is conventionally envisaged in a two-step process: In the first step, biomass is gasified (with heat demand, high T / low P) and in the second step methane is formed (with heat release, low T / high P) in a separate reactor. In this configuration there is no heat integration possible between the two process stages.

In this thesis, a new gasification concept is investigated, termed *self-gasification*, that overcomes, inter alia, the issue of heat integration. The concept entails an intermediate temperature (700-800°C) and pressure (25-35 bar) steam gasifier, where recycled ash components -contained in the biomass itself- serve as potential "catalysts" for char (from biomass pyrolysis) gasification, methane formation, gas conditioning and tar cracking. The focus of the present research lies on process evaluation and study of the influence of biomass ashes on the aforementioned reactions. Ashes are present in different concentrations in targeted biomass feeds for gasification; ranging from ~0.5 wt.% in "clean wood" to ~15 wt.% in chicken litter. For that reason alone, results presented in this thesis are not limited to the self-gasification concept where methane is the final product, but give valuable information for other biomass gasification processes as well. Subjects such as gasification under pressure, methane formation and the effect of naturally occurring ash in biomass are dealt with in this thesis.

Summary

Biomass/char gasification and methane production have been studied in dedicated experimental set-ups. An earlier developed (within the SPT group) fast screening method using quartz capillaries has been modified and improved. In order to study the catalytic activity of ash-rich char for the conversion of CO/H_2 into CH_4 at high pressures (25 bar) a completely new set-up has been designed, constructed and operated.

Process modeling of different possible gasification configurations has indicated that gasifier operation at 700°C and at pressures higher than 20 bar is promising for obtaining high energetic efficiencies toward methane (55-66%). An operation mode including a CO/H_2 recycle to the gasifier combined with a small downstream methanation unit seems most favorable requiring only an additional hot utility of relatively low temperature for CO_2 separation (~100° C), a low electricity consumption and a heat exchanger network of low complexity.

Steam gasification tests of biomass were realized at a temperature range of 600 -900°C in batch capillary reactors. These tests showed that most of the methane, in a once-through process, is a product of tar cracking reactions and that added alkali components do not have a large effect on methane yields under these conditions where no additional synthesis gas (e.g. from a recycle) is added. Thermogravimetric wood pyrolysis tests indicated that impregnation of alkali components in the wood accelerates the pyrolysis reaction and the product char can be completely gasified.

Thermogravimetric analyses, performed to study in detail the steam gasification of char, pointed out that the presence of different ash constituents play an important role in the enhancement of the char gasification rates and demonstrated that biomass gasification can be catalyzed by its own (recycled) ash. Addition of the ash/ash model components to the wood by impregnation before pyrolysis resulted in the highest overall gasification rates. An optimal potassium loading on wood lies between 1.1 and 6.6 wt.% potassium. This yields char where the salt is more evenly distributed resulting in enhanced steam gasification rates, up to a factor 30, compared to wood without impregnation. Therefore, implementation of a wood/biomass ash impregnation step in the process and the use of an active, ash-rich biomass feedstock are attractive.

Tests were realized in a fixed bed reactor at 700°C and 25 bar and these showed that methane production and char gasification rates are comparable under these reaction conditions. Methane formation over a packed bed of char was enhanced in the presence of potassium carbonate and methane production close to equilibrium was realized. Steam gasification rates of char with added potassium at high pressure are lower than measured at atmospheric pressure probably because of inhibition due to high partial pressures of H_2 and CO.

The concept is now ready to be studied in an integrated bench-scale unit for further evaluation.

Samenvatting

Biomassa is zeer geschikt als een alternatief voor fossiele grondstoffen, met name omdat het een hernieuwbare energiebron is die koolstof bevat. Koolstof is een essentiële bouwsteen voor vele chemicaliën en brandstoffen; zo ook voor aardgas, een brandstof die gebruikt wordt voor verwarming, elektriciteitsopwekking en transport. In Nederland levert aardgas ongeveer 50% van het totale primaire energieverbruik (Bron: Energy Research Centre of the Netherlands [ECN]) en daarom is het hier een zeer belangrijke brandstof met een eigen distributienetwerk en infrastructuur.

Om methaan (hoofdcomponent in aardgas) te produceren uit biomassa zijn er verschillende conversieroutes welke afhangen van het watergehalte van de biomassa. Droge biomassa kan omgezet worden naar methaangas door een conventioneel thermochemisch proces dat uit twee stappen bestaat. In de eerste stap wordt biomassa vergast (waarbij warmte nodig is bij hoge temperatuur en lage druk) en in de tweede stap wordt in een separate reactor langs katalytische weg methaangas gevormd (met warmte productie bij lage temperatuur en hoge druk). In deze configuratie is geen warmte-integratie tussen de twee processtappen mogelijk.

In dit proefschrift werd een nieuw vergassingsconcept onderzocht, waarbij warmte-integratie wel mogelijk is. Dit vergassingsconcept wordt *zelfvergassing* genoemd. Biomassa wordt in een stoomvergasser vergast bij een middelhoge druk (25-35 bar) en een temperatuur van 700-800°C. De alkalimetalen, die in de biomassa aanwezig zijn, spelen hier een belangrijke rol als “katalysatoren” voor houtskoolvergassing (houtskool die afkomstig is van de pyrolyse van biomassa na intrede in de reactor), methaanvorming, gas opwerking en het kraken van teren. De focus van dit onderzoek ligt op de procesevaluatie en de invloed van biomassa-as, al dan niet gerecycled, op de genoemde reacties. Asconcentraties in biomassa kunnen variëren tussen de ~0.5 wt.% voor hout en ~15 wt.% voor kippenmest. Hierdoor is het onderzoek niet alleen belangrijk voor het zelfvergassingsconcept, maar ook voor andere processen voor biomassavergassing. Tevens worden onderwerpen zoals vergassing onder druk, methaanvorming en de invloed van biomassa-as, welke ook een bredere

betekenis hebben, in dit proefschrift behandeld.

Verschillende experimentele opstellingen zijn gebruikt voor het bestuderen van biomassa- en houtskoolvergassing en methaanvorming. Een eerdere binnen de SPT-werkeenheid ontwikkelde methode waarbij capillairen van kwartsglas werden gebruikt als batch reactoren voor lage temperatuur en druk, is verder verfijnd en toegespitst op het huidige onderzoek. Daarnaast werd een nieuwe opstelling ontworpen en gebouwd om het effect van de asrijke houtskool op de omzetting van CO/H_2 naar CH_4 bij hoge drukken te onderzoeken.

Procesmodellen van verschillende vergassingsconfiguraties hebben aangetoond dat een vergassingstemperatuur van 700°C en een druk hoger dan 20 bar hoge energetische rendementen naar methaan (55-66%) kan geven. Een configuratie waarbij gevormd CO/H_2 wordt gerecycled naar de vergasser in combinatie met een kleine na-geschakelde methanisatie-unit blijkt het meest gunstig omdat er dan een laag stroomverbruik (voor de compressoren) en slechts een simpel netwerk van warmtewisselaars nodig is. Wel is er dan nog warmte van een laag temperatuur niveau voor CO_2 afscheiding (~100°C) nodig.

Stoomvergassing van biomassa werd bij temperaturen tussen de 600-900°C in de batch capillair reactoren uitgevoerd. Deze proeven hebben aangetoond dat het meeste van het geproduceerde methaangas het product is van decompositiereacties van teer en dat de toegevoegde alkalimetalen geen aanzienlijke invloed hebben op de methaanopbrengst onder deze omstandigheden waarbij geen extra synthese gas (bijv. door een recycle) wordt toegevoegd. Door middel van thermogravimetrische analyses werd aangetoond dat impregnatie van hout met alkalimetalen de pyrolysereacties versnelt waardoor het houtskoolproduct volledig kan worden vergast.

Verder, zijn er meer thermogravimetrische analyses gedaan om de stoomvergassing van houtskool te onderzoeken. De proeven hebben aangetoond dat de aanwezigheid van verschillende as-componenten een belangrijke rol speelt in het versnellen van de vergassingsreactie van houtskool. Bovendien kan de eigen (gerecyclede) as de vergassing van

biomassa versnellen. De hoogste vergassingssnelheden werden bereikt toen het bijgemengde as of de as-modelcomponent via impregnatie aan het hout werd toegevoegd. De optimale belading van hout ligt tussen de 1.1 en 6.6 wt.% Kalium. De houtskool die aldus geproduceerd wordt geeft een betere verspreiding van het zout en stoomvergassingssnelheden worden verhoogd tot een factor 30 in vergelijking met hout zonder impregnatie. Daarom is de implementatie van een hout/biomassa as-impregnatiestap in het proces gunstig en het gebruik van een as-rijke biomassavoeding zeer aantrekkelijk.

Proeven in een gepakt bed reactor bij 700°C en 25 bar hebben aangetoond dat de reactiesnelheden van methaanproductie en houtskoolvergassing vergelijkbaar zijn onder deze reactieomstandigheden. De methaanvorming over een gepakt bed van houtskool werd versneld in aanwezigheid van kaliumcarbonaat en methaanproductie was dichtbij het evenwicht. Reactiesnelheden van de stoomvergassing van houtskool met toegevoegde kaliumzout waren lager bij hoge druk vergeleken met wat gemeten werd bij atmosferische druk. Dit kwam waarschijnlijk doordat hoge partiaalspanningen van H_2 en CO de vergassingsreactie remmen (inhibitie).

Het concept is uitvoerig in deelstappen bestudeerd en kan nu in een geïntegreerde proefopstelling verder ontwikkeld worden.

Περίληψη

Η βιομάζα είναι μια πολλά υποσχόμενη βιώσιμη εναλλακτική της χρήσης ορυκτών πόρων επειδή είναι μια ανανεώσιμη πηγή ενέργειας η οποία περιέχει άνθρακα, τον ακρογωνιαίο λίθο αερίων και υγρών καυσίμων. Το μεθάνιο είναι το βασικό συστατικό του φυσικού αερίου, το οποίο είναι ένα καύσιμο που χρησιμοποιείται για θέρμανση, παραγωγή ενέργειας αλλά και στις μεταφορές. Στις Κάτω Χώρες, η συμμετοχή του φυσικού αερίου στην κατανάλωση πρωτογενούς ενέργειας ανέρχεται σε ποσοστό 50% (Πηγή: *Energy Research Centre of The Netherlands [ECN]*). Το φυσικό αέριο είναι ένα καύσιμο το οποίο διαθέτει ένα καλώς ανεπτυγμένο δίκτυο αγωγών διανομής και υποδομή.

Υπάρχουν διάφορες διεργασίες μετατροπής της βιομάζας σε μεθάνιο ανάλογα με την περιεκτικότητα της βιομάζας σε υγρασία. Η θερμοχημική διεργασία μετατροπής για την παραγωγή μεθανίου από μια σχετικά ξηρή βιομάζα πραγματοποιείται συμβατικά σε δύο στάδια: Κατά το πρώτο στάδιο, η βιομάζα αεριοποιείται (με κατανάλωση θερμικής ενέργειας, συνθήκες υψηλής T/χαμηλής P) και στο δεύτερο στάδιο το μεθάνιο συντίθεται σε έναν ξεχωριστό αντιδραστήρα (με παραγωγή θερμικής ενέργειας, συνθήκες χαμηλής T/ υψηλής P). Σε αυτή τη διάταξη δεν υπάρχει δυνατότητα θερμικής ολοκλήρωσης μεταξύ των δύο σταδίων της διεργασίας.

Στην παρούσα διατριβή, μια νέα έννοια αεριοποίησης τίθεται υπό έρευνα, η επονομαζόμενη *αυτο-αεριοποίηση*, η οποία λύνει το πρόβλημα, μεταξύ άλλων, της θερμικής ολοκλήρωσης. Η έννοια αυτή περιλαμβάνει έναν αντιδραστήρα αεριοποίησης (αεριοποιητή) που λειτουργεί υπό ατμό σε μέση θερμοκρασία (700-800°C) και πίεση (25-35 bar), όπου ανακυκλωμένα συστατικά της τέφρας-που περιέχεται στην ίδια τη βιομάζα-λειτουργούν ως πιθανοί καταλύτες για την αεριοποίηση του βιοάνθρακα (προερχόμενου από την πυρόλυση της βιομάζας), τη σύνθεση μεθανίου, τη ρύθμιση του αερίου και τη θερμική διάσπαση της πίσσας. Η εστίαση της παρούσας έρευνας έγκειται στην αξιολόγηση της διεργασίας και την διερεύνηση της επίδρασης της τέφρας της βιομάζας πάνω στις προαναφερθείσες αντιδράσεις. Η τέφρα περιέχεται στη βιομάζα προς αεριοποίηση σε διάφορες συγκεντρώσεις που κυμαίνονται από

~0.5% κ.β. σε «καθαρό» ξύλο έως ~15% κ.β. σε κοπριά πουλερικών. Για αυτόν το λόγο, τα αποτελέσματα που παρουσιάζονται στην παρούσα διατριβή δεν περιορίζονται στην έννοια της αυτο-αεριοποίησης όπου το τελικό προϊόν είναι το μεθάνιο, αλλά δίνουν πολύτιμες πληροφορίες και για άλλες διεργασίες αεριοποίησης βιομάζας. Η αεριοποίηση υπό πίεση, η σύνθεση μεθανίου και η επίδραση της φυσικής τέφρας της βιομάζας είναι θέματα τα οποία πραγματεύεται η παρούσα διατριβή.

Η αεριοποίηση βιομάζας/βιοάνθρακα και η παραγωγή μεθανίου έχουν μελετηθεί σε σχετικές πειραματικές εγκαταστάσεις. Τροποποιήθηκε και βελτιώθηκε μια προσφάτως ανεπτυγμένη (μέσα στην ερευνητική ομάδα SPT) μέθοδος ταχείας διαλογής που χρησιμοποιεί τριχοειδείς αντιδραστήρες από χαλαζία. Με σκοπό να ερευνηθεί η καταλυτική δράση ενός βιοάνθρακα πλούσιου σε τέφρα στην μετατροπή CO/H_2 σε CH_4 υπό υψηλές πιέσεις (25 bar) σχεδιάστηκε, κατασκευάστηκε και λειτούργησε μια νέα πειραματική εγκατάσταση.

Η προσωμοίωση διεργασίας διαφόρων πιθανών τρόπων αεριοποίησης απέδειξε ότι η λειτουργία του αεριοποιητή στην θερμοκρασία των 700°C και σε πιέσεις μεγαλύτερες των 20 bar είναι οι βέλτιστες συνθήκες για μέγιστες ενεργειακές αποδόσεις προς μεθάνιο (55-66%). Ο τρόπος λειτουργίας ο οποίος περιλαμβάνει ανακύκλωση του μείγματος CO/H_2 προς τον αεριοποιητή, σε συνδυασμό με μια μικρή μονάδα μεθανιοποίησης δείχνει να είναι ο πιο ευνοϊκός, απαιτώντας ένα βοηθητικό δίκτυο θέρμανσης σχετικά χαμηλής θερμοκρασίας για τον διαχωρισμό του CO_2 (~100°C), χαμηλή κατανάλωση ρεύματος και ένα απλό σύστημα εναλλαγής θερμότητας.

Πειράματα αεριοποίησης βιομάζας υπό ατμό διεξήχθησαν σε θερμοκρασίες μεταξύ 600-900°C σε τριχοειδείς, ασυνεχούς λειτουργίας, αντιδραστήρες. Τα πειράματα αυτά απέδειξαν πως η μεγαλύτερη ποσότητα του παραγόμενου μεθανίου, σε μια διεργασία μονής διάβασης, προέρχεται από τη θερμική διάσπαση πίσσας καθώς επίσης ότι προστεθειμένα αλκαλικά συστατικά δεν έχουν κάποια σημαντική επίδραση στην απόδοση παραγωγής μεθανίου υπό τις συνθήκες αυτές, όπου δεν έχουμε διοχέτευση επιπλέον αερίου σύνθεσης (π.χ. από ανακύκλωση). Θερμοσταθμικές αναλύσεις πυρόλυσης ξύλου έδειξαν ότι η εμπότιση του ξύλου με αλκαλικά συστατικά επιταχύνουν την αντίδραση

της πυρόλυσης και ο παραγόμενος βιοάνθρακας μπορεί να αεριοποιηθεί πλήρως.

Θερμοσταθμικές αναλύσεις που πραγματοποιήθηκαν για τη λεπτομερή διερεύνηση της αεριοποίησης υπό ατμό του βιοάνθρακα, οδήγησαν στο συμπέρασμα ότι η παρουσία διαφόρων συστατικών τέφρας παίζουν σημαντικό ρόλο στην επιτάχυνση του ρυθμού αεριοποίησης του βιοάνθρακα και απέδειξαν πως η αεριοποίηση της βιομάζας μπορεί να καταλυθεί από την ίδια της την (ανακυκλωμένη) τέφρα. Η προσθήκη τέφρας ή μοντέλων συστατικών τέφρας μέσω εμπότισης του ξύλου πριν την πυρόλυση σημείωσε τους υψηλότερους συνολικά ρυθμούς αεριοποίησης. Το βέλτιστο φορτίο καλίου στο ξύλο κυμαίνεται μεταξύ 1.1 και 6.6% κ.β.. Ο παραγόμενος βιοάνθρακας περιέχει το άλας κατανεμημένο πιο ομοιόμορφα και μπορεί να σημειώσει βελτιωμένους ρυθμούς αεριοποίησης υπό ατμό, μέχρι και ένα συντελεστή 30, σε σύγκριση με ξύλο χωρίς εμπότιση άλατος. Επομένως, η εφαρμογή ενός σταδίου εμποτισμού του ξύλου/της βιομάζας με τέφρα και η χρήση μιας ενεργού, πλούσιας σε τέφρα βιομάζας ως πρώτη ύλη παρουσιάζουν μεγάλο ενδιαφέρον.

Πειράματα διεξήχθησαν σε έναν αντιδραστήρα σταθερής κλίνης στους 700°C και 25 bar και έδειξαν ότι η παραγωγή μεθανίου και ο ρυθμός αεριοποίησης του βιοάνθρακα είναι τιμές συγκρίσιμες υπό τις συγκεκριμένες συνθήκες αντίδρασης. Η σύνθεση μεθανίου υπό σταθερής κλίνης βιοάνθρακα ενισχύθηκε υπό την παρουσία ανθρακικού καλίου και επιτεύχθηκε παραγωγή μεθανίου σε ποσότητες κοντά στη θερμοδυναμική ισορροπία του συστήματος. Ο ρυθμός αεριοποίησης βιοάνθρακα που περιέχει προστεθειμένο κάλιο είναι χαμηλότερος υπό υψηλές πιέσεις σε σύγκριση με παρόμοιες μετρήσεις που πραγματοποιήθηκαν υπό ατμοσφαιρική πίεση πιθανώς λόγω των υψηλών μερικών πιέσεων H_2 και CO που παρεμποδίζουν την αντίδραση.

Η νέα έννοια αεριοποίησης βιομάζας όπως παρουσιάζεται στην παρούσα διατριβή μπορεί να περάσει στο στάδιο της έρευνας εντός μιας ολοκληρωμένης μικρής κλίμακας μονάδας για περαιτέρω αξιολόγηση.

Chapter 1

Introduction

In this thesis we investigate and discuss the envisaged benefits of gasifying at higher pressures and utilizing the alkali metals in the feed as catalysts. We propose and examine an alternative thermo-chemical process for bio-methane production from lignocellulosic biomass, termed self-gasification. Self-gasification of biomass is envisaged to utilize a high-pressure steam gasifier (30-80 bar) at temperatures of 600-800°C and to use the alkali metal components in biomass as gasification and methanation catalysts. This chapter describes the motivation for and the background of the research performed. In the end of the chapter, the scope and outline of this thesis are presented.

1.1. Biomass and bio-methane

1.1.1. Introduction

Many scientists, including the author, believe that global warming is the result of increased greenhouse gas concentrations in our atmosphere. The largest effect is attributed to anthropogenic CO_2 emissions, which are mainly caused by deforestation and fossil fuel combustion. In order to reduce our net CO_2 emissions and because of rising fuel prices, depletion of fossil resources, security of supply and need for (more) energy, we have to find renewable alternatives for heat, power and transportation.

Biomass is one of these renewable alternatives especially when it comes to fuels because it is the only renewable source that contains carbon which is an essential building block for gaseous (natural gas) and liquid fuels (diesel, gasoline, kerosene, heavy fuel oil, and alcohols).

In our daily lives we use natural gas, with methane as its main component, for cooking, (industrial) heating and transportation, but this gas has fossil origin. A renewable alternative for this would be *bio-methane*. Bio-methane can be injected into the natural gas grid or it can be used as an alternative to LNG in its compressed form for transportation fuels [1].

Routes for obtaining bio-methane depend on the moisture content of the biomass feed. Wet biomass streams (>70 wt.% water) can often be partially converted by biological routes but cannot be economically converted to gas by low pressure thermochemical gasification technologies because of the required energy for water evaporation [2].

1.1.2. Methane from wet biomass

Anaerobic digestion and *hydrothermal gasification* are suitable processes for producing gases from wet feeds. Anaerobic digestion is a biological process and proven technology for small- and medium-scale applications. Typical process conditions are a temperature around 37°C and a pH of about 7 [3]. Its main gaseous products are CH_4 and CO_2. It is a proven and simple technology for small-scale applications, but biomass conversion is relatively low resulting in large waste streams.

Hydrothermal gasification is a thermo-chemical route in the R&D stage. Process conditions are temperatures between 300 and 400°C and a pressure range of 120-340 bar, over catalysts, e.g. Ni or Ru [4]. It produces a gas containing mainly CH_4, CO_2 and H_2. High conversions can be achieved by this

process, ranging from about 70% up to almost 100% carbon conversion. However, operation is costly and the technology is not yet mature.

1.1.3. Methane from dry biomass

Gasification is a thermo-chemical conversion process already known since the 1800's when gas was produced from coal for the first time on commercial scale to provide the London streets with light. Nowadays, gasification is gaining more interest as a means of converting low energy-density biomass feeds or organic waste streams into a transportable higher-value gas for heat and power generation, chemicals and fuels. More details on the history and development of coal, oil and biomass gasification as well as types of gasification processes and products are provided in the next section (1.2).

Fuel gas is produced by gasification with steam and/or oxygen. This process, including heating of the feedstock and reactants, requires energy and is described by overall reactions (1.1) and (1.2). The high energy demand of the gasifier requires air/oxygen addition to the process.

$$C_xH_yO_z + aH_2O/bO_2 \rightarrow cCO + dH_2 + eCO_2 + fCH_4 + gC_{2\text{-}4} + hTars + iC_{(s)} \quad [\textit{pyrolysis/gasification}] \quad (1.1)$$

$$C + \alpha H_2O/\beta CO_2 \rightarrow \gamma CO + \delta H_2 \quad [\textit{carbon gasification}] \quad (1.2)$$

The direct products of gasification are gases, tars and char/ash. The gases are the desired product, which after gas cleaning, secondary reactions and upgrading can lead to methane or syngas ($CO+H_2$) as product. Especially concerning methane production, a low-temperature and high-pressure step is needed as a secondary reaction after gasification, because methane formation is favored under these conditions. Therefore, a two-step process has been proposed [5, 6] and is schematically given in Figure 1.1. Nowadays, biomass gasification technologies for methane production on demonstration scale are of this type of configuration and are presented in more detail in sections 1.3.3 and 1.3.4.

In the second step (after gas cleaning), the produced gases are led to a downstream methanation unit, where methanation (reaction (1.3), which is exothermic) takes place as well as water-gas shift and reforming of C_2-C_3 hydrocarbons [7], according to reactions (1.4) and (1.5), respectively.

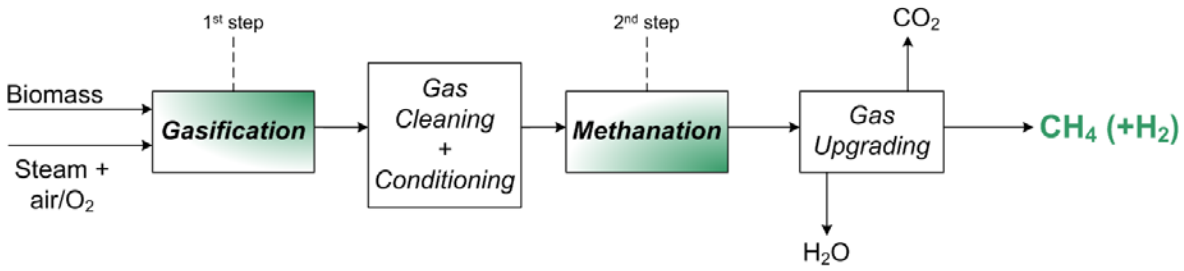

Figure 1.1. Block diagram of the two-step configuration for bio-methane production.

$CO + 3H_2 \leftrightarrow CH_4 + H_2O$ [*methanation*] (1.3)

$CO + H_2O \leftrightarrow CO_2 + H_2$ [*water-gas shift*] (1.4)

$C_xH_y + xH_2O \rightarrow xCO + (y/2 + x)H_2$ [*steam reforming*] (1.5)

The gas exiting the methanation unit, is upgraded by removing water and CO_2 to give the final methane product. An advantage of this two-step process is that the biomass gasifier usually operates near atmospheric pressure [8]. Therefore, no sophisticated materials or complicated feeding systems are needed in this case. However, the product gas has to be pressurized for the second step, to favor methane formation (reaction (1.3), before entering the methanation reactor. Additionally, there is no heat integration possible between the two units because the gasifier requires heat at a much higher temperature level (700-900°C) than the exothermic methanation reactor can provide (350-500°C).

In the literature there is no clear definition of the "methanation" reaction. Therefore, throughout this thesis, specific definitions are used for different methane producing reactions. These are as follows:

$CO + 3H_2 \leftrightarrow CH_4 + H_2O$ [*methanation reaction*]

$C + 2H_2 \rightarrow CH_4$ [*carbon hydrogenation reaction*] (1.6)

$CO_2 + 4H_2 \leftrightarrow CH_4 + 2H_2O$ [*Sabatier reaction*] (1.7)

1.2. Coal and Biomass Gasification

1.2.1. History and development

Coal was first recorded to have been used in China between 220-589 AD, but the actual production of gas from the combustion of coal was noticed much later, in the year 1609 by the alchemist Jean Baptist van Helmont.

The first coal gasifier was put to use by Fontana in the year 1780, by passing a water flow over very hot, glowing coal and in this way producing a mixture of

carbon monoxide and hydrogen, which was called “blue water gas” as it gave off a blue flame when it was burnt. Later, in 1812, the company Westminster and London Gas, Light, and Coke Co. was the first company to produce gas from coal on a commercial scale for providing the streets of London with light [9]. The first gasifiers were air-blown fixed bed reactors with a maximum gasification temperature of about 900°C. In 1926, Winkler introduced the first fluid bed gasifier, the advantages of which over a fixed bed were claimed to be the ability to accept all types of coal, smaller sized coal, and more ash removal flexibility.

Gasification technology developed further and in 1936 the pressurized version (25-30 bar) of the atmospheric fixed bed gasification came to commercial application by Lurgi. The gasifier used O_2 because it could be available commercially via cryogenic air separation (C. von Linde, 1920) and gasification temperatures were lower than 1000°C to avoid ash melting. This was the only pressurized gasification system for many years. In 1938, the Koppers-Totzek entrained-flow gasification process was commercialized. The first commercial units were atmospheric and were mostly built for ammonia production. For the next 40 years there was no significant further development in gasification technology, because of natural gas and naphtha availability in the 1950s. Technology then focused more on the steam reforming of these feeds toward syngas production for ammonia. At the end of the 1940’s (Texaco) and the beginning of 1950’s (Shell) the oil gasification to syngas technology was developed with operating conditions of P=30-80 bar and T=1250-1450°C. In the 1970’s a pressurized version (up to 30 bar) of the Winkler gasifier was introduced, also known as the High Temperature Winkler (HTW) process. In the same period, the U-Gas technology was developed by the Gas Technology Institute. This was an ash-agglomerating fluidized bed, a modified version of which was used in 1993 for a biomass gasification demonstration plant (Renugas technology).

After 1973, coal gasification regained importance as a process for liquid and gaseous fuel production because of the oil crisis and a potential shortage of natural gas. Older processes were further developed: Lurgi and British Gas (BGL) co-operated on the development of the slagging gasifier which operated for some years on a wide range of coals, Shell and Krupp-Koppers developed a pressurized version (P=20-70 bar, T>1400°C) of the Koppers-Totzek gasifier, Texaco (GE Energy) adapted the oil gasification process to accept slurried coal

feed and Dow developed the E-gas process, an entrained-flow slagging gasifier with coal slurry feed (later owned by Conoco Philips). During that time, also a new process by Exxon reached the demonstration stage, the CCG (Catalytic Coal Gasification) process that was used to produce SNG from coal impregnated with K_2CO_3. However, its development was stopped because of the end of the oil crisis [10, 11].
After the end of the oil crisis, interest in coal gasification declined again. In the 1980's the Lurgi CFB technology was adapted for coal combustion and since then it has been applied for biomass gasification. In the 1990's gasification of heavy residues became important in oil refineries aiming at hydrogen production for hydrocracking of heavy oil fractions. In 1998, Lurgi started developing the Multi-purpose Gasification (MPG) process, an entrained flow gasifier operating at T=1250-1450°C for liquids and slurries, originally designed to handle tars produced in the gasifier.

Although the first biomass gasification took place in the middle of the 19th century (Bischof 1839), the first wide-spread use of biomass gasification was around WWII when vehicles, and especially military trucks, were powered by gas produced by built-in wood and waste gasifiers. Much later, in 1983, the first test rig of FICFB biomass gasification was built, more details on which can be found in section 1.3.4 of this chapter. In the same year, the Foster Wheeler CFB atmospheric gasifier was developed to process waste from the pulp and paper industry. Later on, also a pressurized version was developed (20 bar) which was the basis for the Värnämo plant in Sweden (T=950-1000°C). In the mid-1990's the Lurgi/British Gas slagging gasifier was used to gasify municipal solid waste (MSW) and lignite for methanol and power production. It was not until the last two decades that fluid-bed gasification processes incorporate the use of a heat carrier, such as sand, char and/or ash. This also means separate gasification and combustion zones, which eliminates the need for pure O_2 as feed and produces a gas with very low nitrogen content. These processes are so-called "indirect" gasification processes and an example of this was the SilvaGas (Batelle) biomass gasification process (T=650-815°C). For a detailed overview of coal and biomass gasification the reader is referred to Higman and van der Burgt [8].

1.2.2. Types of gasification processes and products

The developments in the coal and oil industry have led to three main gasifier types: fixed bed, fluid bed and entrained flow. Low temperature gasifiers operate in the temperature range of 800-950°C and they produce a so-called fuel gas. This is a mixture of CO, H_2, CO_2, CH_4, H_2O, higher hydrocarbons, tars and N_2 (in air-blown gasification). This type of gas requires intense downstream cleaning and upgrading before it can be used as feed for the production of fuels and chemicals, mainly because of its high tar content. High temperature gasifiers operate at temperatures higher than 1300°C and are usually of the entrained-flow, slagging type. They can handle any coal and liquid feeds and produce a clean, tar-free synthesis gas (CO, H_2, CO_2 and H_2O). Synthesis gas or syngas is a building block for synthesizing many fuels and chemicals [12]. Either produced by low- or high-temperature gasification, the gas still has to be treated in gas cleaning units to remove e.g. particulates, S, Cl and alkali metals before any downstream conversion steps.

For all gasifiers there is a temperature range between the softening and the slagging temperature of the coal/biomass ash where operation is unfavorable. This temperature range can vary between 950 and 1300°C and is feedstock-specific. The ashes of the feed soften in this temperature range and start forming a solid/liquid phase which is difficult to handle in the gasifier [8].

Biomass gasification is essentially the same technology as coal and oil gasification and biomass can actually be considered as very young coal. However, there are differences in oxygen content, reactivity and ash amount and composition to be considered. The differences in reactivity become clear when analyzing the main gas producing step: in coal gasification, gas is produced by the heterogeneous reaction of solid carbon with H_2O and/or CO_2, while for a solid biomass the majority of the gas comes directly from devolatilization reactions of the feedstock. Coal and biomass co-feeding in existing power plants (e.g. Essent, Amercentrale) is nowadays most interesting as a way for accelerating market penetration of biomass technologies.

Biomass ash has a lower ash-melting point than coal and its molten ash is very aggressive. For these reasons, and because it is difficult to obtain small particle sizes with fibrous biomass, entrained-flow gasifiers are not generally used for solid biomass feedstocks. Moreover, the scale of operation of biomass gasification is normally too small to allow for the complexity of entrained flow

operation. Fixed bed gasifiers are also limited by the type and size of biomass feed and therefore, fluid beds are mostly preferred for biomass gasification processes.

1.3. Gasification/methanation technology of dry feedstocks to SNG

This section focuses on the current status of the gasification/methanation technology for methane production from coal or biomass. Many attempts have been made over the years to produce SNG, and especially in the 1970's the oil crisis stimulated further R&D on converting coal directly to SNG. A number of process development units and demonstration plants were built in those years, but most of these projects were terminated because of limited success in handling shredded, low density feedstocks (Renugas Gasification Technology), expensive methane purification (cryogenic) and catalyst make-up units (Exxon's Catalytic Coal Gasification process [CCG]), oil price decrease in the mid 1980's (Comflux methanation process) and low conversion and high catalyst loss in the three-phase fluidized-bed methanation reactor (Liquid-Phase Methanation [LPM]). The TREMP process (Topsøe's Recycle Energy efficient Methanation Process) was initially intended for a methane steam reforming/syngas methanation cycle concept as a heat storage and distribution system. Although the project was terminated because of discontinuation of the high-temperature nuclear reactor technology, Haldor Topsøe still offers this process for the production of SNG from coal-derived syngas [13].

The only commercial plant still in operation since 1984 is the Great Plains Synfuels Plant operated by the Dakota Gasification Company (U.S.A.). Nowadays, R&D activities are focusing on methane/SNG production from biomass, but also the coal-to-SNG processes remain interesting because of rising natural gas prices, effort to decrease dependency on natural gas imports and, in the case of biomass, a renewable alternative for natural gas.

It is noted from current operating pilot or commercial facilities, described further in this section, that gasification concepts utilizing coal as feedstock are direct gasification processes. On the other hand, biomass gasification concepts, which are also more recent technologies, are indirect gasification processes. Indirect gasification seems more promising since it produces a gas with a higher heating value while instead of pure oxygen, air can be used in the process. By indirect gasification, the nitrogen in the air remains separated from

the product gas and complete conversion of the feedstock is achieved.

1.3.1. Dakota Gasification Process

The Great Plains Synfuels Plant is located near Beulah, North Dakota in USA. It was commissioned in 1984 and it is owned and operated by the Dakota Gasification Company since 1988. It converts daily 18,000 tons of lignite coal (d_p≈0.3-10 cm) to about 4.8 million m^3 SNG for home heating and electricity generation. A simplified process scheme is presented in Figure 1.2.

An additional product of this process (6,080 ton/d) is dry CO_2 of high purity (~96%) which is being used for enhanced oil recovery (EOR).

The gasification unit consists of 14 fixed-bed gasifiers (Lurgi type) operating at about 32 bar. The temperature in the combustion zone (lower zone) of the gasifier can reach 1260°C. Methanation of the sulfur-free syngas (S < 20 ppb) is carried out in a fixed-bed with nickel-type catalyst pellets [14].

1.3.2. Great Point Energy (Blue Gas process)

Great Point Energy is developing a process termed *Hydromethanation* (Blue Gas) process and it is schematically given in Figure 1.3. It is designed to run on coal, petroleum coke and biomass feedstocks and the concept resembles Exxon's CCG process. Gasification and methanation occur in a single

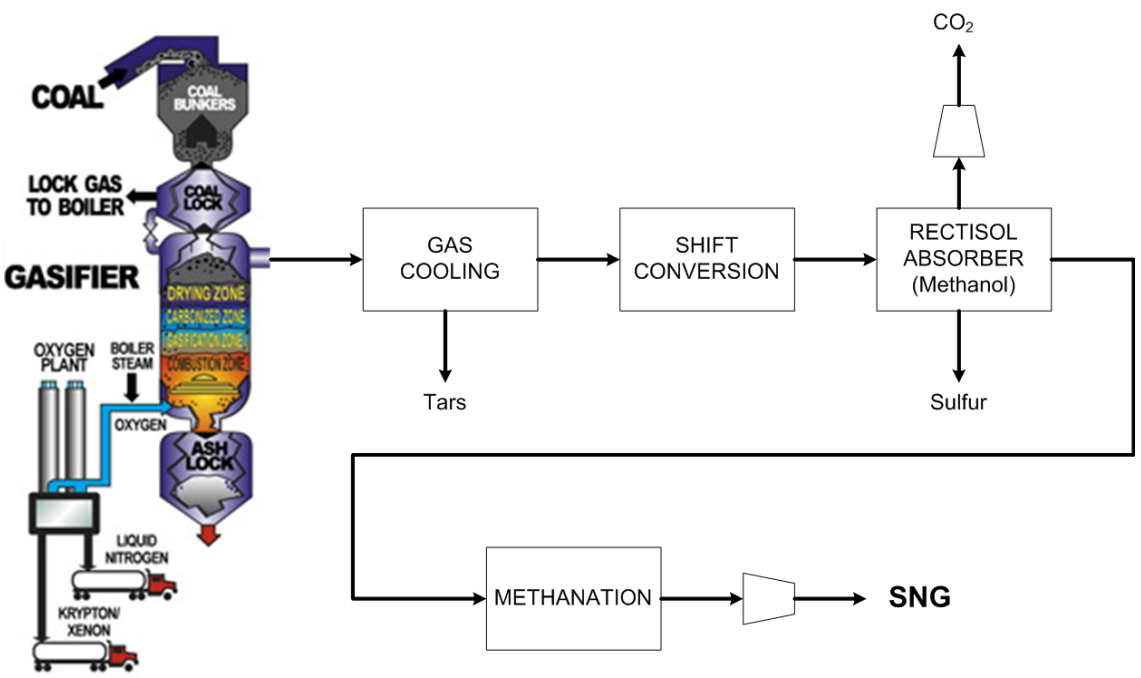

Figure 1.2. The Dakota Gasification Process from coal to SNG. Adapted from [14].

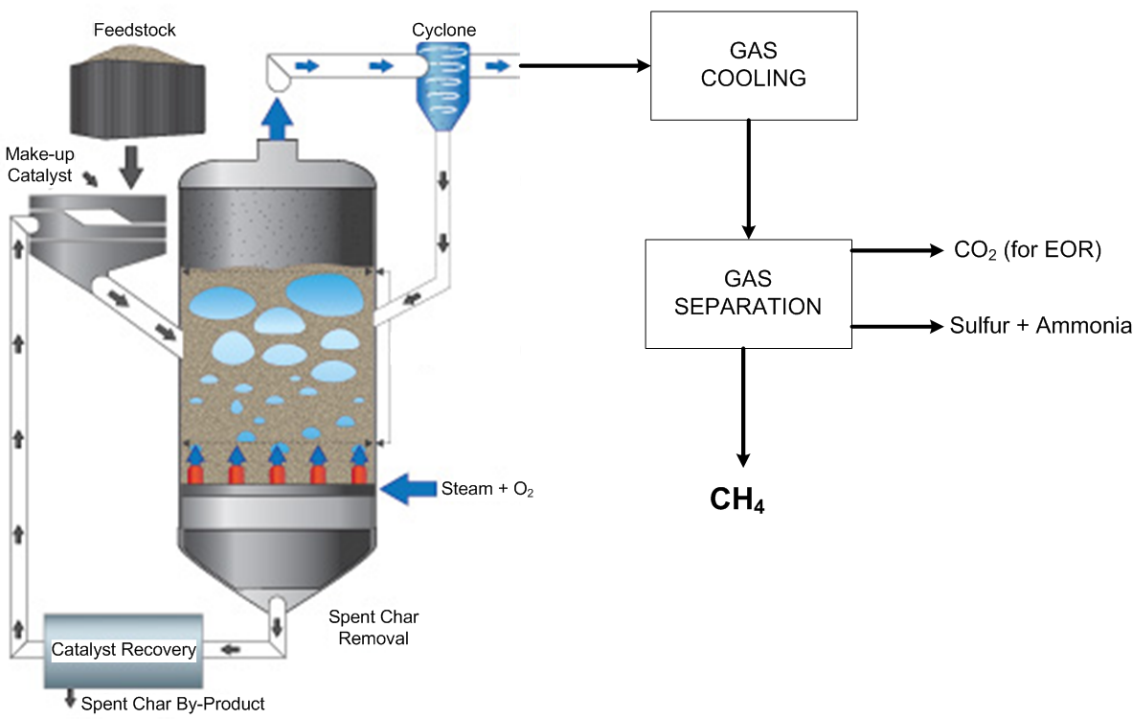

Figure 1.3. The Hydromethanation process from carbonaceous feedstocks to methane by Great Point Energy. Adapted from [15]. The flowsheet is incomplete because of lacking information.

pressurized fluidized-bed gasifier by utilizing a catalyst and steam. A pilot plant was operated at GTI's Des Plains, IL, USA and a pilot plant facility was available at Somerset, Massachusetts, USA. Another pilot plant is operational at the Energy and Environmental Research Center in Grand Forks, North Dakota, USA [15]. There are a number of recent patents by the company that involve gasification of carbonaceous feedstocks and recovery of alkali metals from char [16-18]. Further information or reports are not available.

1.3.3. Energy Research Centre of The Netherlands (ECN)

At ECN the MILENA gasifier technology has been developed for biomass gasification. Gasification reactions occur in a riser under conditions of T=850°C and P≈1 bar. The char combustion section is a bubbling fluidized-bed and methanation occurs in a fixed bed installation. The whole process chain from biomass to SNG is termed BioSNG and is shown in Figure 1.4. A lab-scale unit (30 kW_{th}-5 kg/h) was constructed in 2003 and was operational in 2004. This was also coupled to a lab-scale gas cleaning and methanation set-up. A pilot-scale installation (800 kW_{th}-160 kg/h) was constructed in 2007 and came in

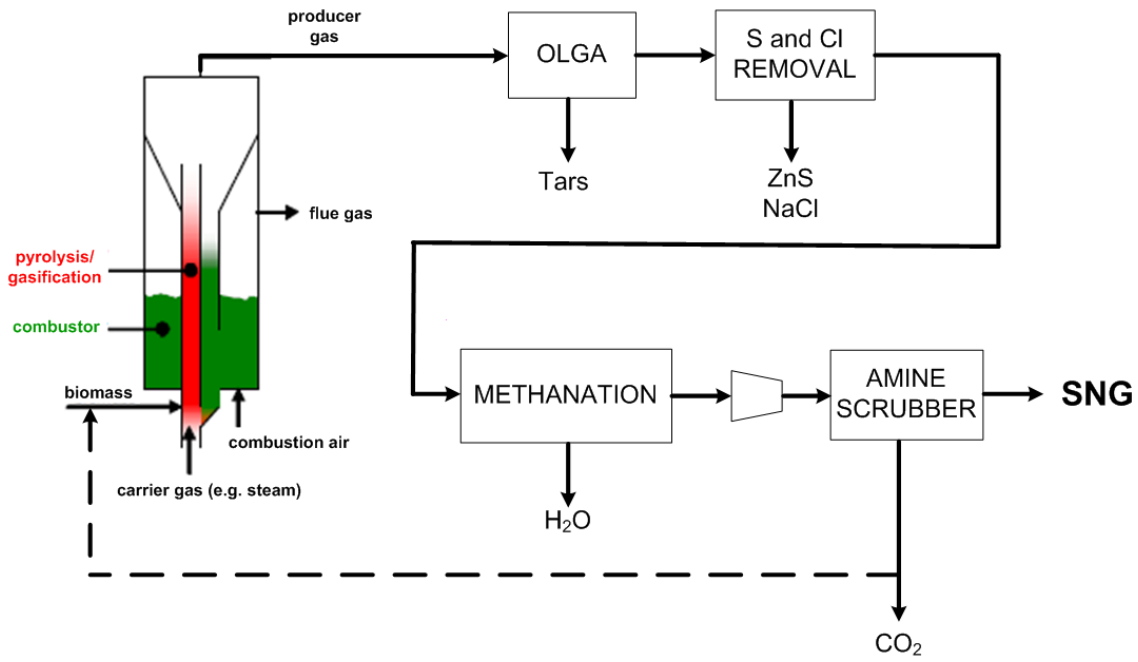

Figure 1.4. The biomass to SNG (BioSNG) concept by ECN. Adapted from [20, 21]. CO_2 is used for pneumatic feeding of the biomass particles.

operation in 2008. The gasifier was connected with the OLGA gas cleaning installation in 2009. A successful duration test with 428 h of operation (out of 500 h test period) of the complete system was realized in 2012. Construction of a demonstration plant (12 MW_{th}) is scheduled for 2013 [19, 20].

1.3.4. Güssing Technology

The initial gasification technology was described as a Fast Internally Circulating Fluidized-Bed (FICFB) developed at TU Vienna, Austria. A 10-kWth test rig was built in 1983 for investigation of fundamental behavior of FICFB. The name *FICFB* remained since then although the design has been changed to an externally circulating fluidized bed. A 100-kW_{th} pilot plant was built in 1997 to gasify various feedstocks (biomass and coal) and for a parameter study. Gasification conditions of T=850-900°C and P≈1 bar are realized in a dual fluidized-bed function. Also, the gas cleaning section was being developed. The design parameters obtained from this pilot plant were used for the 8 MW_{th} demonstration plant which was constructed in 2000-2001 in Güssing, Austria [22]. It operated since 2002 as an industrial gasification power plant by running a 2 MW_e gas engine.

The first methanation experiments (duration of 120 h) were realized in a bench

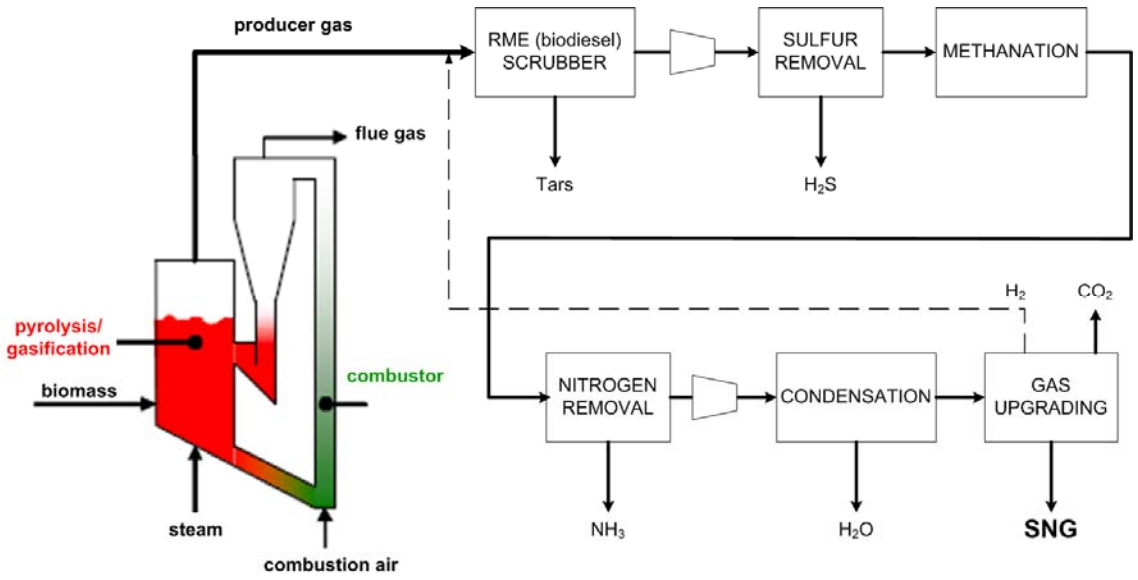

Figure 1.5. The biomass to SNG concept operational at Güssing. Adapted from [20, 23].

-scale reactor using a slipstream of the FICFB gasifier in 2003 [23]. The "Comflux" fluidized-bed methanation technology was selected because of optimum temperature control. Based on the results of this reactor, a 1 MW_{SNG} process development unit was built.

Commissioning of the gas cleaning and methanation step was completed in November 2008. In December 2008 fuel gas was converted to a methane-rich gas for the first time. In April 2009 demonstration of the whole process chain was achieved, which is presented in Figure 1.5.

1.4. New gasification concept for bio-methane production from dry biomass

A new gasification process for methane production from biomass is proposed in this thesis. This gasification concept is termed *self-gasification of biomass*.

Self-gasification is autothermal and (auto)catalytic and utilizes elevated pressures. It is autothermal because it uses, in *one* reactor, the heat provided by the (exothermic) methanation reaction (1.3) to meet the heat demand for the (endothermic) gasification process, expressed by reactions (1.1) and (1.2). It is envisaged that operation is possible without using oxygen/air at all. It is (auto)catalytic because the minerals contained in the biomass itself, are used possibly in combination with a synthesized catalyst to catalyze e.g. gasification, methanation and tar cracking/reforming. The amount of minerals/ash in the reactor can be increased by recycling or creating a hold-up of the ash or components of the ash. Problems related to the presence of

inorganic elements in biomass gasification systems (slagging, fouling and corrosion) will not be a serious issue at biomass self-gasification conditions because of the lower gasification temperatures utilized (600-800°C).

Biomass self-gasification uses elevated pressures (30-80 bar) favoring the equilibrium reaction (1.3) towards methane formation. The same reaction also favors the production of methane at low reaction temperatures, since it is an exothermic equilibrium reaction. On the other hand, however, a higher reaction temperature is favorable to reach sufficient gasification rates. Also, the elevated pressures required in the gasifier may lead to complex biomass feeding systems. Other possible process configurations for this concept, except for the conventional one presented in Figure 1.1, are shown in Figure 1.6. All three possible operation modes are further investigated and discussed in Chapter 2 of this thesis.

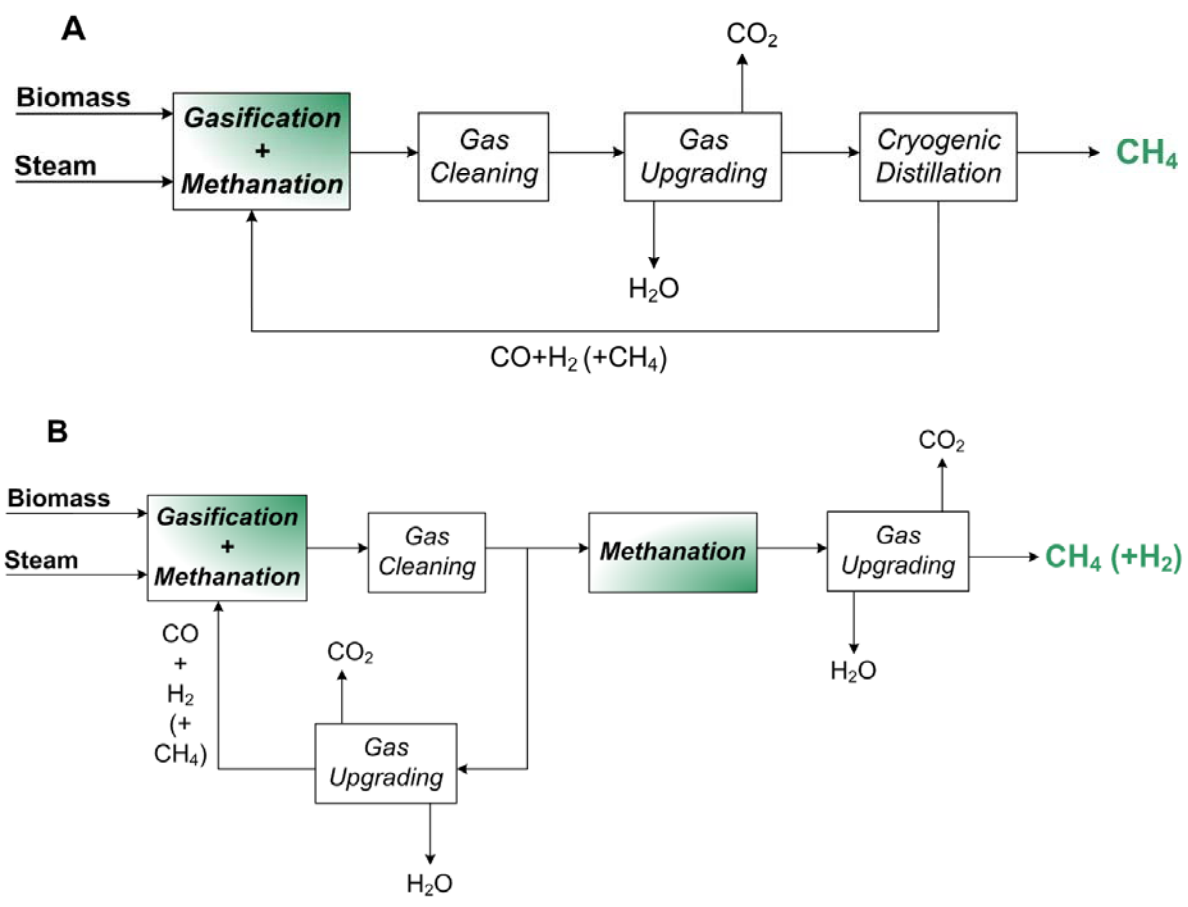

Figure 1.6. Other possible process configurations for the self-gasification concept.

The concept of self-gasification of biomass finds its roots in coal research and specifically the CCG (Catalytic Coal Gasification) process developed by Exxon in the 1980's [10]. Exxon claimed that: (1) impregnation of the coal feed with K_2CO_3 and gasification under pressure with steam produced methane gas at equilibrium and (2) the gasifier needed very little heat input, since the produced CO and H_2 were recycled back to the gasifier to produce more methane [11]. So, the net gaseous products were CH_4 and CO_2. The end of the oil crisis caused the costly CCG process to become uneconomic and its development was stopped. High process costs were involved for the cryogenic unit for CH_4 purification and for the make-up catalyst as well as for the catalyst recovery unit.

CCG research is regaining interest because biomass can be used instead of coal. Biomass already contains a number of minerals that could act as catalysts in the process. These minerals can reach the desired (higher) concentration inside the reactor by partial recovery at the ash exit and recycling to the reactor. Additionally, the ash from the bleed stream of the gasifier can be recycled back to the soil of the biomass production areas. This process is envisaged to be generally suitable for biomass containing high concentration of alkali metals. On the other hand, if the alkali metal content of the feed is low this could be adjusted either by an impregnation step or by co-feeding biomass with a higher alkali content.

Alkali(ne earth) metals that are mostly present in biomass are calcium (Ca), sodium (Na) and potassium (K). Some iron (Fe), magnesium (Mg) and chlorine (Cl) may also be present. Table 1.1. shows their elemental compositions in different types of biomass. This table also includes the elemental composition of Illinois no.6 coal which was used by Exxon in the CCG process. The types of biomass preferred, because of their high alkali metal content, are short rotation crops. Haga et al. [26] indicated that these elements as well as their binary and ternary composites have a catalytic effect on carbon gasification.

1.5. Scope and outline of this thesis

The scope of this current work is the proof of concept of biomass self-gasification as an alternative biomass to SNG gasification process. This entails detailed process simulations as well as experimental studies. The results obtained in this thesis are important not only for the biomass to methane route, but give valuable insights for all biomass gasification processes. These

Table 1.1. Fe, Mg, Ca, Na, K and Cl elemental compositions of different biomass types and of Illinois no.6 coal.

elements in dry material, wt.%	water hyacinth [24]	alfalfa [24]	banagrass [24]	tobacco [24]	sugarcane fibers [24]	grass [24]	rice straw [24]	olive cake [24]	pine wood [25]	Illinois no.6 coal [24]
Fe	n.d.[a]	0.0	0.0	n.d.	1.2	0.0	0.1	0.2	n.d.	1.1
Mg	n.d.	0.1	0.1	n.d.	0.4	0.1	0.2	0.5	0.013	0.1
Ca	1.7	1.0	0.3	2.7	0.8	0.4	0.3	1.3	0.077	0.4
Na	0.3	0.0	0.0	0.0	0.2	0.0	0.1	0.1	n.d.	0.1
K	3.1	3.8	3.5	1.8	1.0	2.4	2.1	0.9	0.003	0.4
Cl	1.9	0.6	0.8	n.d.	0.4	1.0	0.5	0.2	n.d.	0.1
Total	7.0	5.5	4.7	4.5	4.0	3.9	3.3	3.2	0.093	2.2

[a] n.d. : not defined.

issues include: methane formation, gasification under pressure and the effect of naturally occurring ash in biomass and its potential as gasification catalyst.

Chapter 2 focuses on the process performance of biomass gasification to methane. The possible process configurations, including possible recycles, are presented and investigated via process modeling. Efficiencies toward methane production are calculated including heat integration considerations. An appendix at the end of this chapter provides detailed results on the models and technologies used.

Chapter 3 deals with mapping of the operating window by experimental investigation of the influence of model ash components on the different stages of gasification (pyrolysis, char gasification and methanation). A comparison is made between different biomass gasification technologies and the self-gasification concept on basis of operating conditions and methane content of the product gas. An appendix at the end of this chapter gives more insight on the batch capillary technique used for the experimental study.

In *Chapter 4* the steam gasification of pine wood-derived char is investigated, with the focus mainly on the catalytic potential of wood ash as catalyst. Parameters studied involve presence of ash components, their type, concentration and addition method. Inhibition by CO and H_2 is considered as well. Char morphology was examined and ash distribution inside and among biomass/char particles is discussed.

In *Chapter 5* methane formation and gasification of char from potassium-impregnated wood is studied at high pressure. CO and/or H_2 were led over packed beds of catalyst or wood char and methane production was measured. Also, the effect of gasifying medium (H_2O and/or CO_2) and presence of K_2CO_3 in the char were studied for high-pressure gasification. Methane steam reforming was examined as well.

At the end of this thesis, overall conclusions are summarized, the attained experimental data are interpreted qualitatively with respect to reactor and process design, and an outlook is presented.

Literature cited

1. Zhang W., Automotive fuels from biomass via gasification, Fuel Process. Technol. **2010**, 91, 866-876.

2. van Rossum G., Kersten S.R.A., van Swaaij W.P.M., Staged catalytic gasification/steam reforming of pyrolysis oil, *Ind. Eng. Chem. Res.* **2009**, 48, 5857-5866.

3. Sakar S., Yetilmezsoy K., Kocak E., Anaerobic digestion technology in poultry and livestock waste treatment - a literature review, *Waste Manage. Res.* **2009**, 27, 3-18.

4. Matsumura Y., Minowa T., Potic B., Kersten S.R.A., Prins W., van Swaaij W.P.M., van de Beld B., Elliott D.C., Neuenschwander G.G., Kruse A., Antal Jr., M.J., Biomass gasification in near– and super– critical water: Status and prospects, *Biomass Bioenergy* **2005**, 29, 269-292.

5. van der Drift A., Rabou L.P.L.M., Boerrigter H., Heat from biomass via synthetic natural gas, Proceedings of the 14th European Biomass Conference & Exhibition, Paris, France, Oct 17-21, **2005**.

6. Duret A., Friedli C., Maréchal F., Process design of synthetic natural gas production (SNG) using wood gasification, *J. Cleaner Prod.* **2005**, 13, 1434-1446.

7. Hausberger A.L., Knight C.B., Atwood K., Development of methanation

catalysts for the synthetic natural gas processes, *Adv. Chem. Ser.* **1975**, 146, 47-70.

8. Higman C., van der Burgt M., *Gasification*; Gulf Professional Publishing, Houston, TX, **2003**.

9. Kirk-Othmer, Encyclopedia of Chemical Technology; John Wiley & Sons, Inc. , vol. 6, **2002**.

10. Marshall H.A., Smits F.C.R.M., Exxon catalytic coal gasification process and large pilot plant development program, Proceedings of the 9th Annual International Conference on Coal Gasification, Liquefaction and Conversion to Electricity, Pittsburgh, PA, Aug 3-5, **1982**, 357-377.

11. Koh K.K., Integrated catalytic gasification process, US Patent 4,094,650, June 13, **1978**.

12. Levenspiel O., What will come after petroleum?, *Ind. Eng. Chem. Res.* **2005**, 44, 5073-5078.

13. HaldorTopsøe, From coal to substitute natural gas using TREMP, technical report, Haldor Topsøe, **2008**.

14. PGP, Practical experience gained during the first twenty years of operation of the Great Plains gasification plant and implications for future projects, Technical report, Dakota Gasification Company prepared for U. S. Department of Energy (DoE) - Office of Fossil Energy, **2006**.

15. Hydromethanation process, www.greatpointenergy.com. Great Point Energy. (Website accessed on 11-11-2012)

16. Reiling V.G., Robinson E.T., Nahas N.C., Smith J., Mims C., Processes for gasification of a carbonaceous feedstock, US Patent 8,328,890, December 11, **2012**.

17. Rappas A.S., Spitz R.A., Catalytic gasification process with recovery of

alkali metal from char, US Patent 7,897,126, March 1, **2011**.

18. Nahas N.C., Catalytic steam gasification of petroleum coke to methane, US Patent 8,114,176, February 14, **2012**.

19. van der Meijden C.M., Veringa H.J., Vreugdenhil B.J., van der Drift B., Bioenergy II: Scale-up of the MILENA biomass gasification process, *Int. J. Chem. Reactor Eng.* **2009**, 7, A 53.

20. van der Drift A., Zwart R.W.R., Vreugdenhil B.J., Bleijendaal L.P.J., Comparing the options to produce SNG from biomass, Technical Report, ECN report, Presented at 18th European Biomass Conference and Exhibition, Lyon, France, May 3-7, **2010**.

21. van der Meijden C.M., Veringa H.J., Rabou L.P.L.M., The production of synthetic natural gas (SNG): A comparison of three wood gasification systems for energy balance and overall efficiency, *Biomass Bioenergy* **2010**, 34, 302-311.

22. Hofbauer H., Rauch R., Bosch K., Koch R., Aichernig C., Biomass CHP plant Güssing-A success story, Expert Meeting on Pyrolysis and Gasification of Biomass and Waste, Strasbourg, France, Oct **2002.**

23. Rehling B., Hofbauer H., Rauch R., Aichernig C., BioSNG - Process simulation and comparison with first results from a 1-MW demonstration plant, *Biomass Conv. Bioref.* **2011**, 1, 111-119.

24. Phyllis Database for biomass and waste. www.ecn.nl/phyllis. Energy Research Centre of The Netherlands.

25. Westerhof R.J.M., Kuipers N.J.M., Kersten S.R.A., van Swaaij W.P.M., Controlling the water content of biomass fast pyrolysis oil, *Ind. Eng. Chem. Res.* **2007**, 46, 9238-9247.

26. Haga T., Nogi K., Amaya M., Nishiyama Y., Composite catalysts for carbon gasification, *Appl. Catal.* **1990**, 67, 189-202.

Chapter 2

Biomass Gasification for the Production of Methane: Process Performance Analysis

This chapter examines the process performance of biomass gasification to methane. Three gasification configurations were studied via process modeling: the (product) recycle, the (secondary) methanation and the combined (recycle and methanation) mode. The simulations gave insight into the HHV efficiency to methane and process energy demand (hot utility) with varying gasifier temperature (700-800°C) and pressure (1-35 bar). Simulation results show that the overall efficiencies to methane obtained are in the range of 48-66%, of which the combined configuration exhibits the highest overall efficiencies (55-66%). Operation without extra heat input (hot utility) is possible for some cases, but only if the energy requirements for the CO_2 separation unit are lower than 2 MJ/kg CO_2 via an improved or new CO_2 separation technology.

2.1. Introduction

The scope of this chapter is to investigate the performance of the self-gasification process for bio-based methane/SNG production and to examine different possible process configurations via modeling with Aspen Plus.

Conventional proposed biomass gasification processes for methane production from dry biomass are usually two-step configurations [1, 2]. This type of configuration will be referred to as "methanation configuration" in this chapter and is schematically given in Figure 2.1A. An alternative configuration is the recycle mode, which is proved to work for pressurized coal gasification [3, 4] and is presented in Figure 2.1B. Another possible configuration is a combination of the methanation and the recycle mode (termed "combined mode") and is given in Figure 2.1C. These three process configurations are studied in this chapter in view of the newly proposed gasification process for all three configurations, termed *self-gasification of biomass*.

Self-gasification of biomass utilizes a high-pressure steam gasifier, which favors exothermic methane formation via methanation. The process is envisaged to work autothermally and (auto)catalytically without the need of an air/oxygen supply. This can be possible when the heat released in the gasifier due to methane formation fulfills the heat demand for the gasification process. The gasifier works as a dynamic system where the amount of methane produced is controlled by gasifier temperature and vice versa. Therefore, it runs as an auto-tuned system making it an easily controllable unit. Without any air addition, N_2 dilution of the product is avoided and no larger downstream units are necessary. No oxygen addition to the gasifier results in no need for a costly air separation unit (ASU). Initial experimental screening of this process shows that alkali metals greatly enhance the reactivity of char with steam and therefore no separate combustion unit for the char is necessary avoiding the complex heat transfer system that an indirect gasifier entails.

A hot utility expression is used in all simulations of the three process alternatives to have a better basis for comparison among them. A more detailed discussion on the utility/energy demand of the gasifier/process is included in section 2.2.5, where the heat integration analysis is given.

A disadvantage of the methanation and the combined configurations is that the heat released in the methanation reactor cannot be used directly to power the gasifier because the heat is available at a lower temperature (350-500°C) than is needed in the gasifier (700-900°C). A drawback of the recycle configu-

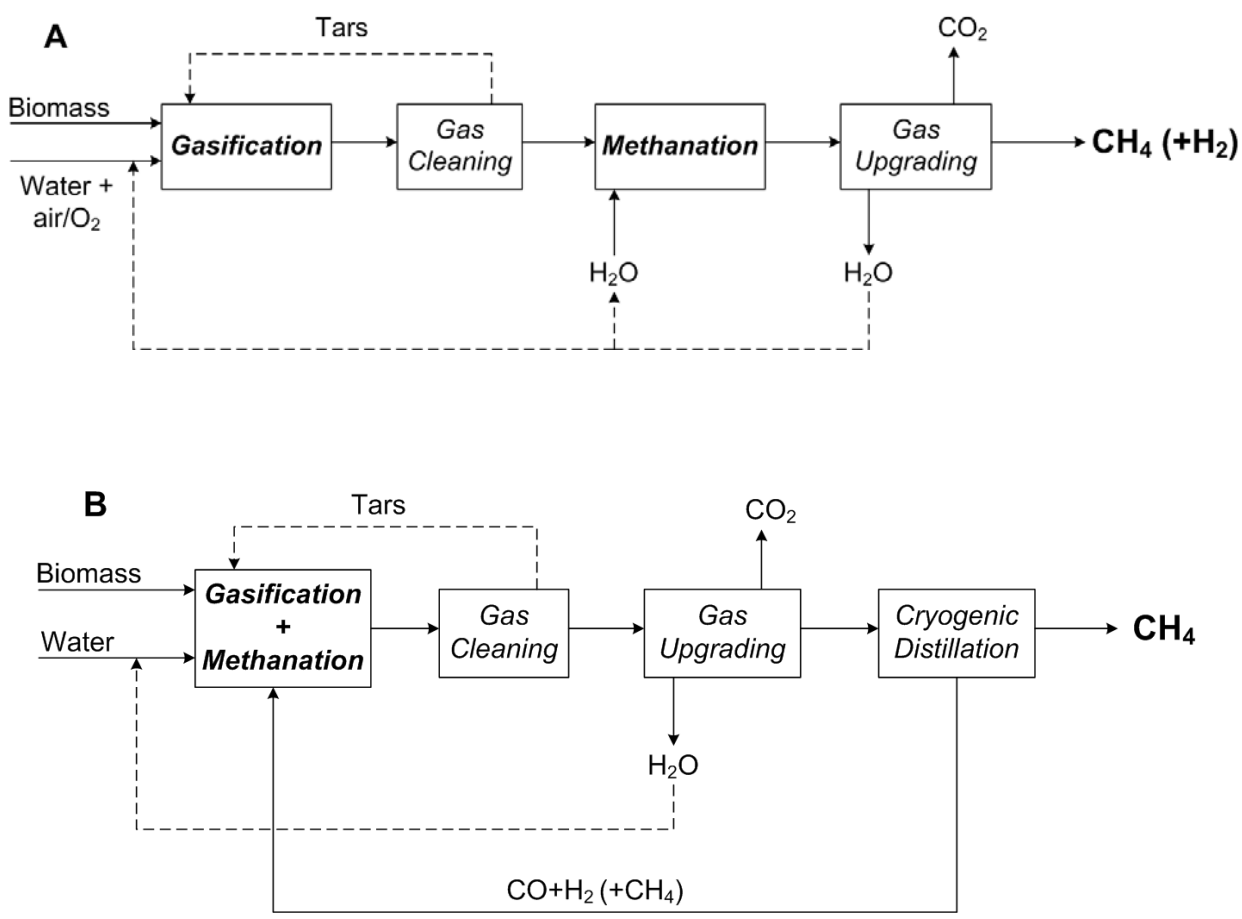

Figure 2.1. Block diagrams of the **(A)** methanation, **(B)** recycle, and **(C)** combined configurations.

ration is the use of the cryogenic distillation unit for methane purification, which is an energy-intensive process. An advantage of the recycle and the combined configurations is that the gas recycle to the gasifier provides a higher potential for autothermal operation of the gasifier without O_2/air addition. Also, the recycle gas can be used for lock hopper pressurization and, therefore, no inert gas is needed at all for biomass feeding. The amount of gas required for pressurization ranges between 0.5 and 0.6 m^3/GJ fuel [5].

In all three configurations, there is possibility for water recycling and for feeding of the tars from the gas cleaning section to the gasifier [6]. These are indicated in Figure 2.1 by the dashed lines only for illustration purposes and are not dealt with in the studied simulations.

The route to methane via gasification of dry biomass is presented and examined for the three aforementioned process configurations: (a) the methanation, (b) the recycle, and (c) the combined types. The three process types are compared with respect to their HHV efficiency to methane with varying gasifier temperature and pressure. At the highest gasifier pressures (~35 bar), the results represent the envisaged self-gasification regime.

Elevated pressures, in practice, may require complex reactor feeding systems. In commercial pressurized gasifier systems, expensive lock hoppers are used for feeding dry solids under a maximum pressure of 100 bar [7]. There is also the possibility of using a piston-type feeder for the solids [8] or dynamic hoppers, which require multi-stage operation for pressures higher than 20 bar. Solids can also be fed to the gasifier in the form of water slurries (30-40 wt.% water for coal-water slurries). In this case, there is also the alternative of using liquid biomass as feed (e.g. pyrolysis oil or bio-slurry [9]) because pumping of liquid feeds is easier. Therefore, liquefied biomass seems to be a promising alternative biomass feed for large-scale self-gasification and especially for very high pressures (~80 bar).

2.2. Process simulations

2.2.1. Model description and methodology

For modeling biomass, $C_1H_{1.33}O_{0.66}$ was chosen as a basis for the calculations. Its enthalpy of formation was defined corresponding to a dry HHV of 20.7 MJ/kg for the biomass (biomass specific) [10]. The process conditions applied in the models are given in Table 2.1.

The gas composition of the gasifier and the methanation reactor effluents were

Table 2.1. Process conditions used in the models.

biomass moisture content (wt.%)	6
biomass input	25°C, 1 bar
water input	25°C, 1 bar
steam/carbon (mol/mol) (gasifier)	1.50 – 2.43
compressors (also cryogenic unit)	multistage (with intercooling)
recycle split (only in combined mode)	50%
methanation reactor	350-500°C, 35 bar
S_1 separator	43°C [10]
S_2 separator	35°C [10]
S_3 separator (only in recycle mode)	-147 to -138°C, 35 bar
CH_4 product	25°C, 35 bar

calculated by minimization of the Gibbs free energy at the operating conditions. The Peng-Robinson property method was used. It was assumed that only the components H_2O, CO_2, H_2, CO and CH_4 were at chemical equilibrium. C_2-C_3 components existed in very small amounts at chemical equilibrium according to the model (<10^{-3} mol%). Therefore, they were not taken into account for further calculations. In practice, also contaminants can exist in the gasifier effluent, which originate from N, S and Cl components of the biomass feed. N can exist in the gas product mostly as NH_3 (0.08 [11]-0.30mol% [12]) and to a lesser extent as HCN (0.0015mol% [6]). S can exist in the gas mainly as H_2S (0.006 [6]-0.010mol% [11, 12]) as well as COS (max. 0.0011mol% [6]). Finally, Cl can appear in the gaseous product as HCl (0.003mol% [6]). Because the scope of this work is to evaluate the process from the efficiency point of view, these specific components were not taken into account for the calculations. However, in an actual gasifier, such removal units could be integrated in the low-temperature operation of the water and CO_2 removal units.

The gasifier was operated isothermally. The methanation reactor was simulated as a series of reactors with intermediate cooling as happens in practice [13-15]. It was not modeled isothermally at a specific temperature (350 or 500°C), but rather as a linear temperature decrease between 500 and 350°C.
Thermodynamic (solid) carbon-free operation of the gasifier is ensured in all cases under the conditions simulated by varying the steam/carbon (mol/mol) ratio (from 1.50 to 2.43). The steam/carbon ratio needed in all cases was 1.5

except for the recycle configuration at 800°C and the combined configuration at 700°C to prevent carbon deposition. The energy requirement for steam production and superheating is also included in the detailed results for these configurations in section A.1 of Appendix A at the end of this chapter.

For (solid) carbon-free operation of the methanation reactor, extra steam was added to the first reactor of the series at reactor temperature (at 350°C; just enough to prevent (solid) carbon formation), as is also done in practice [13]. For the range of operating conditions simulated, the steam/dry gas (mol/mol) ratio entering the first methanation reactor was in the range of 0.00-0.62 depending on gasifier operating conditions. The dry gas in this case is the sum of H_2, CO, CO_2 and CH_4 in the gas. For lower gasifier pressures and higher gasifier temperatures, the needed ratio was low because at these conditions more hydrogen was produced. Carbon can, though, still be formed in the gasifier and/or the methanation reactor depending on kinetics (kinetic (solid) carbon).
Figures 2.2 to 2.4 show the PFDs of the methanation, the recycle, and the combined configurations, respectively. In all cases, the heater for steam production and the cooler before separator(s) S_1 are modeled as three heaters and three coolers in series, respectively, to obtain a better calculation of the enthalpy involved in water evaporation or condensation. In the case of the methanation and combined configurations, hydrogen is included in the final product. This is the result of steam addition to the methanation reactor to prevent thermodynamic (solid) carbon formation and to completely convert the carbon monoxide in the gas stream.

Figure 2.2 shows the PFD of the methanation configuration. Biomass and steam are the feed streams of the gasifier, and its product gas is upgraded (S_1 and S_2), compressed to 35 bar, and led to a downstream methanation reactor, after which the gas is again dried (S_1) and upgraded (S_2). The methane product is cooled to a temperature of 25°C.
Figure 2.3 depicts the PFD of the recycle configuration. Biomass and water in the form of steam are fed to the gasifier. The produced gas is cooled and isothermally compressed to a pressure of 35 bar after water removal in separator S_1. Scrubber S_2 is used for CO_2 separation, the outlet stream of which (a mixture of CO, H_2 and CH_4) is fed to the cryogenic unit S_3 (modeled as a distillation column with a cascade refrigeration system), where the CH_4 product is

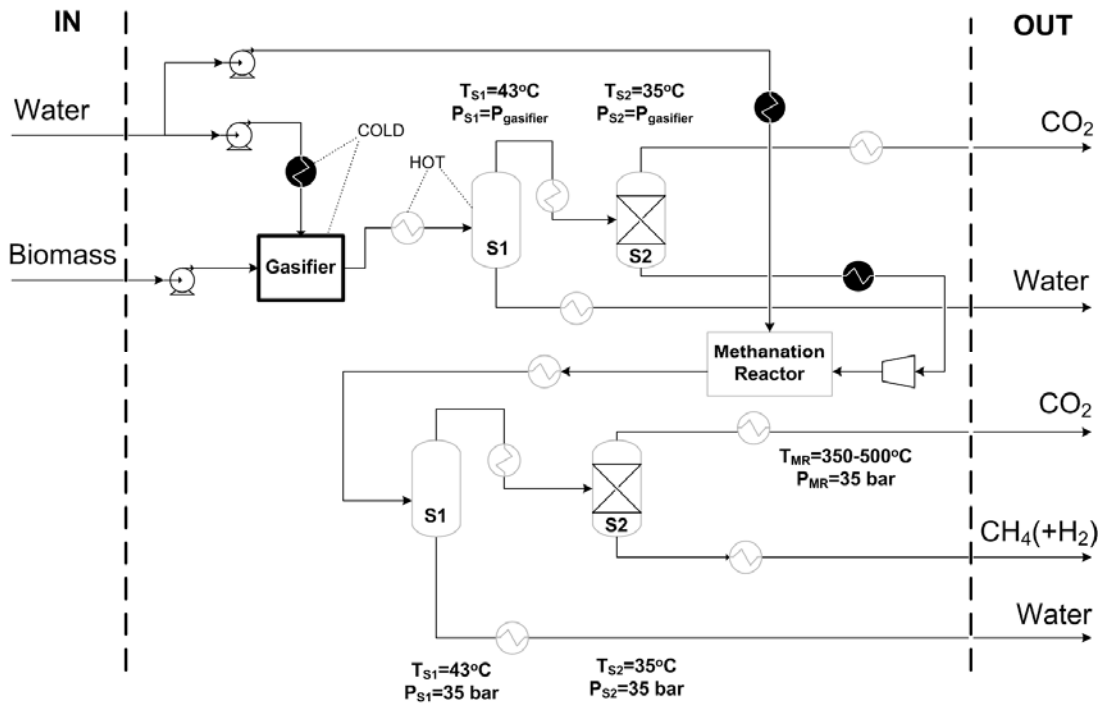

Figure 2.2. PFD of the methanation configuration. Cold units require heat and hot units require cooling (basis for heat exchange network). S_1 = water condensation/ separation, S_2 = CO_2 separation.

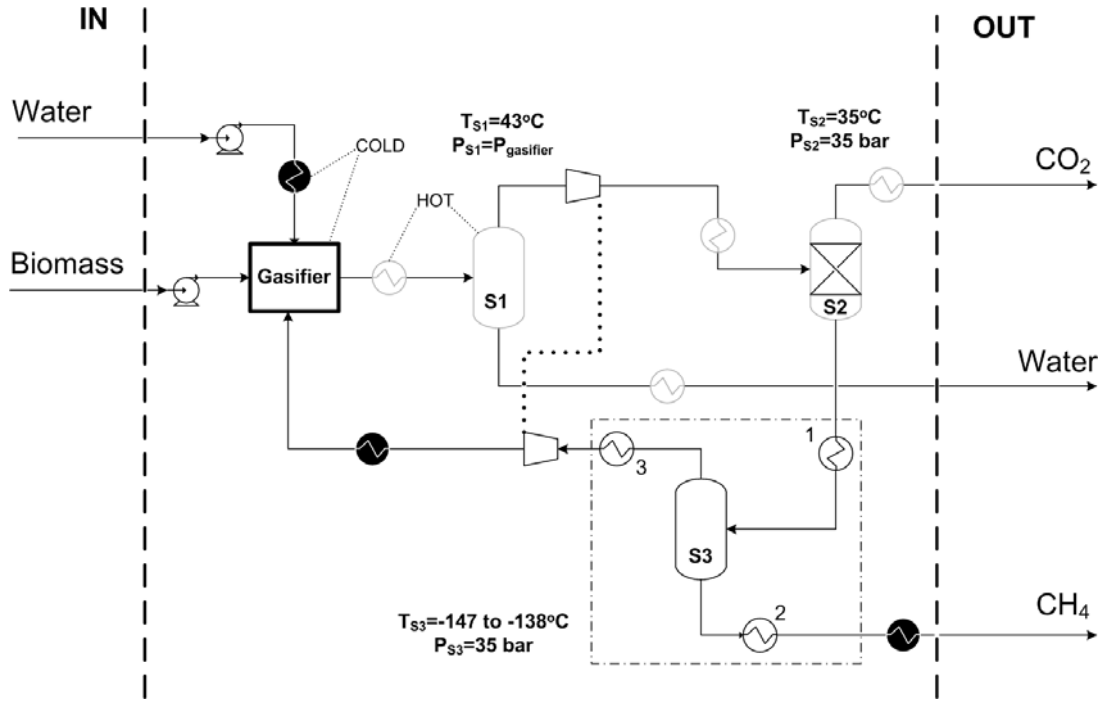

Figure 2.3. PFD of the recycle configuration. Cold units require heat and hot units require cooling (basis for heat exchange network). S_1 = water condensation/separation, S_2 = CO_2 separation, S_3 = cryogenic separation. The numbered heat exchangers (1-3) correspond to the numbers in Figure A.2 in section A.3 of Appendix A at the end of this chapter.

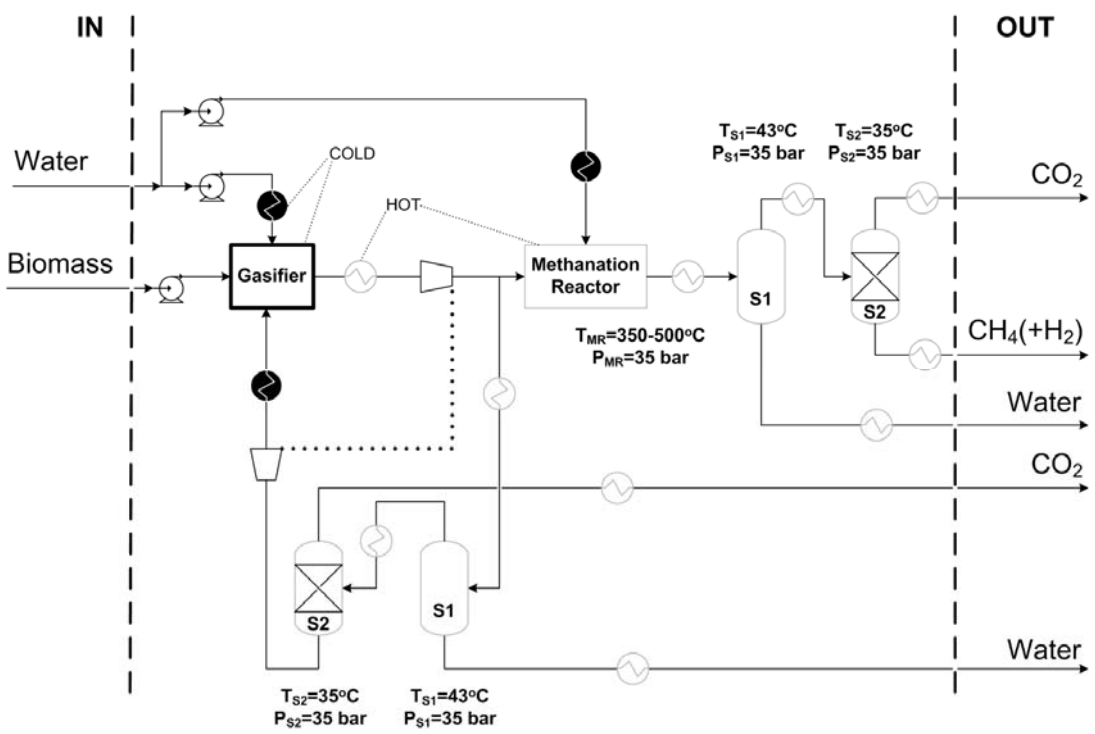

Figure 2.4. PFD of the combined configuration. Cold units require heat and hot units require cooling (basis for heat exchange network). S_1 = water condensation/ separation, S_2 = CO_2 separation.

separated from CO and H_2. The CH_4 product is heated to a temperature of 25° C. The CO and H_2 mixture (containing also some CH_4), after expansion to gasifier pressure and heating, is recycled back to the gasifier. Compressor and turbine are linked together in a system, where heat and work are exchanged (denoted in Figure 2.3 by the dotted line).

Figure 2.4 shows the PFD of the combined configuration. Cold biomass and steam are led to the gasifier, after which the effluent is cooled down and compressed to 35 bar. A total of 50% of the gas stream is led to a downstream methanation reactor and 50% is recycled back to the gasifier, after water (S_1) and CO_2 removal (S_2). The effluent of the methanation reactor is upgraded (water and CO_2 removal), and the final product is obtained. In the compressor-turbine system (denoted in Figure 2.4 by the dotted line), heat and work are exchanged. The choice of a recycle split of 50% is further studied and explained by a sensitivity analysis in section A.2 of Appendix A at the end of this chapter.

For comparison of the different configurations on an equal basis, some common parameters have been chosen: (1) the temperatures of all feeds and products are set to a temperature of 25°C, (2) after the compressor the pressure is

set to 35 bar, so that specific separation technologies are utilized and separation efficiencies are not affected by a change in the pressure (especially the cryogenic separation unit), (3) steam is fed to the gasifier at gasifier operating temperature. As a result, the energy demand of the gasifier could be studied as an effect of the overall reaction enthalpy and heating of the cold biomass entering the gasifier, (4) the hot utility demand is represented by a value. The way this hot utility is generated is not dealt with in this work, (5) the simulation results are presented on a relative basis (biomass input).

2.2.2. Efficiency definition

The HHV efficiency to methane is expressed on primary energy input and is calculated by:

$$\eta_{CH_4} = \frac{HHV_{CH_4}\Phi_{m_{CH_4}} + HHV_{H_2}\Phi_{m_{H_2}}}{(HHV_{biomass} + \sum Q + \sum W)\Phi_{m_{biomass}}} \times 100\% \qquad \text{(eq.2.1)}$$

where $\sum Q = Q_{\text{hot utility}} + Q_{S2}$

$\sum W = 3W_{\text{compressor(-turbine)}} + 3W_{\text{recycle compressor}} + 3W_{\text{pumps}} + 3W_{\text{solid}} + 3W_{S3}$

where all units are expressed in MJ/kg dry biomass feed, unless otherwise stated. The number "3" is preceding each work expression "W" because it is assumed that electricity is produced with an efficiency of $\eta=1/3$ from an energy source. The efficiency expression also includes hydrogen that can exist in the product gas (max 6 mol%) for the case of the methanation and the combined configurations because in these cases it is considered as part of the final product. $Q_{\text{hot utility}}$ is the process energy demand in hot utility, after heat integration analysis, and is read from the cold-hot composite diagrams as explained in section 2.2.5. and Q_{S2} is the energy demand of the CO_2 separation unit. No energy input is included in eq.2.1 for separator S_1 because this is taken into account indirectly through system coolers in the hot composite curve and is therefore incorporated into the $Q_{\text{hot utility}}$ expression.

$W_{\text{compressor(-turbine)}}$ is the net work required for the compressor(-turbine) system, $W_{\text{recycle compressor}}$ is the work required for compression of the recycle stream to overcome the assumed pressure drop of $\Delta P=1$ bar (only in the case of the recycle and the combined configurations), W_{pumps} is the sum of the work required

for the pumps of the gasifier and methanation reactor water feeds, W_{solid} is the energy required for feeding the solid biomass into the gasifier. The latter parameter is added because the model uses a liquid biomass feed, underestimating the actual energy demand. The assumption is made that the solid biomass is pressurized in lock hoppers and a screw feeder is used for biomass injection in the form of 0.5 mm particles [5]. The energy requirement varies from 0.62 to 1.05 MJ_e/kg dry biomass. This includes electricity consumption for compression of the inert gas and the power consumption for size reduction (milling) of the wood to 0.5 mm particle size [5]. In the case of the recycle and combined configurations, the recycle stream (already compressed) can be used for pressurizing the lock hoppers; therefore, the minimum energy requirement is calculated for those cases, which is only the milling of the wood (energy requirement of 0.62 MJ_e/kg dry biomass). W_{S3} (included only in the case of the recycle configuration) is the energy requirement for the cryogenic separation unit S_3. This includes only work expressions for the compressors of the system.

According to this efficiency definition, the maximum efficiency to methane obtained from reaction stoichiometry:

$$C_6H_8O_4 + 2H_2O \rightarrow 3CH_4 + 3CO_2 \quad (2.1)$$

can be calculated as:

$$\frac{3MW_{CH_4}}{MW_{biomass}} \frac{HHV_{CH_4}}{HHV_{biomass}} \times 100\% \quad \text{(eq.2.2)}$$

This gives a maximum efficiency to methane of 89%.

2.2.3. Assumptions

Assumptions that were made for the process calculations are as follows:

- Electricity is assumed to be produced from (fossil) fuel with η=1/3
- Carbon-to-gas conversion in the gasifier is 100%. This is envisaged to be possible according to the *self-gasification* concept
- Reactions are at chemical equilibrium. It is stated in the literature that methanation and water-gas shift can be at equilibrium in the temperature range 700-800°C by the use of alkali metals as catalysts [3, 4]. This is further investigated in Chapters 3 and 5 of this thesis

- The solid biomass is pressurized in lock hoppers, and it is injected in the gasifier in the form of 0.5 mm particles by a screw feeder
- The gasifier effluent is tar-free. The catalyst used in the self-gasification concept is envisaged to enhance vapor cracking/reforming. A tar recycle to the gasifier can also be assumed
- A pressure drop of ΔP=1 bar is assumed only for the recycle stream in the case of the recycle and the combined configurations
- Full heat integration is obtained from the heat analysis of each system
- Hot utility is assumed to be generated with 100% efficiency
- The separation efficiency of S_1 and S_2 is 100%
- For the CO_2 separation unit (S_2) [16]:
  - MEA solution of 30 wt.% in water
  - 2 MJ/kg CO_2 energy needed for heating of the CO_2-rich solution from 80 to 100°C (regeneration temperature)
  - 2 MJ/kg CO_2 energy needed for water evaporation and regeneration reaction of the amine

2.2.4. Gas upgrading/separation units

Separator S_2, which is the CO_2 removal unit, was set to have a separation efficiency of 100%. The technology chosen was the use of MEA via chemical wash. The energy demand was conservatively set at 4 MJ/kg CO_2 [7] (equal to 3.7 MJ/kg dry biomass). The option of in-situ removal of CO_2 with CaO also exists, but because of the high temperature needed for regeneration of $CaCO_3$ (at least 850°C) with recirculation of the solid [17], this is out of the scope of this work and is therefore not a part of the self-gasification concept.

Separator S_3 was modeled as a cryogenic distillation column with a cascade refrigeration system [3, 18], including three consecutive refrigeration cycles (propylene, ethylene, methane). Further details about the modeling of the cryogenic unit can be found in section A.3 of Appendix A at the end of this chapter.

2.2.5. Heat Integration Analysis

In Figures 2.2 to 2.4, all of the black and grey units were included in calculations for heat integration and consequent necessary process utilities. The black units require heating (cold streams), and the grey units require cooling (hot streams). The compressor(-turbine) system was not included in the heat inte-

gration, and the cryogenic separation unit (S_3) was modeled separately with its own utility and heat integration of the adjacent coolers/heaters, as indicated by the dash-dotted line in Figure 2.3. They are both, though, included in the efficiency definition. Heat analysis was realized by constructing composite diagrams for the hot and cold streams. More information on composite diagrams can be found in ref (19).

If the constructed hot and cold composite curves cross, then, the hot composite curve is shifted along the heat axis (Q/HHV), so that theoretically complete heat integration is realized in each case. The curve is shifted so that a ΔT_{min} of 50°C is obtained. The shift of the hot curve is translated as the hot-utility requirement ($Q_{hot\ utility}$) in the efficiency definition (eq.2.1). The hot utility has to be provided to the system at either a low temperature (at the temperature level of the CO_2 separation unit) or a high temperature (at the temperature level of the gasifier) depending on the results of the heat integration analysis for each case. A low-temperature hot-utility source could be residual site heat, and this makes location a very important factor for a future self-gasification plant. This heat could also be delivered by combustion of the biomass feed or the final gas product. This is an undesirable but common practice. In the cases where the hot utility has to be provided at a high temperature, ΔT_{min} is calculated as the temperature difference between the cold composite curve and the high-temperature extension of the hot composite curve (as shown in Figure 2.6A). The high temperature at which the hot utility has to be provided is assumed to be 100°C higher than the gasifier temperature. A high-temperature hot-utility source could be combustion heat, either of the biomass feed itself or of the char produced in the gasifier (indirect gasification) or by the addition of O_2/air to the gasifier (direct gasification). The latter two ways of supplying heat to the gasifier are also applied in practice, but both would result in lower efficiencies to methane for the studied configurations. Indirect gasification leads to less carbon in the system present as methane. It leaves the system as CO_2 in the flue gas of the combustion unit. Direct gasification causes rise in the CO_2 product, resulting in higher energy demand for CO_2 separation and leading to less CH_4 in the final gas product. A high-temperature hot utility could also be provided as waste site heat, but this option seems unlikely.

2.3. Results and Discussion

2.3.1. Methanation configuration

Figure 2.5 presents the efficiency to methane and the hot-utility demand in the process plotted versus gasifier pressure, for two simulated gasifier temperatures (700 and 800°C). The temperature level of the needed hot utility is also included and is denoted in the graph by "H" for high-temperature hot utility and by "L" for low-temperature hot utility.

The efficiency toward methane increases with gasifier pressure and lower gasifier temperature. This is because, under these conditions, methane production shifts from the methanation reactor to the gasifier, and more methane is produced in the gasifier exothermically via the methanation reaction. A high-temperature hot utility indicates the need for the addition of heat at the temperature level of the gasifier (ΔT=100°C). A low-temperature hot utility means that the hot utility has to be provided at the temperature level of the CO_2 separation unit (around 150°C). In general, a high-temperature hot utility is needed when the gasifier consumes energy and a low-temperature hot utility is needed when the gasifier releases energy, and the steam (and recycle) can be fed to

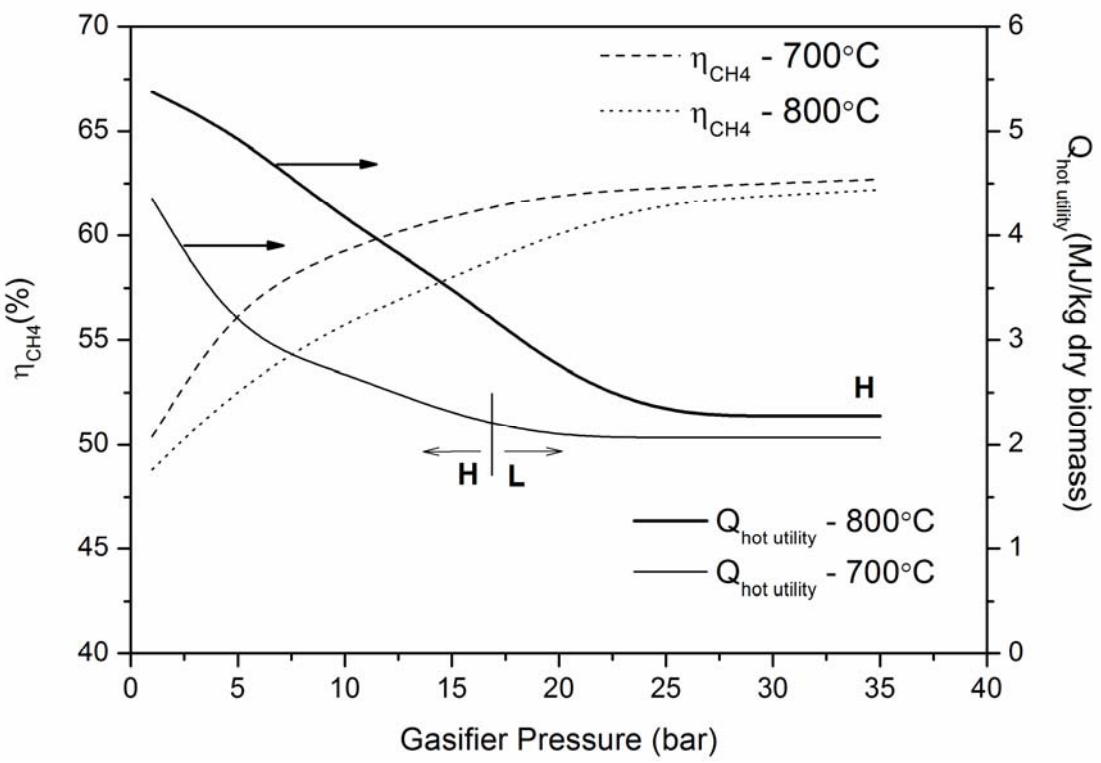

Figure 2.5. Methanation configuration. Effect of gasifier pressure and temperature on efficiency to CH_4 (η_{CH4}) and hot utility demand ($Q_{hot\ utility}$). "H" stands for high-temperature hot utility and "L" stands for low-temperature hot utility.

the gasifier at a temperature of ΔT=50°C lower than the gasifier temperature. Operation of the gasifier at 800°C requires high-temperature hot utility because the gasifier consumes heat throughout the whole simulated pressure range. Operation of the gasifier at 700°C releases heat at operating pressures higher than 15 bar, and therefore at these pressure levels, a low-temperature hot utility is necessary. Thus, autothermal operation of the gasifier itself without O_2/air addition seems to be possible only at 700°C and at pressures higher than 15 bar. Detailed modeling results on the methanation configuration can be found in section A.1 of Appendix A at the end of this chapter.

Figure 2.6 shows two examples of the constructed hot and cold composite curves for the methanation configuration. Figure 2.6A shows the composite curves for operation at 800°C and 1 bar. The cold composite curve consists of three plateaus expressing the energy demand of the isothermal gasifier, the steam production, and the CO_2 separation unit. This case actually represents the focus of the SNG research nowadays [20, 21]. In our study, though, the efficiency for this case is overestimated because there is no separate char combustion unit (indirect gasification) that would provide the needed high-temperature hot utility. This would, consequently, reduce the calculated efficiency to methane. This would occur because the carbon present in the char leaves the system as CO_2 in the flue gas, leading to less methane amount in the final product. Figure 2.6B gives the composite curves for gasifier operation at 700°C and 35 bar. The cold composite curve consists of two plateaus, created by the production of steam for both gasifier and methanation reactor and by the regeneration step of the amine in the CO_2 separation unit. The plateau of the isothermal gasifier, at this pressure, is part of the hot composite curve because it releases heat. The second plateau of the (shifted) hot composite curve at 100°C is the compensating energy usage (in practice, this is a loss) of the CO_2 separation unit. In this case, also the steam can be supplied to the gasifier at lower temperature, to create the necessary ΔT_{min} = 50°C set as the heat integration requirement.

A heat exchanger network (HEN) for the case of Figure 2.6A would provide the necessary heat to the gasifier by the added hot utility and the steam can be generated by the gasifier product, the methanation intercooling and the hot utility. In a HEN for the case of Figure 2.6B, the heat of the gasifier effluent, intercooling of the methanation reactor, and added hot utility could be used to

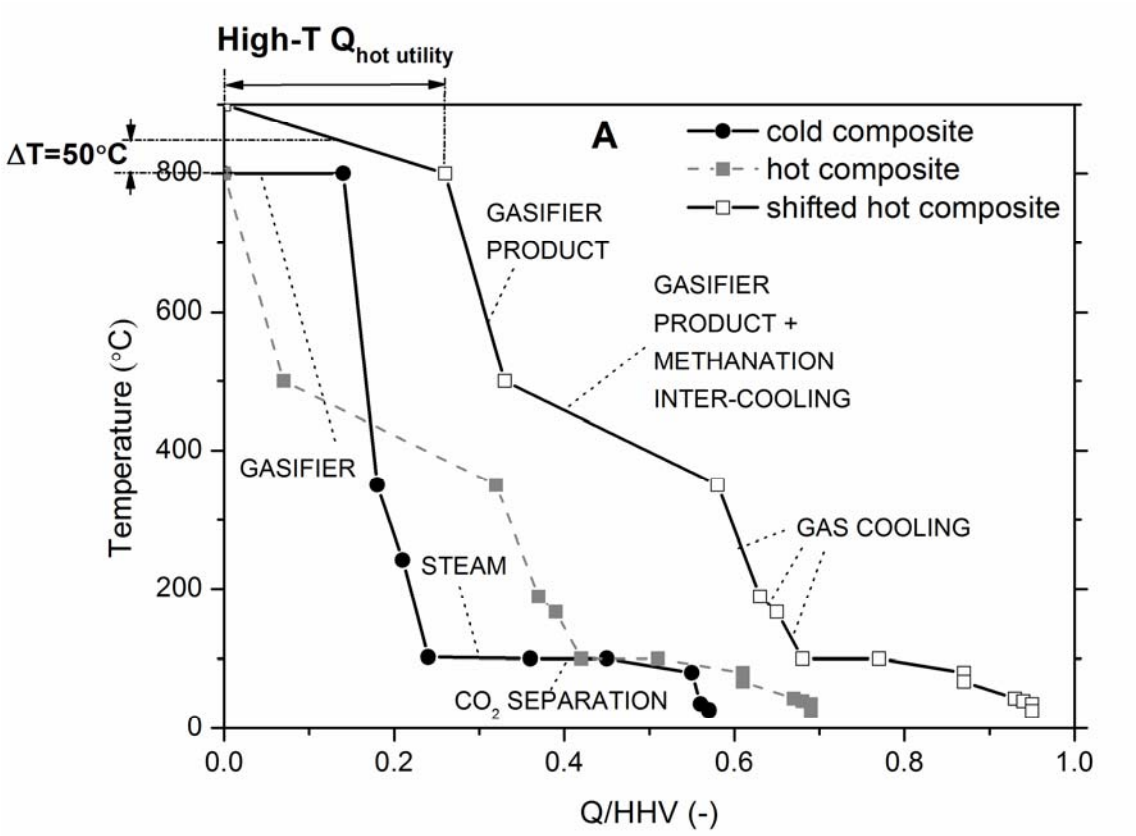

Figure 2.6. Examples of the cold and hot composite curves for the methanation configuration. **(A)** Gasifier temperature = 800°C, gasifier pressure = 1 bar, **(B)** Gasifier temperature = 700°C, gasifier pressure = 35 bar.

produce the steam for both reactors.

In Figure 2.6, the whole hot composite curve is shifted to indicate the necessary hot utility for this configuration. The hot utility does not have to be provided at 800°C in the case of Figure 2.6B, but lower-value heat will be needed at around 150°C.

Simulations also pointed out that it is beneficial for the efficiency to methane to remove water and CO_2 from the gasifier effluent before it enters the methanation reactor. This also happens in practice at the Great Plains Synfuels Plant operated by the Dakota Gasification Company [22]. The efficiency to methane is higher in this case because water and CO_2 are removed before the compression step, and this lowers the power consumption of the compressor. Removal of water steers the equilibrium of the methanation reaction towards higher amounts of methane, although steam addition is still necessary to avoid carbon deposition. Also, CO_2 removal increases the H_2/dry gas ratio of the gas stream entering the first methanation reactor, and therefore less steam has to be added.

The methanation configuration exhibits low efficiency to methane at low gasifier pressure (50%). This was expected because in practice the addition of air/O_2 provides the necessary heat to the gasifier. The calculated extra energy that would be needed in this case for an ASU (if O_2 would be fed to the gasifier) is about 1.2 MJ/kg dry biomass. This is based on experimental (pilot plant) air/biomass feed ratio obtained from ref (6).

2.3.2. Recycle configuration

Figure 2.7 presents the efficiency to methane and the hot utility demand for the recycle configuration versus gasifier operating pressure. The letter "L", which is incorporated into the graph, indicates that the needed hot utility of the system can be added at low temperature (temperature level of CO_2 separation unit) at all simulated gasifier pressures and temperatures. This means that the gasifier produces heat under all conditions. Detailed modeling results on the recycle configuration can be found in section A.1 of Appendix A at the end of this chapter.

Figure 2.8 shows an example of the cold and hot composite curves constructed for the recycle configuration. The two plateaus in the cold composite curve are because of steam production and amine regeneration in the CO_2 separation unit. The plateau in the hot composite curve at 700°C is created by the isother-

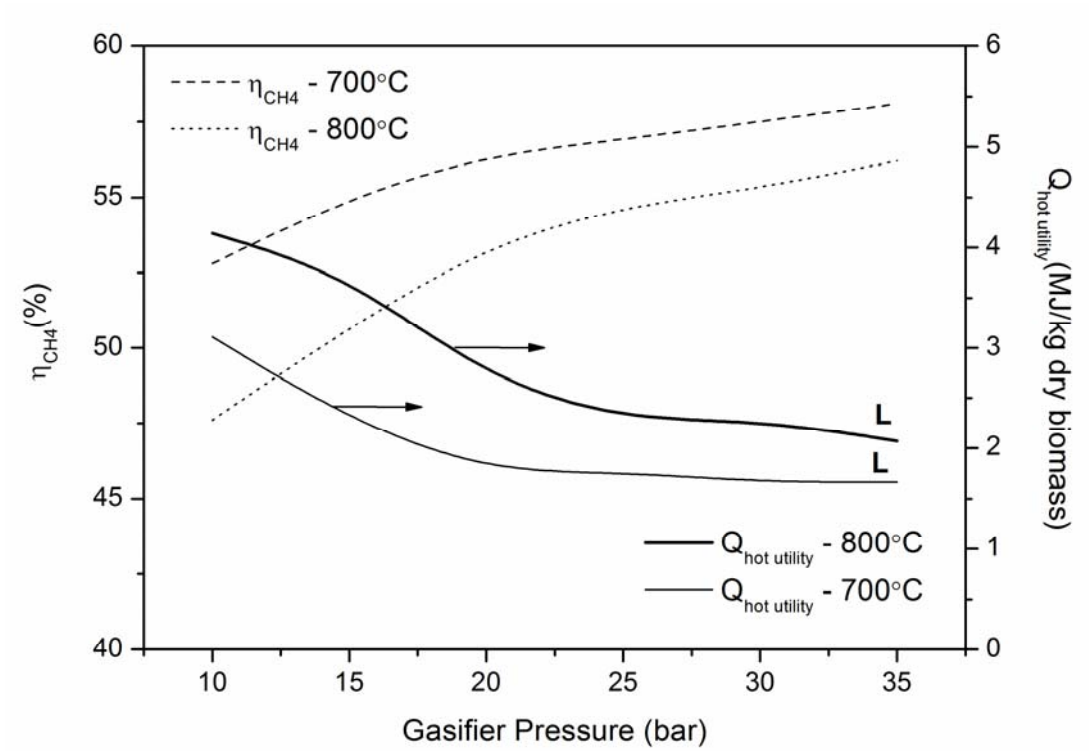

Figure 2.7. Recycle configuration. Effect of gasifier pressure and temperature on the efficiency to CH_4 (η_{CH4}) and hot-utility demand ($Q_{hot\ utility}$). "L" stands for low-temperature hot utility.

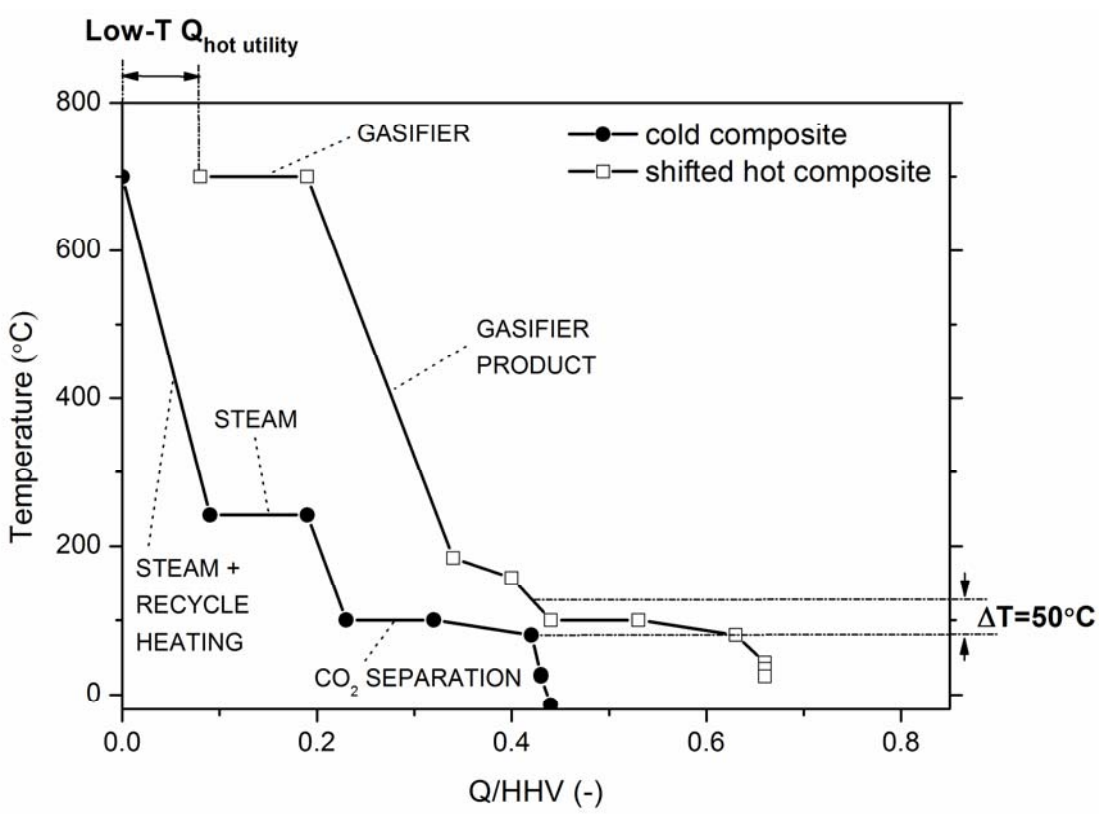

Figure 2.8. Example of the cold and hot composite curves for the recycle configuration. Gasifier temperature = 700°C, gasifier pressure = 35 bar.

mal gasifier operation. The plateau at 100°C is because of the CO_2 separation unit.

In a HEN for this configuration, the gasifier heat and gasifier product can be used for steam production. Because the gasifier releases heat under all simulated conditions, the steam and recycle stream can be fed to the gasifier at a lower temperature (as low as 250°C at 700°C and 35 bar). So, optimized and complete heat integration is theoretically realized.

Temperatures of the cold composite curve that are lower than 25°C correspond to the bottom distillation product of the cryogenic distillation unit. Its temperature, after heat integration with the cryogenic unit (section A.3 of Appendix A at the end of this chapter), can be between -15°C and +15 °C.

2.3.3. Combined configuration

Figure 2.9 shows the efficiency to methane and hot-utility demand versus gasifier pressure for the combined configuration. The letters "H" and "L" included in the plots stand for high- and low-temperature hot utility, respectively. The efficiency toward methane increases with gasifier operating pressure. This is an effect of lower power consumption by the compressor-turbine system, mainly because of the smaller pressure difference that the system has to handle ($\Delta P = P_{methanation} - P_{gasifier}$).

The efficiencies at the two different gasifier temperatures approach the same value at high gasifier pressures (20-35 bar). The difference, though, between them is that gasifier operation at 800°C requires a high-temperature hot utility, while operation at 700°C requires a low-temperature hot utility in the whole studied pressure range. Detailed results obtained with the combined configuration are included in section A.1 of Appendix A at the end of this chapter.

Figure 2.10 presents an example of the plotted cold and hot composite curves for the combined configuration. The two plateaus existing in the cold composite curve are created by steam generation for the gasifier and methanation reactor and by the CO_2 separation unit. For the hot composite curve, the plateau created at 700°C is because of the gasifier. The plateau at 100°C is due to the energy demand of the CO_2 unit.

In a HEN for this specific configuration, the gasifier effluent and inter-cooling of the methanation reactor can be used for steam production of the system. The steam can be injected at a lower temperature into the gasifier.

This system can also work autothermally but only if the total regeneration en-

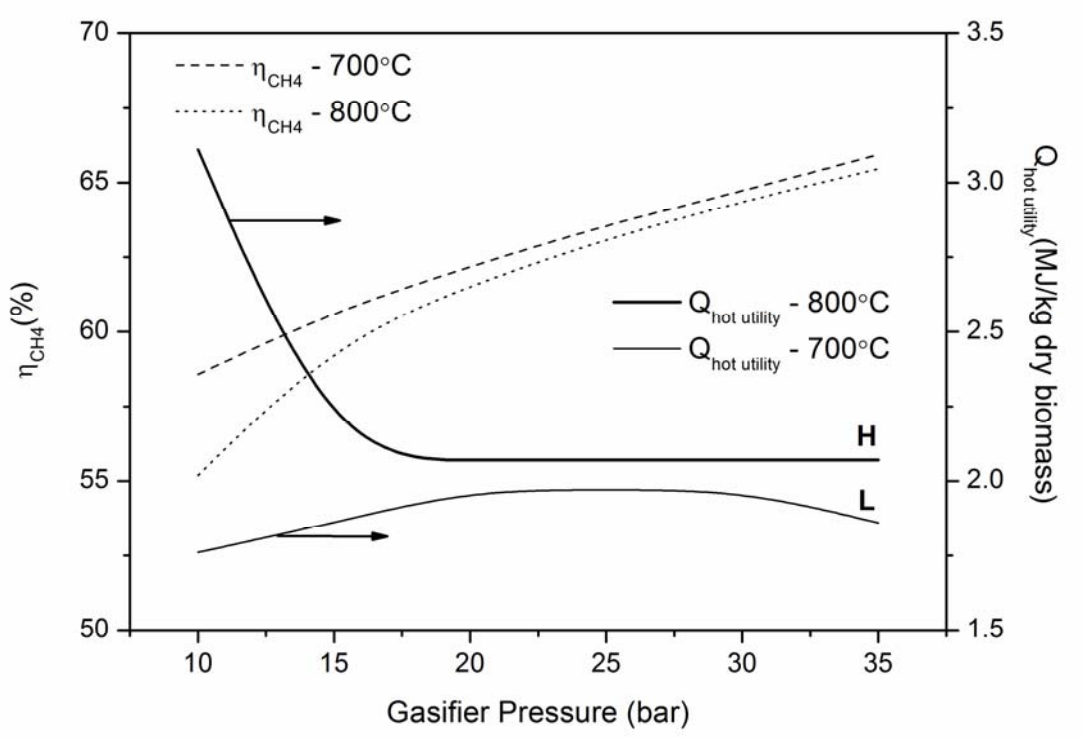

Figure 2.9. Combined configuration. Effect of gasifier pressure and temperature on the efficiency to CH_4 (η_{CH4}) and hot-utility demand ($Q_{hot\ utility}$). "H" stands for high-temperature hot utility, and "L" stands for low-temperature hot utility.

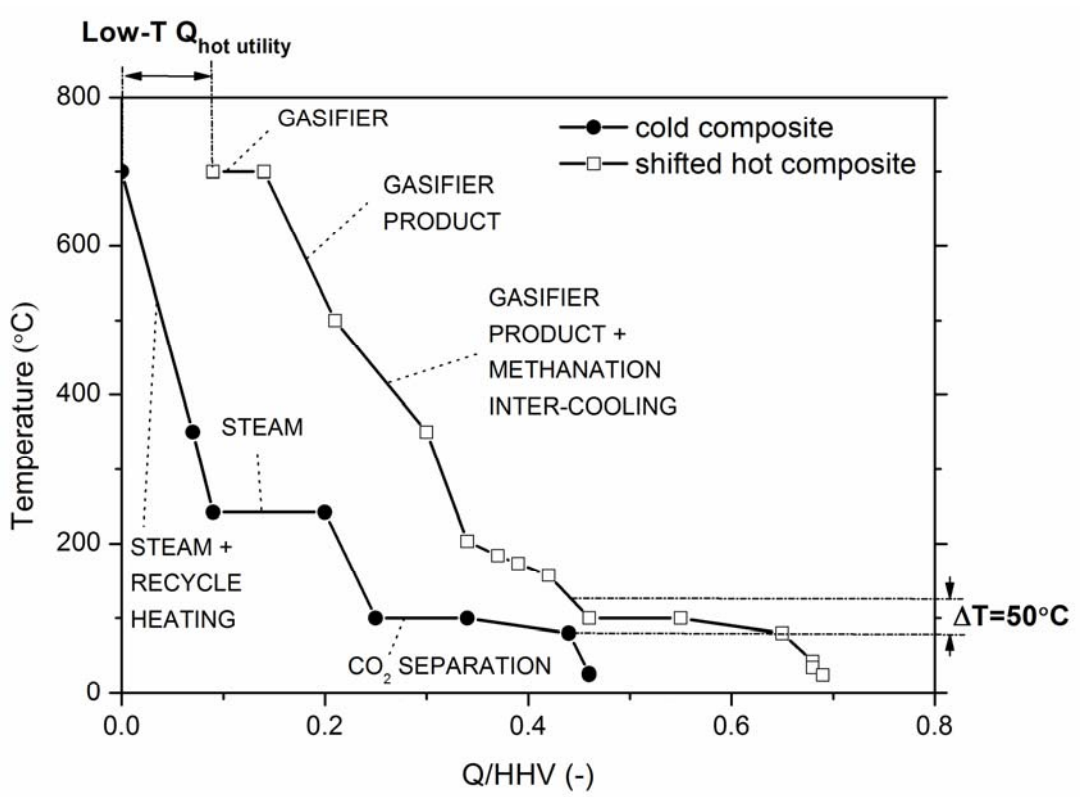

Figure 2.10. Example of the cold and hot composite curves for the combined configuration. Gasifier temperature = 700°C, gasifier pressure = 35 bar.

ergy of the amine in the CO_2 separation unit is lowered from 4 to 2 MJ/kg CO_2. There is important research taking place in the field of CO_2 removal [23-25]. Latest research claims that it is possible to approach such low-energy requirements by employing novel solid amine sorbents [26]. Also, selective CO_2 separation by utilizing membranes seems a promising alternative for a CO_2 separation unit with low-energy consumption [27].

2.4. Discussion

Three possible process configurations for the biomass self-gasification concept for methane production were studied by modeling. These configurations were the methanation, the recycle and the combined modes. The first configuration entailed a gasifier with a downstream methanation reactor, the second one consisted of a gasifier to which CO+H_2(+CH_4) was recycled, and the latter configuration was a combination of the first two. Overall efficiencies to methane obtained were in the range of 48-66%. This corresponds to 54-74% of the theoretical maximum (η_{CH4max}=89%). For the cases where a high-temperature hot utility is needed, the value for the efficiency to methane represents a best-case scenario. The combined process configuration gives the highest overall efficiencies to methane (55-66%), the methanation configuration gives lower efficiencies to methane (49-63%), and the recycle configuration gives the lowest overall efficiencies to methane (48-58%). For gasifier operation at 800°C, the recycle configuration is the only one requiring a low-temperature hot utility, although it has the lowest efficiency to methane. For gasifier operation at 700° C, gas recycle proves to be important, but only at gasifier pressures lower than 20 bar. Also, in the case of the recycle and the combined configurations, CO_2 has a high partial pressure, which is suitable for post-combustion removal. The obtained overall efficiencies to methane in this study are in line with other studies on process efficiencies to syngas [pyrolysis oil reforming (50-60%) [28] and pressurized steam/O_2 blown gasification (58-70%) [29]] or to SNG [steam gasification (67-70%) [30, 31]. However, because of the different model assumptions and efficiency definitions, these efficiencies toward product gases slightly differ.

None of the three studied configurations can operate without extra heat added to the system, unless a CO_2 separation unit with low-energy requirements can be employed (≤ 2 MJ/kg CO_2) in the cases where low-temperature hot utility is required: (1) for the case of the recycle configuration at 700°C (for P=20-35 bar)

and the combined configuration at 700°C (for P=10-35 bar) the energy requirement has to drop from 4 to 2 MJ/kg CO_2 and (2) for the case of the methanation configuration at 700°C (for P=20-35 bar) and the recycle configuration at 700°C (for P=10-15 bar) and at 800°C (for P=10-35 bar) an alternative (low-energy demand) CO_2 removal technology has to be used with energy requirements < 1 MJ/kg CO_2. Membrane utilization could be a promising alternative for these cases. Table 2.2 presents a summary of results for the three above-mentioned configurations. Q/HHV is the total relative amount of heat that has to be exchanged in the process and represents a relative measure of system complexity. Therefore, the higher the Q/HHV, the more complex the HEN will be when the three configurations are compared. W/HHV is the total relative amount of electricity that has to be provided to the system. On this basis, the three configurations are compared. Table 2.2 shows that increasing gasifier pressure and decreasing gasifier temperature lead to less complex HENs and to generally less electricity demand. For high-pressure gasifier operation (35 bar), the combined is the configuration that needs the lowest electricity input and has the least complex HEN at 800°C operation. At 700°C, it does not differ

Table 2.2. Summary of results for the three studied configurations.

	Methanation				**Recycle**				**Combined**			
Gasifier Temperature (°C)	700		800		700		800		700		800	
System requirements	Q/ HHV	W/ HHV	Q/ HHV	W/ HHV	Q/ HHV	W/ HHV	Q/ HHV	W/ HHV	Q/ HHV	W/ HHV	Q/ HHV	W/ HHV
Gasifier Pressure (bar)												
1	0.87	0.13	0.95	0.13	-	-	-	-	-	-	-	-
5	0.76	0.08	0.93	0.09	-	-	-	-	-	-	-	-
10	0.71	0.07	0.87	0.08	0.78	0.12	1.18	0.17	0.67	0.09	0.83	0.10
15	0.67	0.06	0.83	0.07	0.72	0.11	1.03	0.14	0.68	0.07	0.75	0.08
20	0.67	0.06	0.78	0.06	0.68	0.11	0.91	0.12	0.69	0.06	0.74	0.06
25	0.67	0.05	0.75	0.06	0.68	0.10	0.85	0.12	0.69	0.05	0.73	0.05
30	0.67	0.05	0.74	0.05	0.67	0.10	0.83	0.11	0.69	0.04	0.72	0.04
35	0.67	0.05	0.73	0.05	0.66	0.09	0.80	0.11	0.69	0.03	0.71	0.03

much in complexity than the other two configurations.

2.5. Conclusions

The main conclusions of this work can be summarized as follows:

- Overall efficiencies to methane obtained were in the range of 48-66%.
- The combined process configuration gives the highest overall efficiencies to methane (55-66%), the methanation configuration gives lower efficiencies to methane (49-63%) and the recycle configuration gives the lowest overall efficiencies to methane (48-58%)
- For self-gasification (35 bar), the combined configuration has the lowest electricity consumption and a low heat exchanger network complexity
- For gasifier operation at 800°C, the recycle configuration is the only one requiring low-temperature hot utility, although it has the lowest efficiency to methane. Recycling proves to be important only at a gasifier temperature of 700°C and for operation pressures lower than 20 bar
- None of the three studied configurations can operate without extra heat added to the system, unless a CO_2 separation unit with low-energy requirements can be employed (≤ 2 MJ/kg CO_2) in the cases where low-temperature hot utility is required.

Notation

HHV	=	Higher Heating Value, MJ/kg dry biomass feed. For CH_4 and H_2: MJ/kg
MW	=	molecular weight, kg/kmol
P	=	pressure, bar
Q	=	heat, MJ/kg dry feed
R	=	recycle split; defined as the percentage of the stream that is being recycled to the gasifier
S/C	=	steam over carbon molar ratio; defined as the total moles of steam fed to the gasifier, including the moisture content of the biomass feed, divided by the moles of carbon present in the biomass
T	=	temperature, °C
W	=	work, MJ/kg dry feed

Greek symbols

ΔP	=	pressure difference/drop, bar
ΔT	=	temperature difference, °C
η	=	efficiency
Φ_m	=	mass flow, kg/h

Abbreviations

ASU	=	Air Separation Unit
C	=	Compressor
H	=	High-temperature hot utility
HEN	=	Heat Exchanger Network
L	=	Low-temperature hot utility
MEA	=	Monoethanolamine
PFD	=	Process Flow Diagram
S	=	Separator
SNG	=	Substitute/Synthetic Natural Gas

Literature cited

1. van der Drift A., Rabou L.P.L.M., Boerrigter H., Heat from biomass via synthetic natural gas, Proceedings of the 14th European Biomass Conference & Exhibition, Paris, France, Oct 17-21, **2005**.

2. Duret A., Friedli C., Maréchal F., Process design of synthetic natural gas production (SNG) using wood gasification, *J. Cleaner Prod.* **2005**, 13, 1434-1446.

3. Koh K.K., Integrated catalytic gasification process, US Patent 4094650, June 13, **1978**.

4. Marshall H.A., Smits F.C.R.M., Exxon catalytic coal gasification process and large pilot plant development program, Proceedings of the 9th Annual International Conference on Coal Gasification, Liquefaction and Conversion to Electricity, Pittsburgh, PA, Aug 3-5, **1982**, 357-377.

5. van der Drift A., Boerrigter H., Coda B., Cieplik M.K., Hemmes K., Entrained flow gasification of biomass: Ash behaviour, feeding issues, and

system analyses, ECN report ECN-C--04-039, April **2004**.

6. van der Meijden C.M., Veringa H.J., Vreugdenhil B.J., van der Drift B., Bioenergy II: Scale-up of the MILENA biomass gasification process, *Int. J. Chem. Reactor Eng.* **2009**, 7, A53.

7. Higman C., van der Burgt M., *Gasification*; Gulf Professional Publishing, Houston, TX, **2003**.

8. Hamrick J.T., Method of feeding solid particles from a zone of low pressure to a zone of high pressure, US Patent 5,706,742, January 13, **1998**.

9. van Rossum G., Matas Güell B., Balegedde Ramachandran R.P., Seshan K., Lefferts L., van Swaaij W.P.M., Kersten S.R.A., Evaporation of pyrolysis oil: Product distribution and residue char analysis, *AlChE J.* **2010**, 56, 2200-2210.

10. Phyllis Database for biomass and waste. www.ecn.nl/phyllis/. Energy Research Centre of The Netherlands.

11. Pröll T., Siefert I.G., Friedl A., Hofbauer H., Removal of NH_3 from biomass gasification producer gas by water condensing in an organic solvent scrubber, *Ind. Eng. Chem. Res.* **2005**, 44, 1576-1584.

12. Albertazzi S., Basile F., Brandin J., Einvall J., Hulteberg C., Fornasari G., Rosetti V., Sanati M., Trifirò F., Vaccari A., The technical feasibility of biomass gasification for hydrogen production, *Catal. Today* **2005**, 106, 297-300.

13. Ensell R.L., Stroud H.J.F., The British Gas HICOM methanation process for SNG production, Proceedings of the International Gas Research Conference, British Gas Corporation UK, **1983**, 472-481.

14. Höhlein B., Menzer R., Range J., High temperature methanation in the long-distance nuclear energy transport system, *Appl. Catal.* **1981**, 1, 125-139.

15. White G.A., Roszkowski T.R., Stanbridge D.W., The RMProcess, *Adv. Chem. Ser.* **1975**, 146, 138-148.

16. Song Ho-Jun, Lee S., Park K., Lee J., Spah D.C., Park Jin-Won, Filburn T.P., Simplified estimation of regeneration energy of 30 wt.% sodium glycinate solution for carbon dioxide absorption, *Ind. Eng. Chem. Res.* **2008**, 47, 9925–9930.

17. Curran G.P., Rice C.H., Gorin E., Carbon dioxide Acceptor gasification process, Division of Fuel Chemistry, ACS, Philadelphia, Pa., Apr 5-10, **1964**.

18. Barron R.F., *Cryogenic systems*; New York, McGraw-Hill, **1966**.

19. Douglas J.M., *Conceptual design of chemical processes*; McGraw-Hill, **1988**.

20. Seemann M.C., Schildhauer T.J., Biollaz S.M., Fluidized bed methanation of wood-derived producer gas for the production of synthetic natural gas, *Ind. Eng. Chem. Res.* **2010**, 49, 7034-7038.

21. Zwart R.W.R., Boerrigter H., Deurwaarder E.P., van der Meijden C.M., Paasen C.V.B., Production of synthetic natural gas (SNG) from biomass: Development and operation of an integrated bio-SNG system, Technical report, ECN report, ECN-E-06-018, **2006**.

22. PGP, Practical experience gained during the first twenty years of operation of the Great Plains gasification plant and implications for future projects, Technical report, Dakota Gasification Company prepared for U.S. Department of Energy (DoE) – Office of Fossil Energy, **2006**.

23. Singh P., Brilman D.W.F., Groeneveld M.J., Solubility of CO_2 in aqueous solution of newly developed absorbents, *Energy Procedia* **2009**, 1, 1257-1264.

24. Majchrowicz M.E., Brilman D.W.F., Groeneveld M.J., Precipitation regime for selected amino acid salts for CO_2 capture from flue gases, *Energy*

Procedia **2009**, 1, 979-984.

25. van Holst J., Versteeg G.F., Brilman D.W.F., Hogendoorn J.A., Kinetic study of CO_2 with various amino acid salts in aqueous solution, *Chem. Eng. Sci.* **2009**, 64, 59-68.

26. Veneman R., Li Z.S., Hoogendoorn J.A., Kersten S.R.A., Brilman D.W.F., Continuous CO_2 capture in a circulating fluidized bed using supported amine sorbents, *Chem. Eng. J.* **2012**, 207-208, 18-26.

27. Wolf M.J., te Braake J.T.G, Huiskes C., Benes N.E., Nijmeijer A., Bouwmeester H.J.M., Gas separation using hybrid inorganic-organic silica membranes, Book of abstracts, ICOM, Amsterdam, Jul 23-29, **2011**.

28. van Rossum G., Kersten S.R.A., van Swaaij W.P.M., Staged catalytic gasification/steam reforming of pyrolysis oil, *Ind. Eng. Chem. Res.* **2009**, 48, 5857-5866.

29. Hannula I., Kurkela E., A parametric modelling study for pressurized steam/O_2-blown fluidised-bed gasification of wood with catalytic reforming, *Biomass Bioenergy* **2012**, 38, 58-67.

30. van der Meijden C.M., Veringa H.J., Rabou L.P.L.M., The production of synthetic natural gas (SNG): A comparison of three wood gasification systems for energy balance and overall efficiency, *Biomass Bioenergy* **2010**, 34, 302-311.

31. Gassner M., Maréchal F., Thermo-economic process model for thermochemical production of synthetic natural gas (SNG) from lignocellulosic biomass, *Biomass Bioenergy* **2009**, 33, 1587-1604.

Appendix A

Detailed Modeling Results

This appendix includes detailed results of the three modeled configurations in section A.1, the sensitivity analysis of the recycle split for the combined configuration in section A.2, and the modeling of the cryogenic distillation unit in section A.3.

A.1. Detailed modeling results

Methanation configuration

Table A.1 shows detailed results for the methanation configuration at the two simulated gasifier temperatures. The decrease in compressor power consumption with pressure is mainly due to the lower pressure difference (ΔP) that the compressor has to provide in the system ($\Delta P = P_{methanation\ reactor} - P_{gasifier}$). At 35 bar, the compressor power consumption is set to zero, because in this case both gasifier and methanation reactor operate at 35 bar.

The final product, consists mainly of CH_4, but also contains 2-6 mol% H_2. The existence of H_2 in the final product is the result of the water-gas shift equilibrium that also takes place in the methanation reactor, producing CO_2 and H_2. The steam added to the methanation reactor prevents (solid) carbon formation and completely converts CO present in the gas to H_2. The energy demand for pressurizing the solids is denoted in Table A.1 as W_{solids}. It increases with pressure, because the inert gas has to be pressurized to higher pressure levels. The existence, though, of this inert gas (N_2 or CO_2 from producer gas) in the gasifier effluent is not included in the current calculations. Its effect on system behavior would be reduction of efficiency to methane, because of higher energy requirements for compression and cooling/heating of larger process streams.

Table A.1. Detailed results of the **methanation** configuration at **(A)** 700°C and **(B)** 800°C. Values for W and Q are expressed in MJ/kg dry biomass.

A

P gasifier **(bar)**	**W** compressor	**Q** hot utility	**T** hot utility **H(igh)/ L(ow)**	**W** pumps	**W** solid	**Q** gasifier	**Final product composition (mole fractions)**		η_{CH4} **(%)**
							CH_4	**H_2**	
1	2.09	4.35	H	0	0.62	2.32	0.97	0.03	50.4
5	0.93	3.00	H	2×10^{-3}	0.80	1.15	0.96	0.04	57.0
10	0.51	2.69	H	5×10^{-3}	0.89	0.39	0.96	0.04	59.4
15	0.31	2.28	H	7×10^{-3}	0.94	-0.02	0.95	0.05	61.0
20	0.19	2.07	L	9×10^{-3}	0.98	-0.29	0.95	0.05	62.0
25	0.11	2.07	L	1×10^{-2}	1.00	-0.48	0.94	0.06	62.3
30	0.05	2.07	L	1×10^{-2}	1.03	-0.62	0.94	0.06	62.5
35	0.00	2.07	L	1×10^{-2}	1.05	-0.74	0.94	0.06	62.7

B

P gasifier (bar)	W compressor	Q hot utility	T hot utility H(igh)/ L(ow)	W pumps	W solid	Q gasifier	Final product composition (mole fractions)		η_{CH4} (%)
							CH_4	H_2	
1	2.14	5.38	H	0	0.62	2.80	0.98	0.02	48.8
5	1.13	4.97	H	2×10^{-3}	0.80	2.56	0.97	0.03	52.8
10	0.68	4.14	H	4×10^{-3}	0.89	2.12	0.97	0.03	55.9
15	0.43	3.52	H	6×10^{-3}	0.94	1.74	0.97	0.03	58.0
20	0.27	2.69	H	9×10^{-3}	0.98	1.42	0.97	0.03	60.2
25	0.15	2.28	H	1×10^{-2}	1.00	1.17	0.97	0.03	61.6
30	0.07	2.28	H	1×10^{-2}	1.03	0.97	0.97	0.03	61.9
35	0.00	2.28	H	1×10^{-2}	1.05	0.79	0.97	0.03	62.2

Also, dilution of the final gas product and need for larger downstream units would as well have a negative impact on overall process performance.

Recycle configuration

Table A.2 presents the detailed results for the recycle configuration at the two simulated gasifier temperatures. Increasing gasifier pressure and/or decreasing gasifier temperature causes a slight increase in efficiency as the recycle stream, containing CO and H_2 (potential CH_4) as well as some CH_4 (11-20%), becomes smaller. Therefore, the power consumption of the cryogenic unit decreases. As an example, at 700°C and 10 bar gasifier pressure, the recycle stream is 88 wt.% of the biomass feed stream. At 35 bar, the recycle stream decreases to 47 wt.% of the biomass feed stream, indicating also the economy of size of equipment at higher pressures, although more expensive materials would be needed.

The power needed for feeding the solid biomass (W_{solid}) is constant since the recycle stream is assumed to be used for pressurizing the wood in the lock-hoppers. The energy required (0.62 MJ/kg dry biomass) is only the energy needed for milling the wood as discussed in section 2.2.2 (Chapter 2).

The final product in this case is pure methane. This is because it is one of the products of a separation step (cryogenic unit S_3), giving high purity CH_4.

Table A.2B also includes the energy demand for steam production and superheating (Q_{steam}) because at 800°C operation, the steam/carbon ratio (mol/mol) had to be increased from the standard operation of 1.50 to 1.57 (at 35 bar) until 1.75 (at 10 bar) to prevent (solid) carbon formation in the gasifier. The steam/carbon ratio needed reduces with increasing pressure, which is also reflected

in the values of Q_{steam}, because the recycle becomes smaller with increasing gasifier pressure.

The energy production of the gasifier ($Q_{gasifier}$) remains constant throughout the simulated pressure range for both gasifier temperatures, because the absolute amount of methane in the gasifier effluent is constant. At lower gasifier

Table A.2. Detailed results of the **recycle** configuration at **(A)** 700°C and **(B)** 800°C. Values for W and Q are expressed in MJ/kg dry biomass.

A

P gasifier **(bar)**	**W** compressor-turbine	**W** recycle	**Q** hot utility	**T** hot utility **H(igh)/ L(ow)**	**W** pumps	**W** solid	**Q** gasifier	**W_{S3}**	**Final product composition (mole fractions)**		**η_{CH4} (%)**
									CH_4	**H_2**	
10	0.36	0.03	3.11	L	3×10^{-3}	0.62	-2.28	1.54	1.00	0.00	52.8
15	0.22	0.02	2.28	L	5×10^{-3}	0.62	-2.28	1.49	1.00	0.00	55.0
20	0.14	0.01	1.76	L	7×10^{-3}	0.62	-2.28	1.47	1.00	0.00	56.4
25	0.08	0.01	1.76	L	9×10^{-3}	0.62	-2.28	1.42	1.00	0.00	56.9
30	0.04	0.01	1.66	L	1×10^{-2}	0.62	-2.28	1.39	1.00	0.00	57.5
35	0.00	0.01	1.66	L	1×10^{-2}	0.62	-2.28	1.32	1.00	0.00	58.1

B

P gasifier **(bar)**	**W** compressor-turbine	**W** recycle	**Q** hot utility	**T** hot utility **H(igh)/ L(ow)**	**W** pumps	**W** solid	**Q** gasifier	**Q** steam	**W_{S3}**	**Final product composition (mole fractions)**		**η_{CH4} (%)**
										CH_4	**H_2**	
10	0.79	0.12	4.14	L	4×10^{-3}	0.62	-2.05	5.18	1.96	1.00	0.00	47.6
15	0.41	0.05	3.73	L	6×10^{-3}	0.62	-2.05	4.93	1.72	1.00	0.00	50.7
20	0.23	0.03	2.69	L	8×10^{-3}	0.62	-2.05	4.77	1.66	1.00	0.00	53.4
25	0.13	0.02	2.28	L	9×10^{-3}	0.62	-2.05	4.69	1.63	1.00	0.00	54.7
30	0.05	0.02	2.28	L	1×10^{-2}	0.62	-2.05	4.68	1.59	1.00	0.00	55.3
35	0.00	0.01	2.07	L	1×10^{-2}	0.62	-2.05	4.60	1.54	1.00	0.00	56.2

pressures, though, the amounts of CO and H_2 are higher. Therefore, the heat loads of the streams are higher, which is reflected in the increased demand in hot utility. This would also mean utilization of larger equipment.

Combined configuration

Table A.3 presents the detailed results for the combined configuration at the two simulated gasifier temperatures. At a gasifier operating temperature of 700°C, the gasifier produces heat throughout the whole studied pressure range. Therefore, the steam and the recycle stream can be fed to the gasifier at a temperature of at least 50°C lower, also to fulfill the set minimum temperature difference (ΔT_{min}). In fact, both streams can have a temperature as low as 410°C at 35 bar entering the 700°C-gasifier. Operation of the gasifier at 800°C shows that it requires heat for all simulated gasifier pressures.

Table A.3A also includes the energy consumption for steam production and superheating (Q_{steam}) as the steam/carbon ratio (mol/mol) used at 700°C for this configuration had to be higher than the standard used value of 1.5. The fed steam/carbon ratio was in the range of 1.55 (at 10 bar) and 1.65 (at 35 bar). It increases with gasifier pressure, which is also reflected in the increase of the Q_{steam} values as the H_2/dry gas ratio of the recycle stream reduces with increasing pressure causing a higher tendency for carbon deposition.

Table A.3. Detailed results of the **combined** configuration at **(A)** 700°C and **(B)** 800°C. Values for W and Q are expressed in MJ/kg dry biomass.

A

P gasifier **(bar)**	**W** compressor-turbine	**W** recycle	**Q** hot utility	**T** hot utility **H(igh)/ L(ow)**	**W** pumps	**W** solid	**Q** gasifier	**Q** steam	**Final product composition (mole fractions)**		η_{CH4} **(%)**
									CH_4	**H_2**	
10	1.21	0.02	1.76	L	4×10^{-3}	0.62	-0.24	4.29	0.97	0.03	58.6
15	0.81	0.01	1.86	L	6×10^{-3}	0.62	-0.57	4.44	0.97	0.03	60.7
20	0.53	0.01	1.97	L	8×10^{-3}	0.62	-0.78	4.50	0.97	0.03	62.2
25	0.32	0.01	1.97	L	1×10^{-2}	0.62	-0.94	4.50	0.96	0.04	63.6
30	0.15	0.00	1.97	L	1×10^{-2}	0.62	-1.04	4.56	0.96	0.04	64.7
35	0.00	0.00	1.86	L	1×10^{-2}	0.62	-1.14	4.56	0.96	0.04	65.9

B

P gasifier (bar)	W compressor-turbine	W recycle	Q hot utility	T hot utility H(igh)/ L(ow)	W pumps	W solid	Q gasifier	Final product composition (mole fractions)		η_{CH4} (%)
								CH_4	H_2	
10	1.41	0.02	3.11	H	3×10^{-3}	0.62	1.53	0.97	0.03	55.2
15	0.93	0.01	2.07	H	5×10^{-3}	0.62	1.06	0.97	0.03	59.6
20	0.60	0.01	2.07	H	7×10^{-3}	0.62	0.72	0.97	0.03	61.6
25	0.35	0.01	2.07	H	9×10^{-3}	0.62	0.47	0.97	0.03	63.1
30	0.16	0.01	2.07	H	1×10^{-2}	0.62	0.27	0.97	0.03	64.4
35	0.00	0.00	2.07	H	1×10^{-2}	0.62	0.11	0.97	0.03	65.5

A.2. Sensitivity analysis for the combined configuration

The split between the stream to be recycled and the stream to be led to the downstream methanation reactor was set at 50% for this study. Therefore, some simulations were done at 700°C (where the gasifier produces heat) with a recycle split ranging from 0 to 80% for a sensitivity analysis. This was done for the two extremes of gasifier pressure: 10 bar and 35 bar.

In Figure A.1 we can see that the efficiency to methane decreases with increasing recycle split for both pressures. Efficiency decreases because increasing recycle stream causes an increase in the hot utility demand (due to higher heat loads of the streams), increases the net power consumption of the compressor-turbine system and increases the energy penalty for compressing the recycle. At 35 bar, low-temperature hot utility is needed in the system, because the gasifier releases heat at all recycle splits. At 10 bar, though, also high-temperature hot utility is necessary at recycle splits between 0 and 45%. The rest of the recycle splits (50-80%) require low-temperature hot utility as increasing recycle split also causes the gasifier to produce heat since more methane is exothermically produced in the gasifier. On the other hand, a higher steam/carbon ratio has to be fed to the gasifier with increasing recycle split, to prevent thermodynamic (solid) carbon formation because of decreasing H_2/ dry gas ratio in the recycle stream. Also, larger recycle streams would need a larger gasifier, which has a negative impact on process economics. Moreover, increasing recycle streams cause the heat loads of the system to increase leading to more complex heat exchanger networks.

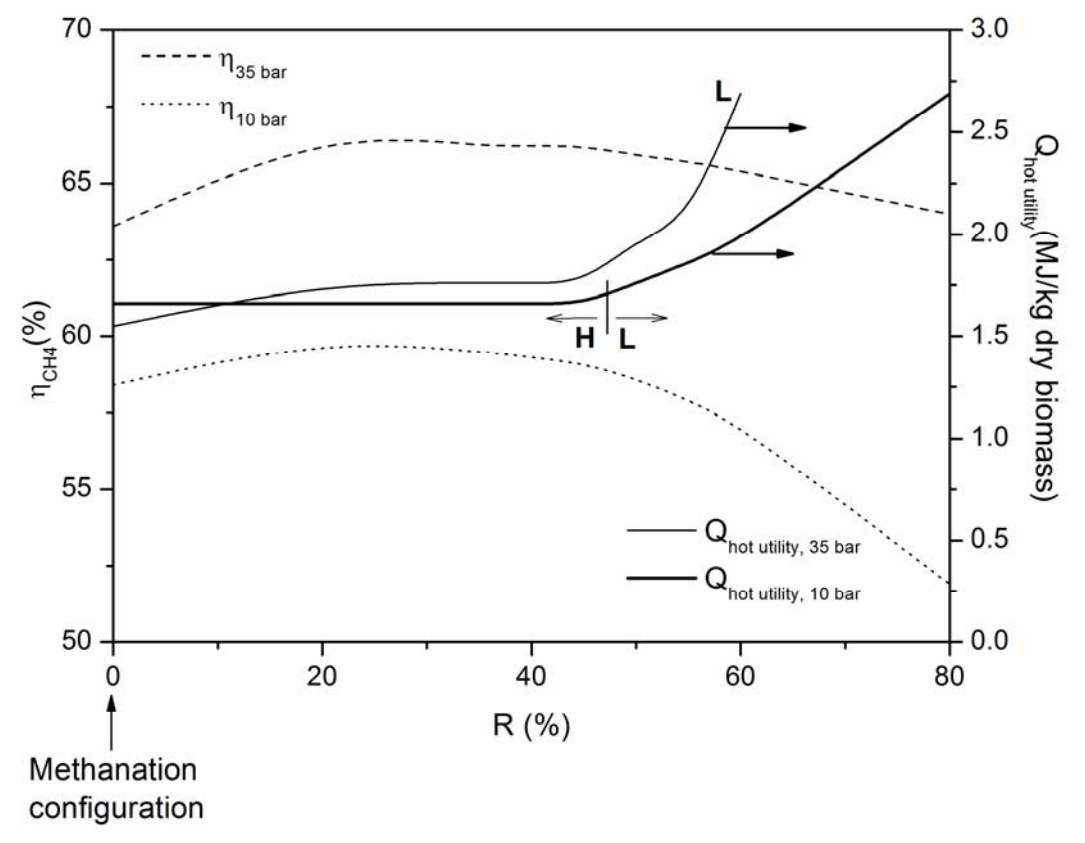

Figure A.1. Combined configuration. Effect of the recycle split on efficiency to methane (η_{CH4}) and hot utility demand ($Q_{hot\ utility}$) at 10 and 35 bar gasifier pressure. "H" stands for high-temperature hot utility and "L" stands for low-temperature hot utility.

Figure A.1 also shows the two extremes of the combined configuration: when the recycle split is 0%, then we actually obtain the methanation configuration (with the CO_2 separation unit after the methanation reactor). When the recycle split is 80%, then we get a configuration close to the recycle type. When the combined configuration approaches methanation operation (at 0% recycle split) the efficiency to methane at 35 bar is 63.6% with a surplus of gasifier energy of 0.73 MJ/kg. For a gasifier pressure of 10 bar (at 0% recycle split) the efficiency to methane is 58.4% with the energy demand of the gasifier giving a value of 0.40 MJ/kg (energy demand of 1.9% compared to the biomass input). These values deviate from the values obtained for the methanation configuration at these gasifier pressures (see Table A.2A). At 10 bar pressure of the methanation configuration at 700°C (Table A.2A), the efficiency to methane is 59.4%. This small deviation is caused by the higher value of hot utility (because of higher steam amount added to the first methanation reactor to avoid carbon deposition), which is to some extent compensated by the lower

power consumption of the compressor (because of smaller stream to be compressed). At 35 bar of the methanation configuration, the efficiency to methane is lower also caused by the higher value of hot utility needed (because of higher steam amount added to the first methanation reactor).
Approach towards methanation configuration gives higher efficiencies to methane especially at 20-40% recycle split, but the system also needs high-temperature hot utility. If the process approaches the recycle type of configuration there is a low-temperature hot utility demand, but more energy is needed for steam production and therefore the efficiency to methane decreases. Also, at 10 bar gasifier pressure, the 50% recycle split is the transition point from high-temperature hot utility to low-temperature hot utility. At 35 bar, the whole range of recycle splits need low-temperature hot utility. For all aforementioned reasons, a split of 50 wt.% seems to be the most favorable operation mode for this configuration.

A.3. Modeling of the cryogenic distillation unit

The PFD of the cryogenic unit is schematically presented in Figure A.2. The top product of the distillation column (stream no. 18, Figure A.2) was used to cool the gas stream to the distillation unit from 35°C to a temperature range of -126 to -77°C, depending on process flows and conditions. The refrigeration unit was employed to cool the gas stream entering the distillation unit (stream no. 16, Figure A.2) further to a temperature range of -147 to -138°C, which is the temperature of the top part of the distillation column.
Each temperature or pressure variation in the gasifier produces a different gas amount and gas composition that flows downstream to the cryogenic unit. Therefore, the temperature of the top part of the distillation column varies as well as the temperatures of other streams from the process itself. The flows in Figure A.2 are set depending on the heat exchange that the process streams can provide. The rest of the heat exchange has to be provided by the refrigeration utility. All heat exchangers are assumed to be of a single pass.
In practice, the actual power consumption of the cryogenic distillation unit is dependent on the power consumption of its condenser, which is powered by the refrigeration cycles and is therefore dependent on the reflux of the distillation column. By this configuration of cryogenic utility as given in Figure A.2, we can calculate the minimum power consumption of the cryogenic unit. This is equal to the sum of the energy demand of the compressors of the unit:

$$3W_{S_3} = 3\sum W_C = 3W_{C1} + 3W_{C2} + 3W_{C3} \qquad \text{(eq.A.1)}$$

where W is the work expressed in MJ/kg dry biomass feed. The number "3" preceding each work expression "W" derives from the assumption that electricity is produced with an efficiency of η = 1/3.

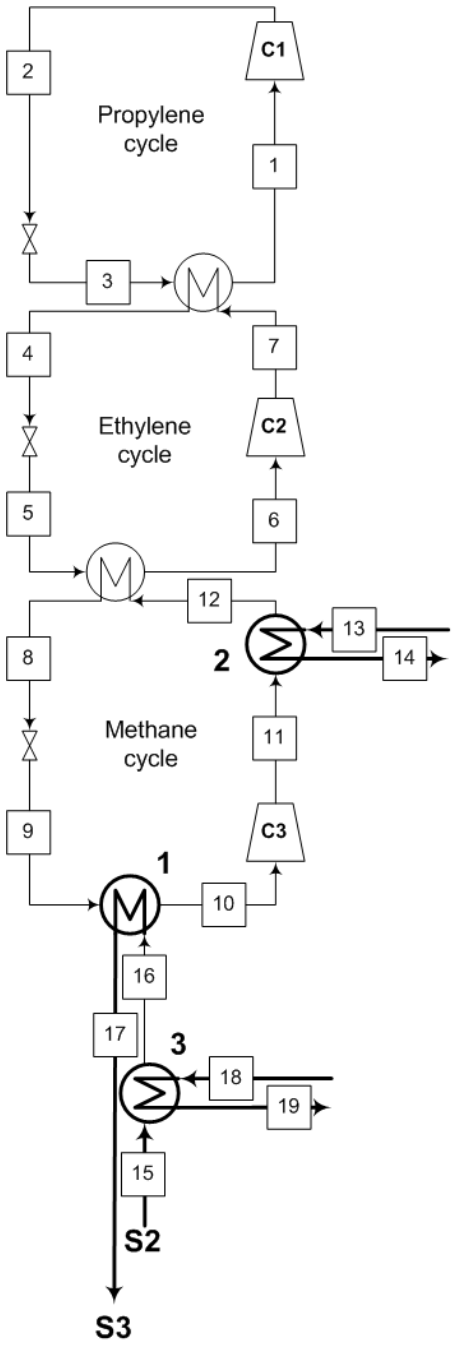

Propylene cycle		
Stream	T (°C)	P (bar)
1	15	1
2	25	17
3	-48	1

Ethylene cycle		
Stream	T (°C)	P (bar)
4	-37	17
5	-104	1
6	-85	1
7	25	17

Methane cycle		
Stream	T (°C)	P (bar)
8	-90	38
9	-162	1
10	-131 to -82	1
11	25	38
12	-80	38
13	-91	35
14	-15 to 15	35

Stream	T (°C)	P (bar)
15	35	35
16	-126 to -77	35
17	-147 to -138	35
18	-147 to -138	35
19	25	

Figure A.2. PFD of the refrigeration unit. C_1, C_2, and C_3 are the compressors of the unit. The numbered heat exchangers (1-3) correspond to the numbers in Figure 2.3 of Chapter 2. S_2 = CO_2 separation, S_3 = cryogenic distillation. Streams denoted in bold are process streams, the rest are cryogenic utility streams.

Chapter 3

Evaluation of Catalytic Effects during Biomass Pyrolysis and Gasification

The biomass to methane gasification (biomass self-gasification) concept was studied by performing several screening experiments with wood. After screening tests of different alkali metals, KOH was chosen as a model compound for biomass-derived ash for further experimentation. It improves char reactivity by more than an order of magnitude and thermogravimetric data interpreted by a first-order reaction model showed that it accelerates the pyrolysis reaction reducing the activation energy from E_a = 143 kJ/mol to E_a = 65 kJ/mol. Methane amounts higher than dictated by equilibrium are produced with and without impregnated KOH.

3.1. Introduction

In this chapter the new gasification concept of biomass to methane, which was introduced in Chapter 1, is investigated by screening experiments. The gasifier is envisaged to run on steam as oxidizing agent without addition of any O_2/ air. Alkali metal components contained in the biomass itself are used to catalyze gasification, methanation and tar cracking/reforming. Mostly, potassium hydroxide (KOH) was used in the tests as a model compound for biomass-derived ash. Pine wood was chosen as feed because it is an ash-lean biomass and therefore the effect of any added catalyst could be investigated more accurately. Coal research proved that potassium is a good gasification (and methanation) catalyst and biomass often contains substantial amounts of potassium.

This chapter entails the mapping of the operating window by screening of the activity of model ash components as well as their influence on the different stages of gasification (biomass pyrolysis and bio-char gasification).

3.2. Experimental Section

3.2.1. Materials

The tested feed material was ash-lean pinewood sawdust, purchased from Rettenmaier & Söhne GMBH, Germany. A type of wood with a very low ash content was chosen in order to investigate the activity of the catalysts more accurately and in a more controlled manner. Mainly, KOH was used as a model compound for biomass-derived ash. The KOH used was synthesis grade powder (Merck). K_2CO_3 (Sigma Aldrich), KCl (Merck) and NaOH (Fluka) were also tested as model components.

Also a Ru catalyst was tested because of its known good reforming/ methanation activity. The Ru catalyst used was 0.5 wt.% Ru on alumina (Ru/ Al_2O_3, Aldrich).

The catalyst-impregnated wood samples were prepared by adding the desired salt in aqueous solution to the wood and then by oven-drying the mixture at 105°C until all the moisture evaporated.

Char from wood was prepared by pyrolyzing the wood in a N_2 flow up to 800° C, with a reaction time of two hours. Similarly, the char from KOH-impregnated wood was prepared by pyrolysis of the KOH-impregnated wood up to 800°C in a N_2 flow, with a reaction time of two hours. The resulting potassium loading of the char was quantified by X-ray fluorescence spectrometry

(XRF). For this analysis, char together with lithium tetraborate ($Li_2B_4O_7$) was fused at 1100°C into a glass bead sample. This bead was then measured directly for its K content.

Elemental compositions (wood, KOH-wood for batch capillaries and char from wood) were analyzed with an EA 1108, Fisons Instruments. The rest of the wood/salt samples were analyzed with a Flash 2000, Thermo Scientific (column temperature for both analyzers: 900°C). The elemental compositions, water and ash contents of the various tested feeds are presented in Table 3.1. The determination of the carbon content of the char produced from KOH-impregnated wood suffered from a low reproducibility. This was probably due to the reaction and/or evaporation of the K salt during the analysis and possibly also due to the heterogeneity of the char.

The moisture content of each feed material was determined by drying at 105°C for 24h.

The ash content was determined by combustion of each sample in air at 550°C for 24 h, according to the procedure developed by Fernández Llorente and Carrasco García [1].

Ash seems to react and/or evaporate during pyrolysis and combustion as can be derived from the analyses given in Table 3.1. The ash contents of the impregnated wood samples are lower (3-20% deviation in ash balance) than the sum of the amount of impregnated salt and ash already contained in the wood itself. Also, the measured absolute ash content of the char presented is lower than the absolute ash content of the wood. Research by Keown et al. [2] sup-

Table 3.1. Elemental composition (C, H) of the tested materials on "dry, ash-free" basis[a].

	wood	**KOH - wood (batch capillaries)**	**KOH - wood (TGA)**	**K_2CO_3 - wood**	**KCl - wood**	**NaOH - wood**	**Char from wood at 800°C**
compound	**wt.%**	**wt.%**	**wt.%**	**wt.%**	**wt.%**	**wt.%**	**wt.%**
C	49.1	49.8	49.4	50.1	49.2	49.3	94.1
H	5.4	5.5	5.6	5.5	5.6	5.4	0.9
Difference (100-C-H)	45.5	44.7	45.0	44.3	45.2	45.3	5.0
Ash	0.4	12.8	9.5	10.6	12.3	6.2	0.8
Moisture	6.8	0.0	0.0	0.0	0.0	0.0	0.0

[a]The difference is mainly oxygen (O), with some traces of nitrogen (N) and sulphur (S). The ash and moisture contents are expressed on an "as received/prepared" basis.

ports this finding as they showed that during pyrolysis of sugar cane bagasse and cane trash up to 900°C at a heating rate of 10 K/min, alkali metal species volatilize. The maximum volatilization observed by them was about 20 wt.% for each of the initial species (Na, K, Mg, Ca) present in the biomass.

3.2.2. Experimental set-ups

In the present work, a TGA, a fixed bed steam gasification set-up and batch capillary micro-reactors were used.

The TGA equipment that was used was a Netzsch STA 449 F3 thermogravimetric analyzer. It was set at a sample heating rate of 5 K/min, in 20 ml/min N_2 flow and 40 ml/min N_2 protective gas. The weight decrease of the sample contained in an Al_2O_3 crucible was recorded and the end temperature of the samples was 800°C. The initial weight of the samples was determined with an external balance.

A schematic overview of the fixed bed set-up used for the char steam gasification experiments is given in Figure 3.1. This arrangement was a modification of the one used by Bleeker et al. [3]. The reactor consisted of a quartz glass tube with an inner diameter of 4 mm and was operated close to atmospheric pressure at a system pressure drop of $\Delta P \approx 0.5$ bar. The reactor was loaded with the char sample (~20 mg). A low steam fraction (0.2 bar) was led through the reactor which was achieved by using a N_2-water saturator. The N_2 gas flow was controlled by a digital mass flow controller (Brooks Instruments).

At the reactor exit, the gas was cooled to about 15°C to condense out the water, which was then separated in a gas-liquid (G-L) separator. A micro-GC (Varian CP-4900; 10m Molsieve 5A He, 10m PPQ He) was used for detecting H_2, O_2, N_2, CH_4, CO, CO_2, C_2H_4, C_2H_6, C_3H_6 and C_3H_8 every 3.3 min.

The char sample was heated to the desired temperature under a N_2 flow. Then the flow was switched to the by-bass (nr.9 in Figure 3.1) and to a N_2/steam flow. After obtaining a constant pressure, the N_2/steam mixture was switched to the reactor for the start of the experiment. At the end of an experiment, the set-up was flushed with N_2 to ensure evaporation of possibly remaining water in the tubes.

Carbon conversion of the char was determined from the amount of carbon initially present in the char sample and from the carbon content of the produced gases CO, CO_2, CH_4 and C_2-C_3. These were measured as a function of time by GC and by using the N_2 flow as an internal standard. In the case of char from

KOH-impregnated wood the initial carbon content was difficult to measure as explained in Section 3.2.1. Its carbon conversion was determined only by the measured carbon-containing gases. Because of the high reactivity of this specific char, the carbon to gas conversion was assumed to reach 100% when no more carbon-containing gases were measured and only grey-white ash remained at the end of the experiment. The steam conversion was at its very peak at about 72% for the catalyzed char and around 4% for the uncatalyzed char. This was calculated by the oxygen balance of the tests, assuming that the char is pure carbon. The steam conversion was high for the catalyzed char, be-

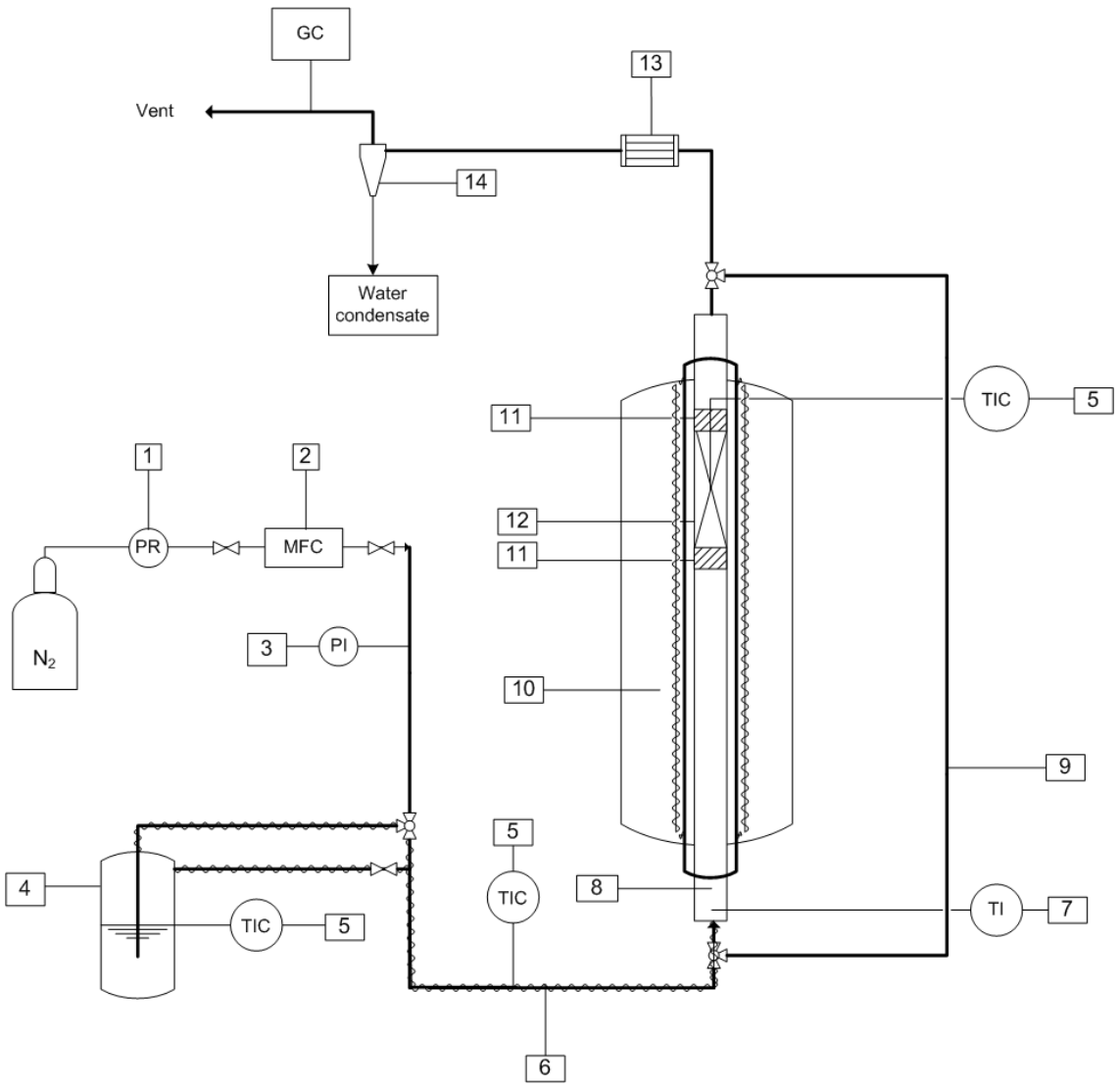

Figure 3.1. Char steam gasification set-up. 1.Pressure regulator (PR), 2.Mass flow controller (MFC), 3.Pressure indicator (PI), 4.N_2 saturator, 5.Temperature indicator/ controller (TIC), 6.Heating element/Tracing, 7.Temperature indicator (TI), 8.Quartz tube reactor, 9.By-pass, 10.Oven, 11.Quartz wool packing, 12.Char sample, 13.Condenser, 14.G-L separator.

cause of set-up limitations. The (initial) reaction rate is therefore underestimated because it is derived at a lower average steam pressure.
In the batch capillary micro-reactor technique the capillaries were filled with reactants, flushed with N_2 and then closed. The capillaries were then rapidly heated up in a fluidized bed and subsequently broken and their gas content was analyzed. Full details of this technique are described by Potic et al. [4] and Knežević et al. [5]. The capillaries used in the present work had an internal diameter of 2 mm.

3.3. Experimental results

This section, presents the results obtained from the three different types of experiments: TGA measurements (Section 3.3.1), Fixed bed-Preliminary char steam gasification experiments (Section 3.3.2) and Batch capillary micro-reactor tests (Section 3.3.3). First, the results obtained by thermogravimetric measurements demonstrate the effect of the model components on the pyrolysis reaction. The second section shows the effect of the catalyst on char reactivity in steam. The third experimental section presents the effect of catalysts on the overall gasification reaction, focusing on carbon to gas conversion and methane yield. These observed results are explained based on the output of the first two sections.

3.3.1. TGA measurements

TGA measurements were performed for wood, catalyst-impregnated wood and wood mixed with Ru/Al_2O_3. The results are shown in Figures 3.2 and 3.3, where the wood conversion rate is plotted against the temperature trajectory. The conversion rate for each sample is expressed on the same initial weight basis, excluding additives, which are assumed to remain unchanged during the measurement. All of the samples were dried before the measurement.
From Figure 3.2 it can be observed that the conversion rate for wood (plot A) starts to increase at about 200°C and it further increases until it reaches a maximum conversion rate at 353°C. After this peak, the conversion rate sharply decreases until a temperature of 373°C is reached. Further temperature increase results in a slower decreasing devolatilization rate until 500°C after which slow degassing of the char takes place up to 800°C. The increased conversion rate for KOH-impregnated wood (plot B) starts around 160°C, which is a lower temperature compared to that of wood. The peak in this case appears at a tem-

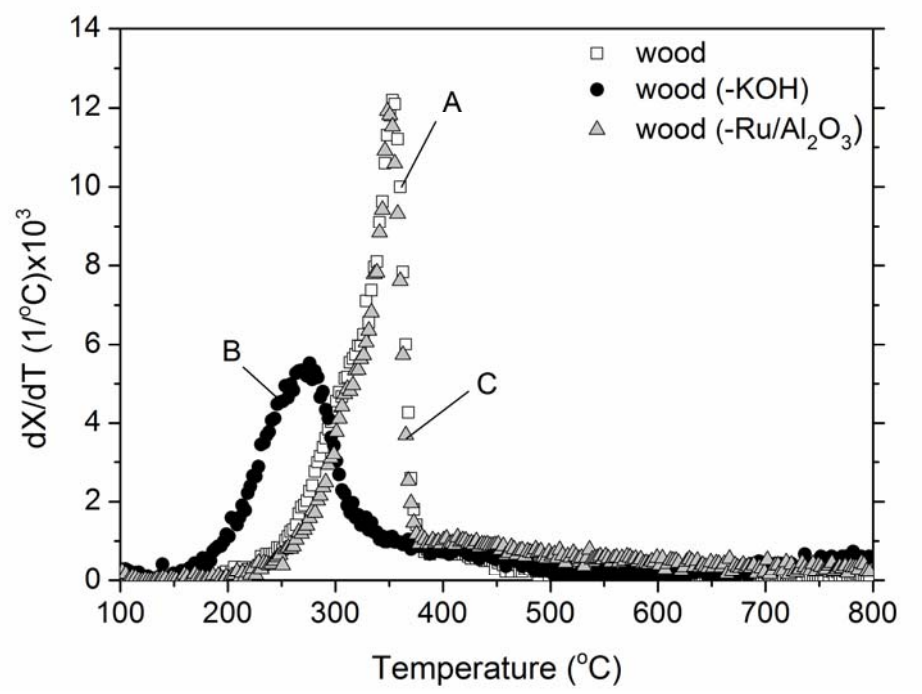

Figure 3.2. Conversion rate vs. temperature for **(A)** wood (Y_{char} = 13.5 wt.%), **(B)** KOH -impregnated wood (Y_{char} = 26.1 wt.%), K = 6.5 wt.% (KOH = 9.4 wt.%) and **(C)** wood mixed with Ru/Al_2O_3, Ru/Al_2O_3 = 59.8 wt.%. TGA settings: heating rate 5 K/min, gas flow N_2, protective gas N_2, sample cup Al_2O_3.

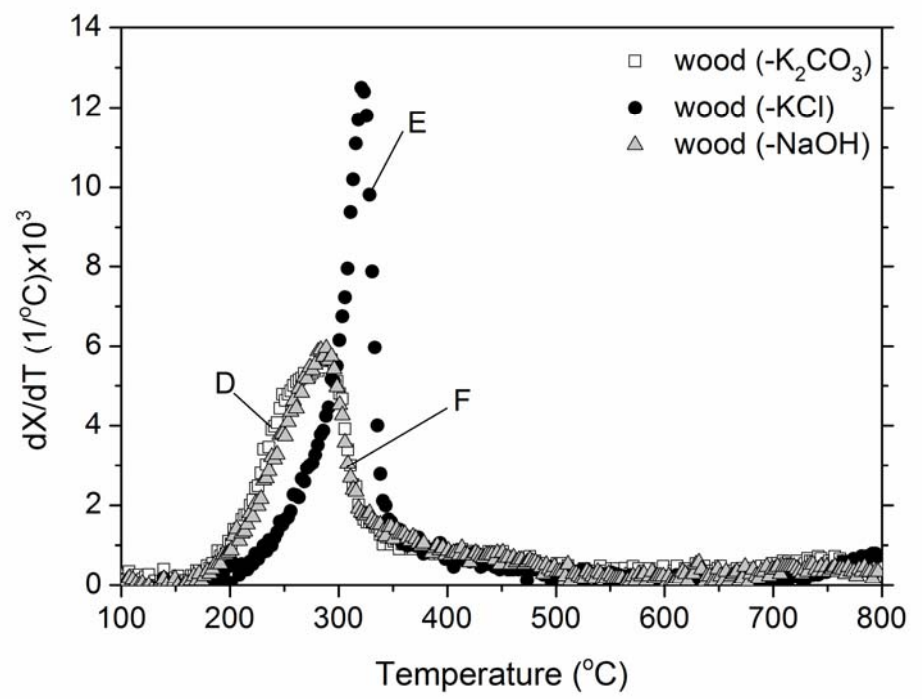

Figure 3.3. Conversion rate vs. temperature for **(D)** K_2CO_3-impregnated wood (Y_{char} = 12.2 wt.%), K = 6.3 wt.% (K_2CO_3 = 11.1 wt.%), **(E)** KCl-impregnated wood (Y_{char} = 13.8 wt.%), K = 7.2 wt.% (KCl = 13.7 wt.%) and **(F)** NaOH-impregnated wood (Y_{char} = 23.0 wt.%), Na = 4.3 wt.% (NaOH = 7.4 wt.%). TGA settings: heating rate 5 K/min, gas flow N_2, protective gas N_2, sample cup Al_2O_3.

perature of 275°C, after which the devolatilization rate gradually decreases until 500°C. This shows that impregnated KOH substantially lowers the pyrolysis temperature of wood, which is in agreement with results by other researchers [6-9]. On the other hand, wood mixed with Ru/Al_2O_3 (plot C) follows the same trend in conversion rate as wood only. This indicates that Ru/Al_2O_3 does not affect the pyrolysis reaction, which also follows from the fact that the areas defined by plots 3.2A and 3.2C are the same. This can be explained by the poor solid-solid contact for a Ru/Al_2O_3-wood system as compared to KOH-impregnated wood.

The areas defined by plots 3.2A and 3.2B are not equal, leading to a measured absolute difference in amount of produced char of 1.40 mg (KOH-free basis). X-ray powder diffraction (XRD) of a char made at 500°C from KOH-impregnated wood indicated the existence of $KHCO_3$ in the char. If the KOH would transform completely into $KHCO_3$ this would mean a weight increase of KOH by 79%. Correcting for this extreme, an absolute calculated difference in the char amount between 3.2A and 3.2B would be 1.21 mg. This reveals that while the impregnated KOH reacts during conversion of the wood to char, even the complete transformation of KOH to $KHCO_3$ cannot account for the measured difference in char weight between 3.2A and 3.2B. Therefore, also other transformations of KOH are probably taking place. The fact that KOH can partly transform into other forms of potassium compounds during pyrolysis (e.g. K, K_2O and K_2CO_3) is also put forward by Di Blasi et al. [6] and is experimentally investigated by Lillo-Ródenas et al. [10].

From our work, the KOH-impregnated wood gave Y_{char} = 26.1 wt.% (on a KOH-free basis) while only wood itself resulted in Y_{char} = 13.5 wt.%. The increase in char yield by KOH was also noted in pyrolysis experiments of KOH-impregnated wood done by Di Blasi et al. [6]. They observed for the impregnated case a char yield of about 32 wt.% (KOH-free basis), while without KOH the char yield was around 22 wt.%. Their tests were realized at a temperature of 527°C and a KOH loading of 7.7 wt.% on dry wood.

Apart from KOH, also K_2CO_3, KCl and NaOH were tested as model components in order to study the influence of the anion as well as the type of cation on wood pyrolysis. Figure 3.3 presents the results obtained for these model components. K_2CO_3- and NaOH-impregnated wood (plots D and F, respectively) show very similar behavior. As in the KOH case, devolatilization starts at about 160°C for both model components and is increasing with temperature,

exhibiting their peak weight loss at around 288°C. Devolatilization continues up to a temperature of 500°C. Conversion rate of KCl-impregnated wood (plot E) starts increasing at about 200°C and after its peak of maximum weight loss at a temperature of 321°C it drops sharply until 346°C. This plot is very similar to that of wood (Figure 3.2, plot A).

KCl was the salt with the least effect on wood pyrolysis temperature and did also not affect wood char yield (Y_{char} = 13.8 wt.%). The rest of the tested model components (KOH, K_2CO_3 and NaOH) all lowered pyrolysis temperature yielding a different product distribution (char and gas/vapor), which is in accordance with findings by Di Blasi et al. [11] on the pyrolysis of fir wood impregnated with these alkaline compounds. Our results showed that both K^+ and Na^+ cations, as well as OH^- and CO_3^{-2} anions, play an important role in the pyrolysis reaction. KOH was chosen as model component for further tests, because biomass can contain significant amounts of potassium, which was also proved to be a good gasification catalyst by coal research. Also, the hydroxide allows for an accurate carbon balance determination, since it is an alkaline compound that does not contain any carbon. NaOH influenced product distribution by increasing the char yield of wood (Y_{char} = 23.0 wt.%) as did KOH, demonstrating possible similar transformation during pyrolysis as observed with NaOH and KOH by Lillo-Ródenas et al. [10].

A first-order reaction model with an Arrhenius type of equation for temperature dependency was used to describe wood pyrolysis and to estimate the pre-exponential factor k_0 (s^{-1}) and the activation energy E_a (kJ/mol):

$$\frac{dX}{dT} = \frac{k_0}{\beta} e^{-E_a/RT}(1-X) \qquad \text{(eq.3.1)}$$

with

$$\beta = \frac{dT}{dt} \qquad \text{(eq.3.2)}$$

where β is the heating rate of the wood sample (K/min), R is the universal gas constant (J/mol K), T is the temperature (K) and X is the conversion of wood.

Table 3.2 presents the results obtained by the model for wood and for catalyst-impregnated/mixed wood.

It can be noted from Table 3.2 that impregnated KOH, K_2CO_3 and NaOH con-

Table 3.2. Estimated values for k_0 and E_a for wood and catalyst-impregnated/mixed wood, according to a first-order reaction model (data on wood pyrolysis by other researchers are included for comparison).

	E_a (kJ/mol)			**k_0 (s^{-1})**			**Temperature range (°C) for this work**
wood	143 [a]	141 [12]	150 [13]	$5.3x10^{9}$ [a]	$4.4x10^{9}$ [12]	$1.4x10^{10}$ [13]	200 - 500
wood + Ru/Al_2O_3	143 [a]			$5.3x10^{9}$ [a]			200 - 500
wood + KOH	65 [a]			$3.8x10^{3}$ [a]			150 - 500
wood + K_2CO_3	65 [a]			$3.4x10^{3}$ [a]			150 - 500
wood + NaOH	67 [a]			$4.6x10^{3}$ [a]			150 - 500
wood + KCl	113 [a]			$3.6x10^{7}$ [a]			200 - 500

[a] This work

siderably lower the activation energy of the wood decomposition reaction. KCl also lowers the activation energy of the reaction but to a lesser extent. The estimated k_0 and E_a values for wood are well in agreement with results for wood pyrolysis obtained by other researchers [12, 13].

3.3.2. Fixed bed-Preliminary char steam gasification experiments

While the reactivity of catalyzed (by alkali metals/potassium) and uncatalyzed char (derived from wood, coal or pyrolysis oil) in steam has been measured before by other researchers [14-22], here we concentrate on steam gasification of wood-derived chars containing impregnated or added alkaline compounds to the wood before it was pyrolyzed, in line with the envisaged operation of the self-gasification concept studied here.

Two char samples (with and without K(OH)) obtained by pyrolysis up to 800° C, were reacted at 750°C in a 0.2 bar steam environment. Figure 3.4 shows the carbon to gas conversion of the chars measured as a function of time. The form in which K exists in the char is unknown since KOH can react and evaporate during pyrolysis of wood as discussed previously (TGA results). Therefore, it is denoted as *K(OH)* and is expressed as elemental K content in the char determined by X-ray fluorescence spectrometry (XRF) (11 wt.% K). If no K would evaporate during pyrolysis of the wood, then it should have been 26 wt.% K. This was calculated from the KOH loading of the impregnated wood, assum-

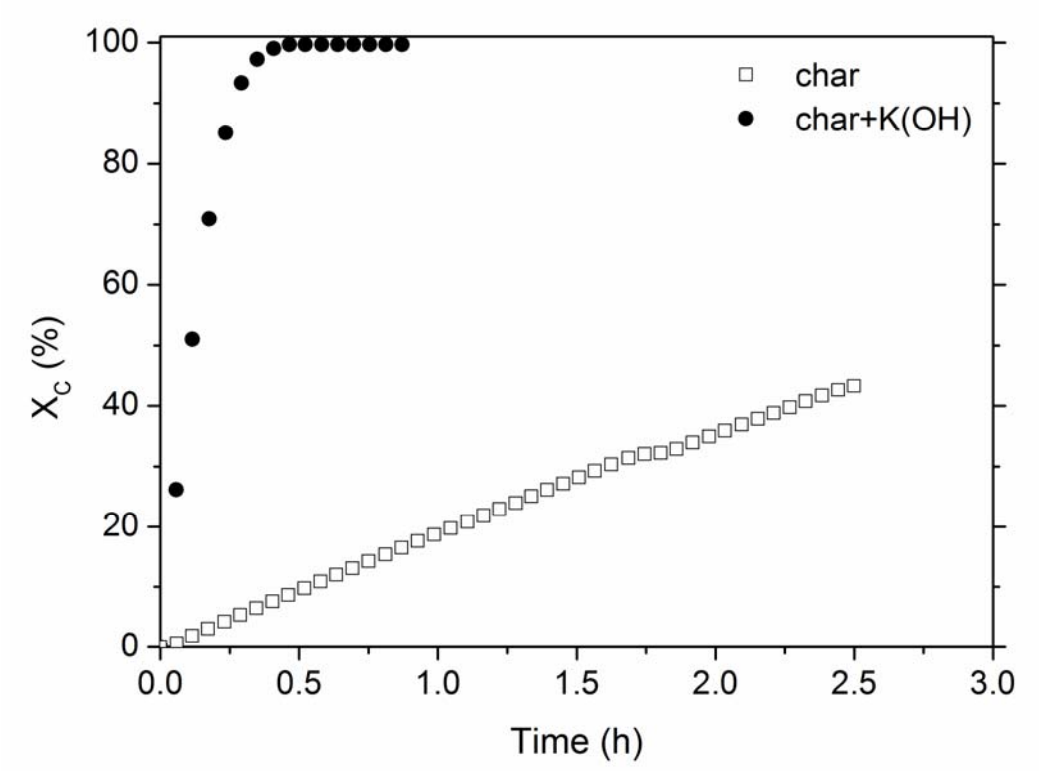

Figure 3.4. Carbon to gases conversion of a batch of char as a function of time. Results for char from wood and char from KOH-impregnated wood. Both chars were produced by pyrolysis up to 800°C and were reacted in a 0.2 bar steam environment, at 750°C. K = 11 wt.%.

ing that all of the elemental K present in the wood ends up in the char product after pyrolysis. It can be concluded that more than half of the K evaporated during pyrolysis. This is a point of consideration concerning gasifier operating temperature since this specific char was made at 800°C. A lower operating temperature would decrease the amount of evaporated potassium.

It is noted from Figure 3.4 that K(OH) drastically enhances the reactivity of wood char ($0.94x10^{-3}$ s^{-1}, at X=0-85%). The actual reactivity of this char would be even higher if a lower maximum steam conversion had been reached (maximum steam conversion was ~72% compared to wood char steam gasification of ~4%). Due to this high steam conversion for the K(OH)-char the actual conversion during the initial period took place at a lower average steam partial pressure. This specific char appears to be so reactive that, even at an average steam partial pressure <0.2 bar, the steam is able to completely convert the char by a factor ~17 faster than wood char reacted under more or less similar conditions ($0.055x10^{-3}$ s^{-1}, at X=0-20%) and at a steam partial pressure of 0.2 bar.

The char was made at 800°C and was reacted in steam at 750°C. Because of the higher temperature at which the char was produced it is somewhat less active compared to char produced at lower temperatures. This phenomenon is known as *aging* of the char [14].
During wood pyrolysis, impregnated KOH most possibly reacts and K evaporates indicating that KOH is actually not a catalyst in the process, but should rather be considered as an additive/reactant which transforms into a steady-state compound that works catalytically.

3.3.3. Batch capillary micro-reactor tests
Capillary micro-reactors were used for the steam gasification of wood, KOH-impregnated wood and wood mixed with Ru/Al_2O_3 catalyst. The steam pressure obtained in the capillaries was about 30 bar. Figures 3.5 and 3.6 express the total carbon to gas conversion and the methane yield and selectivity

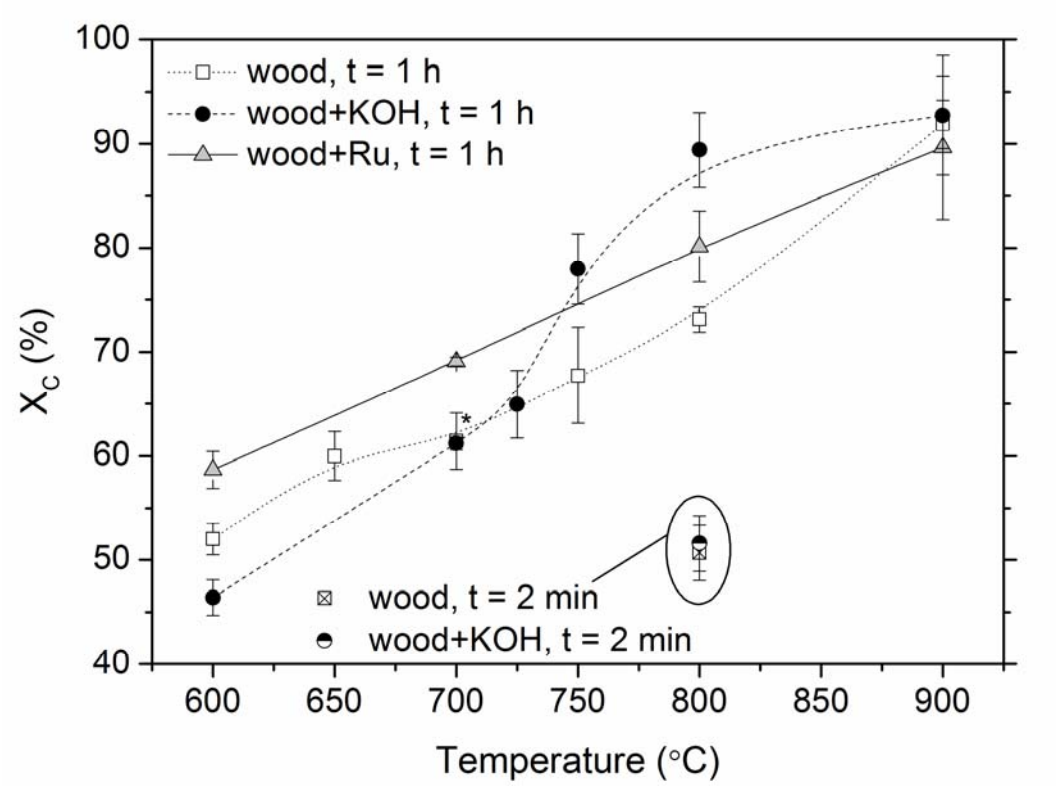

Figure 3.5. Effect of temperature on total carbon to gas conversion for three different samples in quartz capillary reactors: wood, KOH-impregnated wood and wood with Ru/Al_2O_3. P = 60 ± 5 bar, t = 2 min and 1 h, S/C (mol/mol) = 1.5 ± 0.2, K = 9.1 wt.% (KOH = 13.1 wt.%), Ru/Al_2O_3 = 71.1 ± 2.8 wt.%. Each data point represents the average of four samples. The lines are drawn for illustration purposes. *The data points for wood, t = 1 h and wood+KOH, t = 1 h coincide.

against temperature.

Figure 3.5 shows that carbon to gas conversion increases with temperature for all three samples. In the low temperature range up to 700°C (pyrolysis range), wood exhibits higher carbon to gas conversion compared to KOH-impregnated wood, which was also observed indirectly by the TGA measurements (in terms of the carbon residue). With increasing temperature beyond 700°C (gasification range) it is noted that KOH-impregnated wood gives higher carbon to gas conversion than wood. This difference is ascribed to the catalytic action of KOH on steam gasification of char (see also Figure 3.4 and accompanying discussion). This is in contrast to the TGA results (high char yield) but these tests did not include steam addition. For short reaction times (t = 2 min) at 800°C, KOH does not seem to have any measurable effect on the carbon to gas conversion. This result, combined with the information obtained from Figure 3.4 on char steam gasification, means that KOH acts on the conversion of the char to further gas formation with reaction time.

Our experimental data show the same trend with results obtained by Hallen et al. [23] who did tests on Douglas fir steam gasification with and without sodium carbonate at temperatures between 550-850°C and at atmospheric pressure. Their tests gave maximum conversion at 850°C with Na_2CO_3 (95% carbon to gas conversion). The largest difference they noted between catalyzed and uncatalyzed samples was at a temperature of 750°C (increase from 75% to 95% carbon to gas conversion), a result which we obtained for KOH with our quartz capillary technique at 800°C.

Addition of Ru/Al_2O_3 results in a higher carbon to gas conversion than wood only, throughout the whole temperature range tested, except at 900°C where thermal reactions dominate the result for all three samples. The increased conversion to gas at lower temperatures under the influence of Ru can be explained by the high reforming activity of the produced vapors to gases for which Ru is known.

Figure 3.6 shows results on the methane yield (A) and selectivity (B) in the quartz capillary experiments.

Figures 3.6A and 3.6B show one dotted line and one dashed line. The dotted line is the calculated equilibrium methane yield/selectivity for 100% carbon to gas conversion. The dashed line is the calculated equilibrium methane yield (Figure 3.6A) and equilibrium selectivity to methane (Figure 3.6B) based on the experimentally obtained carbon to gas conversion of the wood+Ru/Al_2O_3

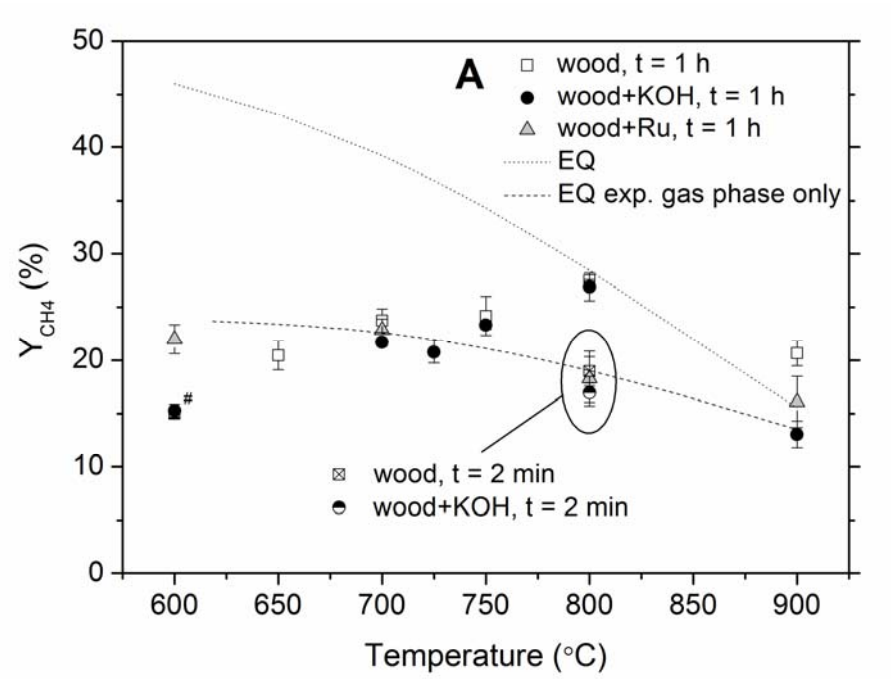

Figure 3.6. Effect of temperature on **(A)** methane yield and **(B)** selectivity to methane in the quartz capillary reactors for three different samples: wood, KOH-impregnated wood and wood with Ru/Al_2O_3. Two lines in each graph are presented as well, showing the calculated equilibrium selectivity to CH_4 for 100% carbon to gas conversion (⋯) and for the experimentally obtained carbon to gas conversion from the wood+Ru/Al_2O_3 samples (----). P = 60 ± 5 bar, t = 2 min and 1 h, S/C (mol/mol) = 1.5 ± 0.2, K = 9.1 wt.% (KOH = 13.1 wt.%), Ru/Al_2O_3 = 71.1 ± 2.8 wt.%. Each data point represents the average of four samples. #The data points for wood, t = 1 h and wood+KOH, t = 1 h coincide. *The data points for wood, t = 1 h and wood, t = 2 min coincide.

samples. The latter line is included in the figure, since under the tested temperature regime there is no complete carbon to gas conversion.

Wood only gives higher methane yields and selectivities than predicted by (gas-carbon-corrected) equilibrium for temperatures higher than 700°C as can be seen in Figure 3.6. On the other hand, the use of Ru/Al_2O_3 catalyst, which is known for its methanation activity [24, 25], causes methane to be driven back to equilibrium amounts. The methane yield of wood without using a catalyst increases with increasing temperature up to 800°C which is opposed to the expectation based on chemical equilibrium and is in all the cases higher than what thermodynamics dictates. Therefore, the formed methane is rather a primary pyrolysis product and/or a secondary product from vapor/gas cracking than being formed via methanation [26, 27].

Additionally, there is a difference between the measured methane yields and the ones indicated by equilibrium calculations, especially at low temperatures. This is because, although methane formation is favored thermodynamically at lower temperatures, in practice this does not happen since the carbon to gas conversion is limited, even with the addition of a catalyst and at long reaction times.

The methane yield (Figure 3.6A) increases with increasing temperature until it reaches an apparent maximum at 800°C and then decreases at 900°C. A similar maximum methane yield close to 800°C and higher than equilibrium was also demonstrated by Liinanki et al. [28] and van Rossum et al. [29] using different experimental techniques. Liinanki et al. performed tests with peat at temperatures between 700-1100°C and pressures in the range of 10-20 bar. They attribute the maximum in the methane yield curve to competition between the methane-producing and the non-methane-producing tar cracking reactions.

When examining the selectivity to methane (Figure 3.6B), though, KOH appears to have a negative effect on the relative amount of produced methane. Possibly it suppresses its formation or enhances its reforming at temperatures higher than 700°C. Although a 1h residence time is a practical value for the solids in large scale gasification, residence times of the produced gases lie in the range of a few seconds or even less. So, less catalytic reforming activity is expected in a large-scale gasifier, because of the reduced gas-solid contact time. On the other hand, the lower methane production could be the result of KOH changing the reaction mechanism that leads to methane.

Figure 3.7 presents the production of C_2-C_3 components as a function of the

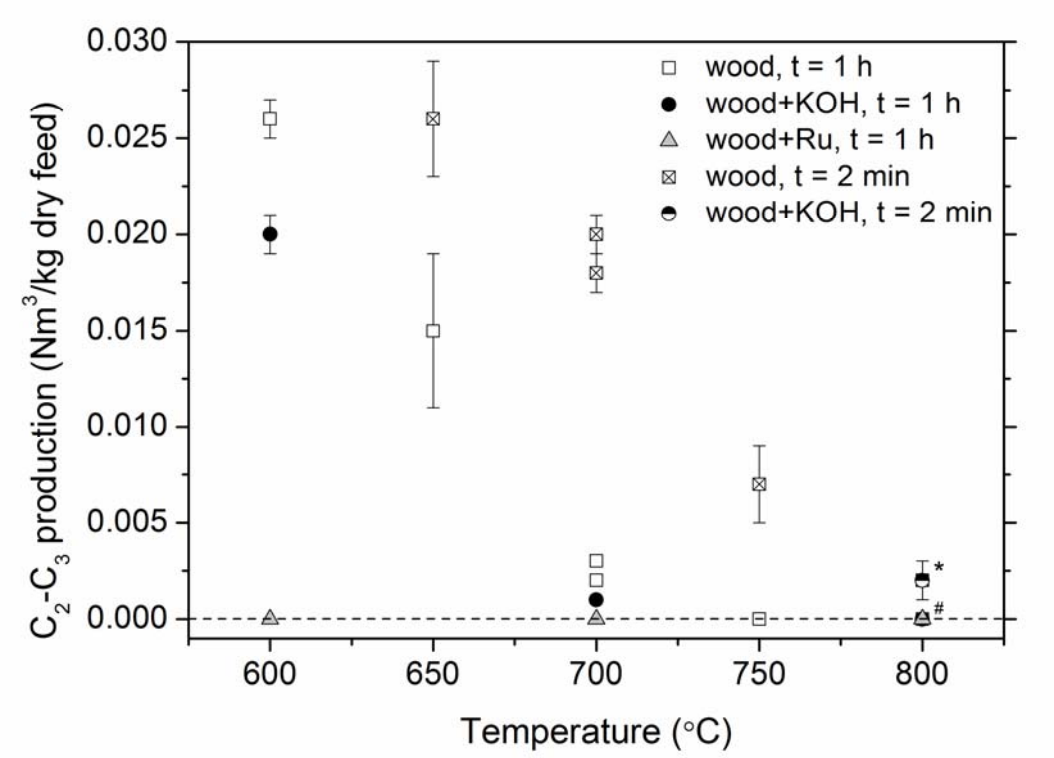

Figure 3.7. Effect of temperature, reaction time and use of catalyst on the production of total C_2-C_3 components for three samples: wood, KOH-impregnated wood and wood with Ru/Al_2O_3. P = 60 ± 5bar, t = 2 min and 1 h, S/C (mol/mol) = 1.5 ± 0.2, K = 9.1 wt.% (KOH = 13.1 wt.%), Ru/Al_2O_3 = 71.1 ± 2.8 wt.%. Each data point represents the average of four samples. *The data points for wood, t = 2 min and wood + KOH, t = 2 min coincide. # The data points for wood, t = 1 h, wood + KOH, t = 1 h and wood + Ru, t = 1 h coincide.

temperature, reaction time and use of catalyst for wood samples reacted with steam. Production of C_2-C_3 components in Figure 3.7 designates the total amount of produced C_2H_4, C_2H_6, C_3H_6 and C_3H_8 (80-100% of the C_2-C_3 components was C_2H_6). These components are considered as tar indicators for non-catalytic gasification [30]. The amount of these components reduces with increasing temperature and reaction time, which implies their conversion to CO, CO_2, H_2 and CH_4 and is an indication of the conversion of higher hydrocarbons to gases (and/or to heavy tars/soot).

Furthermore, the product gas of atmospheric biomass gasifiers operating around 850°C contains at least 0.02-0.04 Nm^3/kg dry biomass of C_2 components [31, 32]. This amount is about a factor 10 higher than the value experimentally obtained here for self-gasification at 800°C for the C_2-C_3 components (Figure 3.7). Wolfesberger et al. [33] attributed a similar lower C_2-C_3 produc-

tion observed in their pressurized experiments to higher gas residence times because of higher gasifying pressure.

Impregnated KOH seems to have minimal effect on C_2-C_3 conversion/ suppression at low temperatures (600°C). However, Ru/Al_2O_3 gives a product gas free of C_2-C_3 even at the lowest temperatures, catalyzing vapor cracking/ reforming reactions [34]. The non-existence of C_2-C_3 components is also predicted by equilibrium in this temperature range. At higher temperatures the presence of either catalyst does not have much of an effect any more when compared to wood only, at the same reaction time of 1 h. This indicates that thermal decomposition dominates the result at high temperatures. Although gas residence times are not that high in practice as discussed previously, the gaseous product should contain preferably a negligible amount of C_2-C_3 components at temperatures higher than 750°C. At lower temperatures a catalyst will be required like Ru/Al_2O_3.

3.4. Comparison to other biomass gasification technologies

Data were gathered and summarized from the literature on various conventional gasification technologies of solid biomass. However, there are not many complete and consistent sets of information available from a single literature source and therefore an extensive and complete comparison between the different gasifiers/gasification technologies is difficult. A simple overview of operating conditions and gas compositions of different technologies is given in Table 3.3. Experimental data on self-gasification obtained here (denoted in table as SG) are also included. These experimental results are the ones corresponding to Figure 3.5, for wood reacted at 700 and 800°C, respectively and for t = 1 h.

From Table 3.3 it can be noted that for high pressure steam gasification, an increase in gasifier pressure has an effect on the methane yield, which was also shown experimentally by Valin et al. [35]. Moreover, the gasifying agent has an influence on the produced methane as can be concluded from comparing the Renugas with the Värnamo technology. They both run on relatively high temperatures and at about the same pressure. The difference that can have a strong effect on the product distribution is the different oxidizing agent (air or air/steam). The Värnamo gasifier runs solely on air as oxidizing agent and the fact that it operates at higher gasification temperatures compared to the Renugas gasifier results in lower methane percentages in the product gas.

Table 3.3. Overview of operating conditions and gas compositions (dry and N_2-free) of different (solid) biomass gasification technologies.

Gasification Technology	Operating T (°C)	Operating P (bar)	Oxidizing Agent	D(irect)/ I(ndirect)	CH_4 (vol%)	CO (vol%)	H_2 (vol%)	CO_2 (vol%)	C_2 (vol%)	Ref.
BIVKIN	850	1	Air	D	8.3	29.4	24.6	34.0	3.0	[31]
MILENA	850	1	Steam/Air	I	15.4	41.3	24.3	13.1	5.5	[32]
RENUGAS	911	22	Steam/Air	D	16.8	15.9	28.0	38.4	0.0	[36]
SG	700	60	Steam		31.3	7.0	19.6	41.6	0.5	This work
SG	800	60	Steam		27.8	8.7	26.1	37.4	0.0	This work
VÄRNAMO	950-1000	20	Air	D	13.2	34.7	21.3	31.6	n.r.[a]	[37]
BATELLE	650-815	1	Steam/Air	I	15.6	44.4	22.0	12.2	5.8	[38]
GÜSSING	850-900	1	Steam/Air	I	11.0	24.0	40.0	22.0	3.0[b]	[39]
	800	10	Steam		9.0	9.0	52.0	30.0	n.r.[a]	[35]

[a] not reported

[b] includes C_3 components.

Self-gasification of biomass, as developed on lab scale until now, produces a gas containing higher amounts of methane compared to other biomass gasification technologies. The calorific value of the dry gas produced by self-gasification of biomass is around 15.7 MJ/Nm^3.

3.5. Mechanism

It is possible to summarize some of the results obtained in this present work with the help of Figure 3.8. It schematically represents the different stages biomass goes through during gasification and on which of these stages KOH or/ and Ru/Al_2O_3 have an effect on product distribution (denoted in Figure 3.8 within brackets).

The obtained results show that KOH is an active catalyst in pyrolysis and steam gasification of char, while its influence on gas phase reactions and especially methanation was found to be minor and this still has to be further investigated. These results indicate that biomass-derived ash containing K and Na can have a catalytic effect on these reactions especially in combination with a methanation catalyst.

In the two-step configuration for methane production from biomass which was discussed in the introductory part of this paper, biomass ash can promote carbon to gas conversion (especially at increased concentration via recycling)

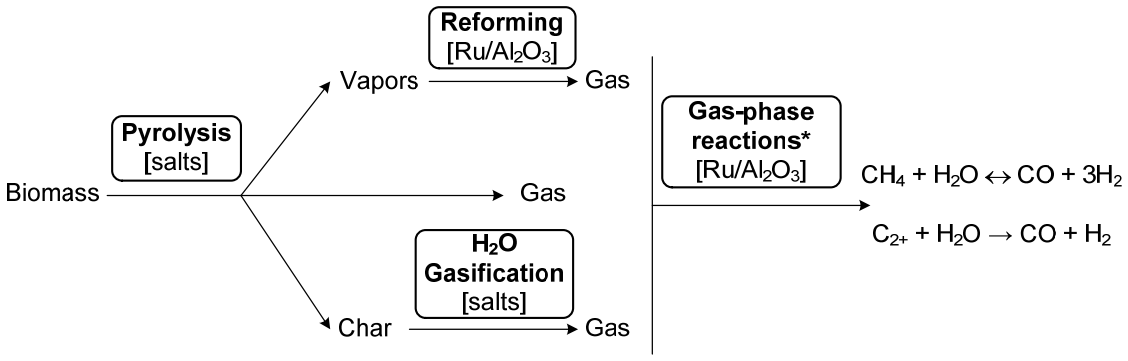

Figure 3.8. Schematic representation of the obtained results. Indication on which reactions K and Ru could act. *In the literature it has been shown that potassium-impregnated carbon is an active methanation catalyst [40]. We could not observe this from our experiments.

and produce methane in amounts higher than equilibrium. The amounts of tar present in the gaseous product are expected to be minimal.

In the case of the recycle and combined configuration, the presence of Ru or other methanation catalyst will play a crucial role in the methane production via the exothermic methanation reaction ($CO + 3H_2 \leftrightarrow CH_4 + H_2O$). This means possible autothermal operation of the gasifier without using oxygen/air. The catalytic ash build-up will provide the high carbon to gas conversion and the Ru catalyst will act on vapor/gas cracking, producing a clean, tar-free gas.

Ash is also known to crack vapors [41], something which we did not clearly observe in our experimental results with the model ash compound.

3.6. Conclusions

The concept of biomass self-gasification was studied by mapping of the operating window and investigating the effect of model ash on pyrolysis, char steam gasification and gas production. The main conclusions of this work can be summarized as follows:

- Solid-phase reactions, pyrolysis and char steam gasification, are both catalyzed by (a steady-state reaction product of) KOH
    - KOH and other salts tested accelerated the pyrolysis reaction in the decreasing order: $KOH \approx K_2CO_3 \approx NaOH > KCl$ (> Ru)
    - Char made from KOH-impregnated wood showed at least 17 times higher reactivity than char derived from wood only and could be completely gasified under continuous steam addition. In the batch ca-

pillary micro-reactors this was not observed probably because of limited supply of steam

- Gas-phase reactions are clearly catalyzed by Ru. There was no large effect observed by model ash (KOH) on the gas composition. A slight negative effect on the amount of methane produced could suggest that KOH has an effect on the reaction mechanism leading to methane. While it is stated in the literature that K-impregnated carbon is an active methanation catalyst, we could not demonstrate this activity based on these experiments
- Biomass self-gasification (as our envisaged process is termed) gives the highest amounts of methane compared to other solid biomass gasification technologies as far as literature data are available
- Non-catalytically formed methane was above equilibrium amounts. Therefore, in the two-step configuration for biomass self-gasification, methane can be obtained at amounts higher than equilibrium
- The presence of a methanation catalyst will be necessary in the recycle and the combined configurations for biomass self-gasification.

Notation

dX/dT	=	conversion rate; defined by: $\frac{dX}{dT} = \frac{dm}{m_0 dT}$ where dm is the sample mass change (mg) for a temperature change of dT and m_0 is the initial sample weight of the wood (mg).
E_a	=	Arrhenius activation energy, kJ/mol
HHV	=	Higher Heating Value, MJ/kg dry biomass feed.
k_0	=	Arrhenius pre-exponential factor, s^{-1}
P	=	pressure, bar
R	=	universal gas constant, 8.314 J/mol K
S_{CH4}	=	selectivity to methane; defined as: $S_{CH_4} = \frac{Y_{CH_4}}{X_C} \times 100\%$
t	=	reaction time, min or h
T	=	temperature, K
X	=	conversion of wood; expressed as:

$$X = 1 - \frac{m(T)}{m_0}$$

where m is the sample weight of wood (mg) and m_0 is the initial sample weight of the wood.

X_C = carbon to gas conversion; defined as the total amount of carbon evolved during gasification in the form of carbon-containing (permanent) gases divided by the initial amount of carbon present in the feedstock:

$$X_C = \frac{mol_C(t)}{mol_{C0}} \times 100\%$$

where mol_C is the cumulative moles of carbon evolved in the gaseous phase in time t and mol_{C0} is the initial moles of carbon present in the char or wood. The char samples for which mol_{C0} could not be defined, the mol_{C0} was assumed to be equal to the final mol_C since at the end of each experiment X_C was 100%, after reaction and visual observation.

Y_{CH4} = methane yield; defined as:

$$Y_{CH_4} = \frac{mol_{C_{CH_4}}}{mol_{C_{feed}}} \times 100\%$$

where $molc_{CH4}$ is the moles of carbon present in the gas product as methane and $molc_{feed}$ is the moles of carbon present in the feed.

Y_{char} = char yield; defined as:

$$Y_{char} = \frac{m_{char}}{m_{wood}} \times 100\%$$

where m_{char} is the char weight on an additive-free basis and m_{wood} is the weight of the initial wood sample on an additive-free basis.

Greek symbols

β = heating rate, K/min

ΔP = pressure difference, bar

Abbreviations

C_2-C_3 = total amount of C_2H_4, C_2H_6, C_3H_6 and C_3H_8 components

D	=	Direct
EA	=	Elemental Analyzer/Analysis
GC	=	Gas Chromatograph(y)
G-L	=	Gas-Liquid
I	=	Indirect
MFC	=	Mass Flow Controller
PI	=	Pressure Indicator
PR	=	Pressure Regulator
S/C	=	Steam over Carbon molar ratio; defined as the total moles of steam feed, including the moisture content of the biomass feed, divided by the moles of carbon present in the biomass.
SG	=	Self-Gasification
TGA	=	Thermogravimetric Analyzer/Analysis
TI	=	Temperature Indicator
TIC	=	Temperature Indicator/Controller
XRD	=	X-Ray powder Diffraction
XRF	=	X-Ray Fluorescence spectrometry

Literature cited

1. Fernández Llorente M.J., Carrasco García J.E., Concentration of elements in woody and herbaceous biomass as a function of the dry ashing temperature, *Fuel* **2006**, 85, 1273-1279.

2. Keown D.M., Favas G., Hayashi J.–ichiro, Li C.-Zhu, Volatilisation of alkali and alkaline earth metallic species during the pyrolysis of biomass: Differences between sugar cane bagasse and cane trash, *Bioresour. Technol.* **2005**, 96, 1570-1577.

3. Bleeker M.F., Veringa H.J., Kersten S.R.A., Deactivation of iron oxide used in the steam-iron process to produce hydrogen, *Appl. Catal., A* **2009**, 357, 5-17.

4. Potic B., Kersten S.R.A., Prins W., van Swaaij W.P.M., A high-throughput screening technique for conversion in hot compressed water, *Ind. Eng. Chem. Res.* **2004**, 43, 4580-4584.

5. Knežević D., Schmiedl D., Meier D., Kersten S.R.A., van Swaaij W.P.M., High-throughput screening technique for conversion in hot compressed water: Quantification and characterization of liquid and solid products, *Ind. Eng. Chem. Res.* **2007**, 46, 1810-1817.

6. Di Blasi C., Galgano A., Branca C., Effects of potassium hydroxide impregnation on wood pyrolysis, *Energy Fuels* **2009**, 23, 1045-1054.

7. Nowakowski D.J., Jones J.M., Uncatalysed and potassium-catalysed pyrolysis of the cell-wall constituents of biomass and their model compounds, *J. Anal. Appl. Pyrolysis* **2008**, 83, 12-25.

8. Fahmi R., Bridgwater A.V., Darvell L.I., Jones J.M., Yates N., Thain S., Donnison I.S., The effect of alkali metals on combustion and pyrolysis of *Lolium* and *Festuca* grasses, switchgrass and willow, *Fuel* **2007**, 86, 1560-1569.

9. Vamvuka D., Troulinos S., Kastanaki E., The effect of mineral matter on the physical and chemical activation of low rank coal and biomass materials, *Fuel* **2006**, 85, 1763-1771.

10. Lillo-Ródenas M.A., Cazorla-Amorós D., Linares-Solano A., Understanding chemical reactions between carbons and NaOH and KOH: An insight into the chemical activation mechanism, *Carbon* **2003**, 41, 267-275.

11. Di Blasi C., Galgano A., Branca C., Influences of the chemical state of alkaline compounds and the nature of alkali metal on wood pyrolysis, *Ind. Eng. Chem. Res.* **2009**, 48, 3359-3369.

12. Di Blasi C., Branca C., Kinetics of primary product formation from wood pyrolysis, *Ind. Eng. Chem. Res.* **2001**, 40, 5547-5556.

13. Wagenaar B.M., Prins W., van Swaaij W.P.M., Flash pyrolysis kinetics of pine wood, *Fuel Process. Technol.* **1993**, 36, 291-298.

14. van Rossum G., Matas Güell B., Balegedde Ramachandran R.P., Seshan K., Lefferts L., van Swaaij W.P.M., Kersten S.R.A., Evaporation of pyrolysis oil: Product distribution and residue char analysis, *AlChE J.* **2010**, 56, 2200-2210.

15. Groeneveld M.J., van Swaaij W.P.M., Gasification of char particles with CO_2 and H_2O, *Chem. Eng. Sci.* **1980**, 35, 307-313.

16. Barrio M., Gøbel B., Risnes H., Henriksen U., Hustad J.E., Sørensen L.H., Steam gasification of wood char and the effect of hydrogen inhibition on the chemical kinetics, Progress in Thermochemical Biomass Conversion; IEA Bioenergy, Cornwall, U.K., **2001**; Vol. 1, pp 32-46.

17. Matas Güell B., van Rossum G., van Swaaij W.P.M., Kersten S.R.A., Lefferts L., Seshan K., Challenges in the production of sustainable fuels from pyrolysis oil: Design of efficient catalysts for gasification of char, *Appl. Catal., B* **2010**, 101, 587-597.

18. DeGroot W.F., Shafizadeh F., Kinetics of wood gasification by carbon dioxide and steam, Fundamentals of Thermochemical Biomass Conversion, International Conference Proceedings, Estes Park, CO, Oct 18-22, **1982**.

19. Yip K., Tian F., Hayashi J-i., Wu H., Effect of alkali and alkaline earth metallic species on biochar reactivity and syngas compositions during steam gasification, *Energy Fuels* **2010**, 24, 173-181.

20. Nandi S.P., Onischak M., Gasification of chars from maple and jack pine woods, Fundamentals of Thermochemical Biomass Conversion, International Conference Proceedings, Estes Park, CO, Oct 18-22, **1982**.

21. Exxon Catalytic Coal Gasification-Process Development Program. Final Project Report; Technical Report, Nov. 1, **1981**.

22. McKee D.W., Spiro C.L., Kosky P.G., Lamby E.J., Catalysis of coal char gasification by alkali metal salts, *Fuel* **1983**, 62, 217-220.

23. Hallen R.T., Sealock Jr., L.J., Cuello R., Influence of alkali carbonates on biomass volatilization, Fundamentals of Thermochemical Biomass Conversion, International Conference Proceedings, Estes Park, CO, Oct 18-22, **1982**.

24. Randhava S.S., Rehmat A., Camara E.H., Methanation of low-concentration carbon monoxide feeds over ruthenium, *Ind. Eng. Chem. Process Des. Dev*. **1969**, 8, 482–486.

25. Tucci E.R., Streeter R.C., Gas processing developments. Ruthenium catalysts improve methanation, *Hydrocarbon Process.* **1980**, 59, 107-112.

26. Font R., Marcilla A., Verdú E., Devesa J., Fluidized-bed flash pyrolysis of almond shells: Temperature influence and catalysts screening, *Ind. Eng. Chem. Prod. Res. Dev.* **1986**, 25, 491-496.

27. Boroson M.L., Howard J.B., Longwell J.P., Peters W.A., Product yields and kinetics from the vapor phase cracking of wood pyrolysis tars, *AlChE J.* **1989**, 35, 120-128.

28. Liinanki L., Lindman N., Sjöberg S.-O., Ström E., Methane yield from biomass gasification at high temperature and pressure, Fundamentals of Thermochemical Biomass Conversion, International Conference Proceedings, Estes Park, CO, Oct 18-22, **1982**.

29. van Rossum G., Kersten S.R.A., van Swaaij W.P.M., Catalytic and noncatalytic gasification of pyrolysis oil, *Ind. Eng. Chem. Res.* **2007**, 46, 3959-3967.

30. Jess A., Reaktionskinetische Untersuchungen zur thermischen Zersetzung von Modellkohlenwasserstoffen, *Erdöl Erdgas Kohle* **1995**, 111, 479-484.

31. Kersten S.R.A., Prins W., van der Drift A., van Swaaij W.P.M., Experimental fact-finding in CFB biomass gasification for ECN's 500 kW_{th} pilot plant, *Ind. Eng. Chem. Res.* **2003**, 42, 6755-6764.

32. van der Meijden C.M., Veringa H.J., Vreugdenhil B.J., van der Drift B., Bioenergy II: Scale-up of the MILENA biomass gasification process, *Int. J. Chem. Reactor Eng.* **2009**, 7, A 53.

33. Wolfesberger U., Aigner I., Hofbauer H., Tar content and composition in producer gas of fluidized bed gasification of wood-Influence of temperature and pressure, *Environ. Prog. Sustainable Energy* **2009**, 28, 372-379.

34. Dũng N.A., Klaewkla R., Wongkasemjit S., Jitkarnka S., Light olefins and light oil production from catalytic pyrolysis of waste tire, *J. Anal. Appl. Pyrolysis* **2009**, 86, 281-286.

35. Valin S., Ravel S., Guillaudeau J., Thiery S., Comprehensive study of the influence of total pressure on products yields in fluidized bed gasification of wood sawdust, *Fuel Process. Technol.* **2010**, 91, 1222-1228.

36. Gissy J., Knight R.A., Onischak M., Carty R.H., Babu S.P., Technology development and commercialization of the Renugas process, U.S.-Finland Biofuels Workshop II, Espoo, Finland, Aug 24-30, **1992**.

37. Ståhl K., Neergaard M., IGCC power plant for biomass utilisation, Värnamo, Sweden, *Biomass Bioenergy* **1998**, 15, 205-211.

38. Paisley M.A., Overend R.P., Verification of the performance of future energy resources' *SilvaGas*® biomass gasifier-Operating experience in the Vermont gasifier, Proceedings of the 19th Annual International Pittsburgh Coal Conference, Pittsburgh, PA, Sept 23-27, **2002**.

39. Hofbauer H., Rauch R., Bosch K., Koch R., Aichernig C., Biomass CHP plant Güssing-A success story, In: Pyrolysis and Gasification of Biomass and Waste; Bridgwater A.V., CPL Press, Newbury, UK, **2003**; pp 371-383.

40. Otake T., Tone S., Kimura S., Hino Y., Methane formation over potassium carbonate catalyst loaded on coal char, *J. Chem. Eng. Jpn.* **1984**, 17, 503-508.

41. Abu El-Rub Z., Bramer E.A., Brem G., Experimental comparison of biomass chars with other catalysts for tar reduction, *Fuel* **2008**, 87, 2243-2252.

Appendix B

High-Throughput Screening Technique for Biomass Conversion in Hot Compressed Water

This appendix presents a study regarding the quartz capillary technique which was developed in our research group for performing screening tests of different biomass conversion routes. The aspects examined are flushing of the capillary with an inert gas, diffusion of gases through the quartz reactor wall and the catalytic activity of this wall. It was shown that hydrogen diffuses through the quartz reactor wall, which shows slight catalytic activity. This has, however, a negligible effect on previously obtained results for reactions at 250-800°C up to 60 min reaction time. Flushing of the capillary micro-reactor with N_2 prior to sealing and reaction is essential, especially for low organics concentrations, in order to avoid partial product combustion by atmospheric O_2 in the capillary.

B.1. Introduction

The quartz capillary technique has been used extensively in our group (Sustainable Process Technology [SPT]) for research into hydrothermal conversion of wood, pyrolysis oil and model compounds [1-4] as well as for supercritical gasification of wood and model compounds [5-7] and high pressure gasification of wood and char, which was presented in this chapter.

The technique utilizes batch micro-reactors (1-2 mm internal diameter) made of quartz. Experimentation is done in a quick, cheap and safe way and allows operation at high temperatures (up to 900°C) and pressures (up to 600 bar). Additionally, the reaction can be inspected visually since quartz is a transparent material and the micro-reactors can undergo rapid heating and cooling because of their small size. The gaseous products can be analyzed and quantified by crushing the micro-reactors in a specially designed chamber with a hammer mechanism. Therefore, for reactions that have gases as their main products, this technique gives sufficient accuracy for detecting trends, mapping of the operating window and for estimating reaction kinetics [5-7].

On the other hand, some limitations of the technique have been identified by Potic et al. [5] regarding liquid and/or solid product quantification and analysis for mass balance closure. This was further investigated and implemented in the technique by Knežević et al. [2-4]. Remaining limitations of the technique are: (1) only solid or liquid feedstock can be used as a reactant, (2) the gaseous sample is entirely consumed by analysis and (3) mixing of the loaded feedstock inside the capillary is limited.

This study was initiated after obtaining unexpectedly low hydrogen yields under reaction conditions of high temperature (800°C) or long reaction times (t>1 h). This was further investigated and previously obtained results with this specific experimental technique were re-examined. Some additional aspects of this experimental technique are presented and discussed, namely flushing of the capillaries with N_2, diffusion of gases through the quartz wall and its catalytic effect. Previously obtained results included overall low reaction temperatures (250-350°C) at long reaction times (up to 10,000 min) and high reaction temperatures (400-800°C) at short reaction times (up to 60 min). In order to investigate this, model compounds had to be used that would completely decompose to detectable gaseous products which can be readily analyzed and quantified, without any liquid and/or solid end by-products other than water. Therefore, formic acid and ethanol were used for this study. Noncatalytically, formic acid

is known to completely decompose to CO_2 and H_2 at 800°C [8], while ethanol also produces CO and CH_4. Formic acid has been used extensively for validation purposes of this experimental technique. Ethanol was used because it completely decomposes to gaseous products which are also generated by biomass conversion processes.

B.2. Experimental Section

B.2.1. Materials

Formic acid (98%, Fluka) and pure ethanol were used (100%, LP) for making the aqueous solutions with distilled water. The Ru/Al_2O_3 catalyst used was 0.5 wt.% Ru on alumina (Aldrich/ 3.2mm pellets, product number: 206199).

The quality of the quartz material used for manufacturing the capillary micro-reactors was electrically fused quartz glass of the type HSQ 300, purchased from LSP Quartz B.V.

B.2.2. Experimental Set-up

The quartz capillaries that were used as batch micro-reactors in our experimental method had dimensions of 2 mm ID, 4 mm OD and lengths ranging from 131 to 151 mm. For some tests, capillaries of 1 mm ID and 2 mm OD were used. After loading the capillaries with the desired feed (0.008-0.024 g), they were flushed with N_2 before sealing. For some tests, where the effect of an inert reaction environment is investigated, the capillaries were then not flushed.

A detailed description of the experimental method is given by Knežević et al. [2-4], Potic et al. [5] and Kersten et al. [6].

For each data point, four capillaries were used which were placed on a specially designed holder and inserted into a preheated fluidized sand bed. After the specified reaction time, the capillaries were quenched in a water bath to ambient temperature to ensure that no further reactions take place.

The gaseous products were analyzed as described by Potic et al. [5] by crushing the capillary in a specially designed chamber (V=46 ml) and by using a gas chromatograph with TCD detectors (Varian Micro GC CP-4900, 10m MS5A He (70°C, 150 kPa) and 10m PPQ He (80°C, 150 kPa)). The final pressure build-up inside the capillary micro-reactor at reaction temperature was calculated by the known amount of produced gaseous compounds and the remaining net amount of water/steam.

Formic acid was tested in aqueous solutions of 1-17 wt.% which were reacted

at a temperature of 800°C and pressures of 111-280 bar. The reaction time ranged between 5 and 1580 min. The ethanol aqueous solution prepared was 9.5 wt.%. and was reacted at a temperature of 800°C and a pressure of 94-95 bar. The reaction time varied between 3 and 2880 min. The Ru/Al_2O_3 catalyst was used at a 93 wt.% concentration on dry ethanol feed basis.

Some capillaries loaded with formic acid (see also Figure B.1) were subjected to lower temperatures, 350 or 600°C, after a reaction time of 800°C for 10 min. For this, two fluidized sand beds were employed, using air as fluidization gas. The first one was kept at a temperature of 800°C and the second one at 350 or 600°C, respectively. The capillaries were initially introduced in the first fluidized bed were they were reacted for 10 min. Afterwards, they were taken out and quickly introduced into the second fluidized bed for a time exposure to either 350 or 600°C.

Equilibrium concentrations were calculated according to the Gibbs free energy minimization method. Fugacity coefficients were calculated with the Modified Soave-Redlich-Kwong equation of state [9].

B.3. Results and Discussion

B.3.1. Tests with formic acid (HCOOH)

Figure B.1 shows the hydrogen fraction plotted against time at different temperatures. The initial hydrogen fraction is defined as the hydrogen present after 10 min of reaction time at 800°C (indicated in Figure B.1 by the gray area).

The lower dotted line represents the H_2 fraction for a HCOOH sample reacted at 800°C. The dotted line in the middle and the upper dotted line are the results obtained for HCOOH samples that were first reacted for 10 min at 800°C to reach full conversion to gases and were then further exposed to temperatures of 600 and 350°C, respectively. The time indicated in Figure B.1 is the total exposure time of the samples (t = 10 min (800°C) + t (350/600/800°C)).

The tests show that the highest capillary temperature, 800°C, has the largest effect on H_2 decrease in time, for which after 1440 min the H_2 almost reaches zero. Even after 30 min at 800°C, the H_2 faction is lowered by 10%. This effect decreases with decreasing reaction temperature. A capillary temperature of 600°C still causes a decrease of H_2 by 65% from its initial value after about 1580 min. The lowest tested temperature, 350°C, has the smallest effect on H_2 and causes a H_2 decrease by 11% from its initial value after 930 min, after which it seems to have reached a constant value.

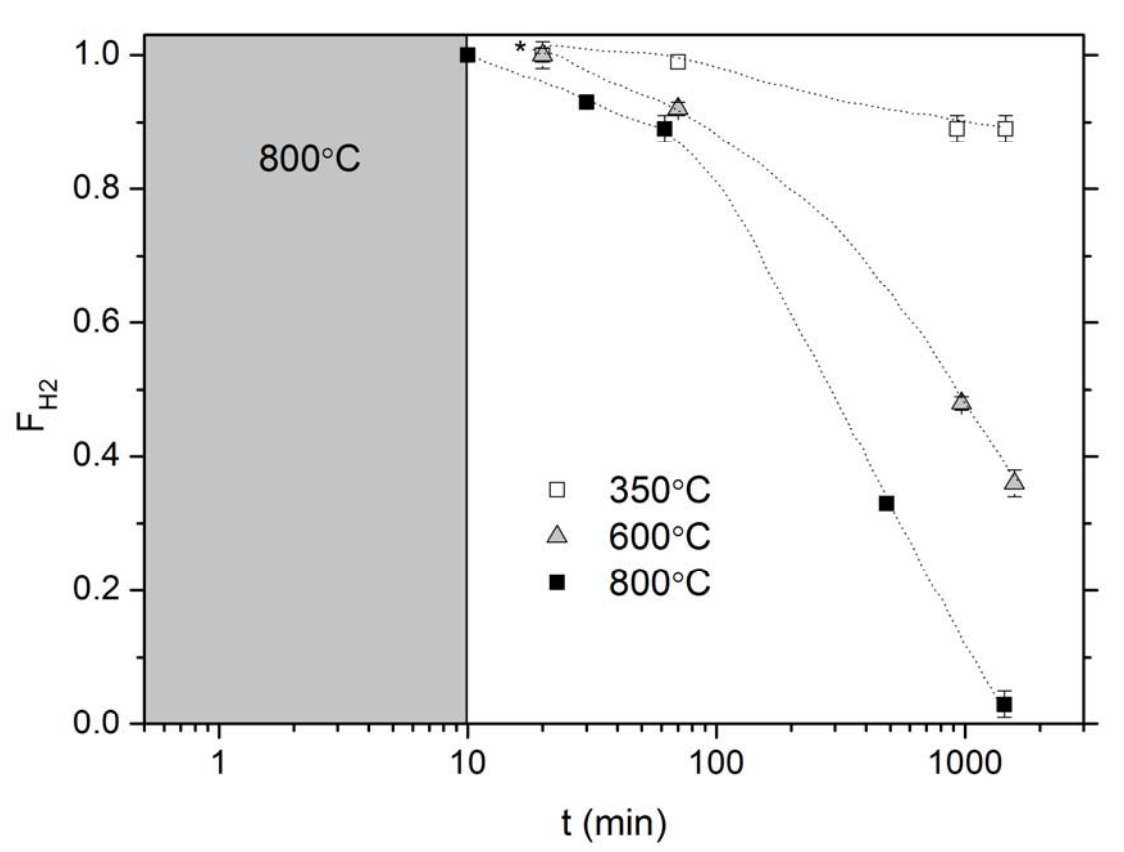

Figure B.1. H_2 fraction (F_{H2}) of initial H_2 content after 10 min exposure to 800°C vs. time of a 17 wt.% aqueous HCOOH solution at 800, 600 and 350°C. P = 111 ± 5 bar (estimated at 800°C). Each data point is the average of four samples with complete carbon to gas conversion (100% ± 2). t = 10 min (800°C) + t (350/600/800°C). The dotted lines are drawn for illustration purposes. *Data points for 350 and 600°C coincide at t=20 min.

Formic acid is known to be converted completely to gaseous products, mainly CO_2 and H_2 at high temperatures [8]. In Figure B.1, the decreasing H_2 with reaction time is attributed to the diffusion of H_2 through the quartz wall of the micro-reactor. It is known that hydrogen can diffuse through quartz material from earlier studies [10-12]. For all tests, the carbon to gas conversion was 100% ± 2 showing that no carbon-containing gases diffused through the quartz. The main carbon-containing gaseous product was CO_2 (with initially ca. 0.5 mol.% CH_4 and about 1 mol.% CO). At ambient temperatures (between 20-25°C) no H_2 diffusion was noted.

The quartz shows, though, water-gas shift activity by the gradually decreasing amount of CO with reaction time of the samples (decrease from 1 mol.% to 0 mol.%), which is converted to CO_2. The water-gas shift equilibrium (B.1) could also have an effect on the H_2 amount with decreasing temperature. Calculation

of this specific equilibrium pointed out that the H_2 yield should increase from 99% at 800°C to 100% at 350°C. These values are far from the ones experimentally obtained (3% at 800°C and 90% at 350°C) and therefore the decrease in H_2 yield observed cannot be explained solely by water-gas shift activity. In order to exclude the possibility that some oxygen has diffused into the quartz from the air which is used for fluidization (and therefore consuming H_2), some additional tests were done. The reaction temperature was 800°C and N_2 was used instead of air for fluidization of the sand bed. The results obtained were identical to the tests done at 800°C in Figure B.1, where air was used for fluidization. Therefore, the decrease in H_2 yield due to consumption by oxygen is excluded as well.

The results of the work by Knežević et al. [1-4] who did tests in capillary micro-reactors at 350°C and for typical reaction times of 60 min are not compromised by these new findings and have a negligible effect on the results of Potic et al. [7] where 1 mm ID and 2 mm OD quartz capillaries were used for supercritical gasification tests. The maximum reaction times and temperatures used in their work were 1 min at 800°C and 1.5 min at 600°C. These reaction conditions were repeated in this work using a 17 wt.% aqueous formic acid solution (P=310 ± 5 bar) and it was found that the permeation of hydrogen through the reactor wall was negligible at such short reaction times. This proves that also the results obtained by Potic et al. [7] are not compromised by the results reported here.

What can be further noted in Figure B.1 is that there seem to be two diffusion regimes for the cases of exposure temperature at 600 and 800°C. The first diffusion regime extends until about 100 min of exposure time and the second one follows. Quartz undergoes a change in its physical structure around a temperature of 573°C [13]. It changes from α-quartz to β-quartz, where β-quartz has a higher diffusion coefficient than α-quartz [14]. Therefore, this could be the explanation for the trend observed.

Figure B.2 presents the amounts of carbon dioxide and hydrogen gas recovered vs. the concentration of formic acid in the aqueous feed, with and without flushing the capillary with N_2 before sealing. The concentration of the aqueous formic acid solution affects the amount of recovered CO_2 and H_2 for the lowest concentrations (1 and 2 wt.%) where the highest inaccuracies were

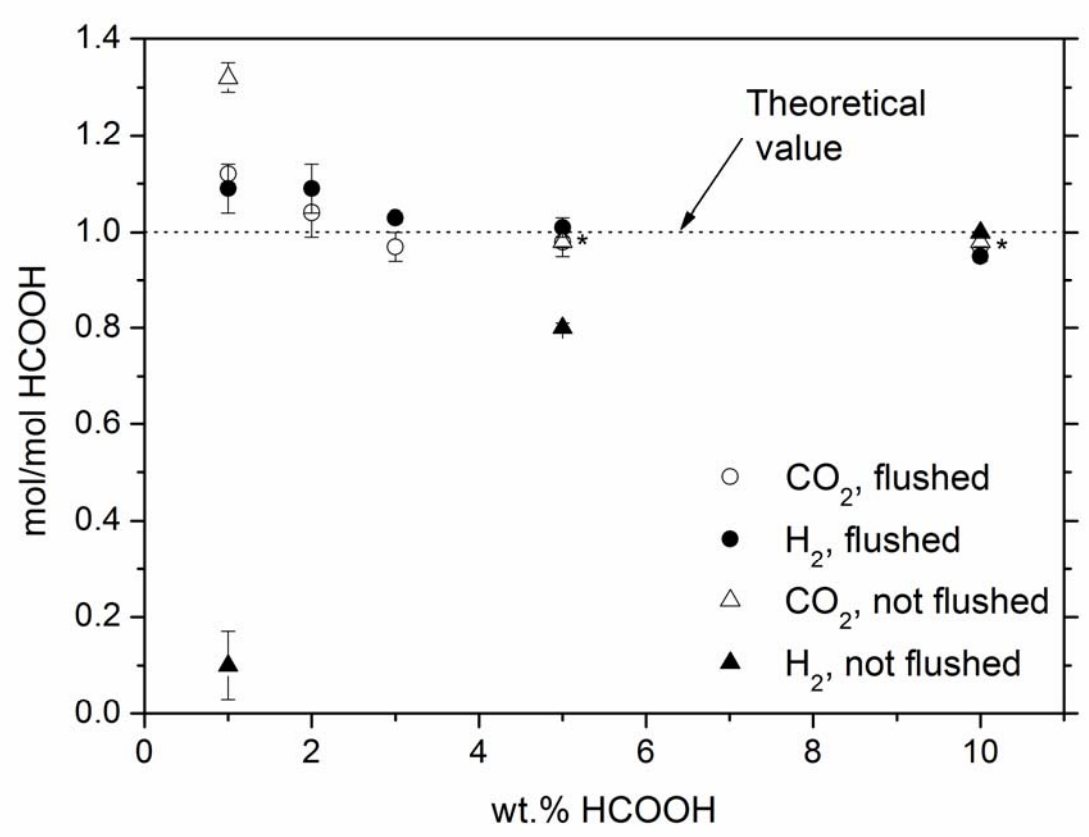

Figure B.2. Recovered carbon dioxide and hydrogen gas vs. formic acid concentration, with and without flushing with N_2. P = 280 ± 8 bar, T=800°C, t = 5 min. Each data point is the average of four samples. *Data points for CO_2 flushed and CO_2 not flushed coincide at 5 and 10 wt.% HCOOH.

found. This is because weighing errors have the largest effect on these results, with an apparent overweighing trend.

For the capillaries that were flushed with N_2 gas before sealing and for concentrations higher than 3 wt.%, the obtained CO_2 and H_2 amounts are very close to the theoretical value. On the other hand, for feeds that were not subjected to an inert environment (were not flushed with N_2), the CO_2 was completely recovered, whereas the H_2 not, up to a concentration of 10 wt.% HCOOH.

This result is in agreement with findings by Kersten et al. [6] who did not flush the micro-reactors and therefore obtained a noticeable difference in the hydrogen yield for very low glucose concentration (1 wt.%) at 800°C. In their case, only half of the theoretical amount of hydrogen gas was recovered. They attributed this to the consumption of the hydrogen by atmospheric oxygen trapped inside the capillary after sealing. Therefore, this clearly shows the importance of flushing with an inert gas before sealing the micro-reactor, espe-

cially for low organics concentrations.

B.3.2. Tests with ethanol (C_2H_6O)

This experimental part of the paper gives results from reacted aqueous solutions of ethanol (Figure B.3) and ethanol with Ru/Al_2O_3 catalyst (Figure B.4). Figure B.3 presents the product yields for H_2, CO, CO_2 and CH_4 as well as the total obtained carbon to gas conversion with reaction time (t). The reacted sample was a 9.5 wt.% aqueous ethanol solution.

The H_2 and CH_4 yields decrease with reaction time, while the CO_2 yield increases. What can be noted at reaction times longer than 60 min and up to 1035 min is that the carbon distribution slowly shifts to carbon dioxide. If this observation is combined with the decreasing hydrogen yield due to diffusion with reaction time, this indicates possible catalytic action on the otherwise very slow gas-phase reaction (B.3):

$$CO + H_2O \leftrightarrow CO_2 + H_2 \qquad (B.1)$$

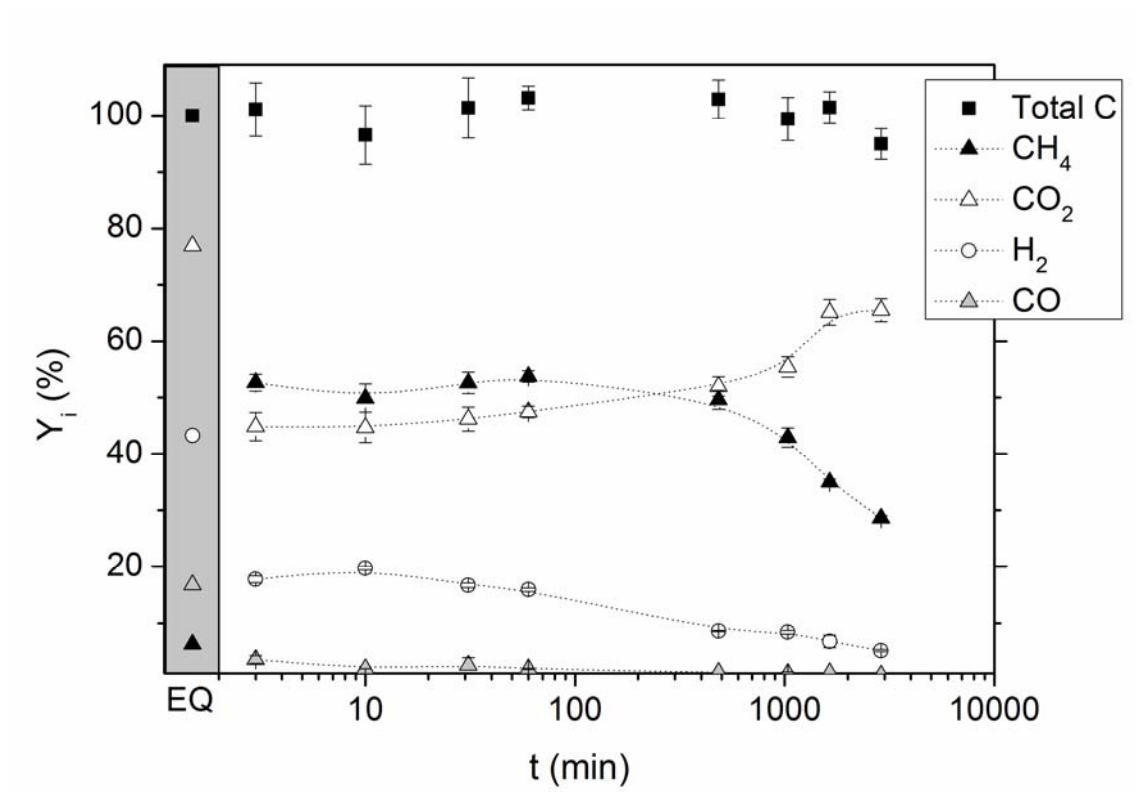

Figure B.3. Product yields vs. reaction time for a 9.5 wt.% aq. ethanol solution. P = 95 ± 3 bar, T=800°C. The gray area contains the equilibrium values (EQ) for 100% carbon to gas conversion. Each data point is the average of four samples. The dotted lines are drawn for illustration purposes.

$$CH_4 + H_2O \leftrightarrow CO + 3\,H_2 \qquad (B.2)$$

$$\underline{\text{Overall:}}\quad CH_4 + 2\,H_2O \leftrightarrow CO_2 + 4\,H_2 \qquad (B.3)$$

Experimental findings from Schoderböck and Lahaye [13] showed that impurities which are present in quartz are responsible for the catalytic activity of the reduction of nitric oxide by carbon monoxide. In their study, catalytic activity of the quartz actually depended on the amount of impurities present. Typical impurities present in the type of quartz glass used in this study are presented in Table B.1.

Table B.1. Typical trace elements in HSQ 300 electrically fused quartz glass (ppm by weight oxide) [15].

Al	Ca	Cr	Cu	Fe	K	Li	Mg	Mn	Na	Ti	Zr	OH Content
15	0.5	<0.05	<0.05	0.1	0.4	0.6	0.05	<0.05	0.3	1.1	0.7	< 30

Figure B.4 shows the product yields vs. the reaction time for a 9.5 wt.% aqueous ethanol solution with Ru/Al_2O_3 used as catalyst. The ruthenium catalyst actually drives the product distribution towards equilibrium amounts. In general, as the reaction time proceeds to 60 min, there is a slight change in the product distribution with CH_4 amounts decreasing while CO_2 is increasing, indicating that reactions (B.1) and (B.2) take place. The hydrogen, though, seems to have a steady value up to about 60 min of reaction time. This indicates that hydrogen diffusion rate through the quartz wall equals the hydrogen production rate from 3 min up to 60 min reaction time. Also, the same trend is observed as in Figure B.1 for the hydrogen concentration profile. In this case as well, two different diffusion regimes seem to exist: the first extends up to about 100 min of exposure time and a second one follows with an apparent higher diffusion coefficient. This could be attributed, similarly, to the change in crystalline structure of the α-quartz to β-quartz [14].

In Figure B.3, there is no significant change for all gas components up to 60 min reaction time when compared to the results in Figure B.1. This occurs probably because the absence of a catalyst in this case slows down reactions. In Figure B.1 at the same reaction time (60 min) the hydrogen yield had decreased by more than 10%. In that case, there was little CO and CH_4 present to

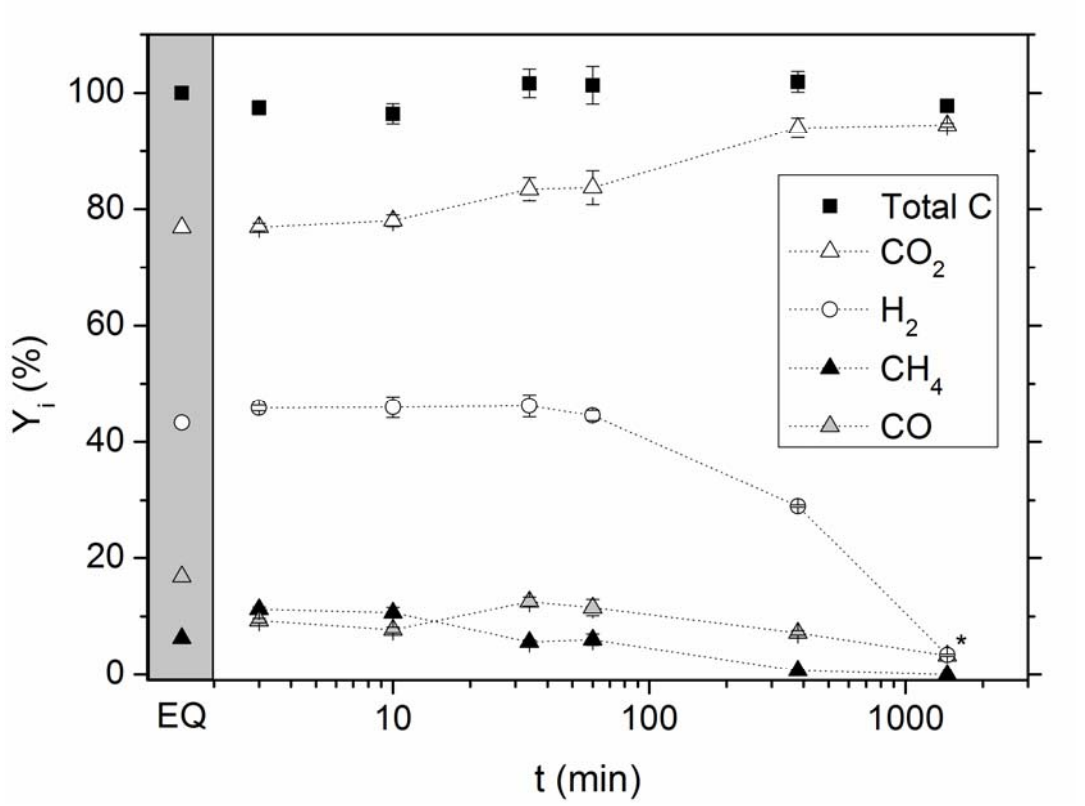

Figure B.4. Product yields vs. reaction time for a 9.5 wt.% aq. ethanol solution with Ru/Al_2O_3 catalyst. Ru/Al_2O_3 = 93 ± 1 wt.% (on dry ethanol feed basis). P = 94 ± 3 bar, T=800°C. The gray area contains the equilibrium values (EQ) for 100% carbon to gas conversion. Each data point is the average of four samples. The dotted lines are drawn for illustration purposes. *Data points for H_2 and CO at t=1455 min coincide.

further react to H_2 and maximum hydrogen partial pressure was higher.

The decrease in hydrogen yield in both Figures B.3 and B.4 occurs because of hydrogen diffusion, otherwise the hydrogen yield should have been much higher according to the stoichiometry of the water-gas shift (B.1) and methane reforming reactions (B.2).

For all samples obtained in Figures B.3 and B.4 the carbon in the feed is completely converted to gases showing that no carbon-containing gases diffuse through the quartz wall as well as in the case of the tests with formic acid. The latter also showed that no O_2 diffuses through the quartz capillary.

B.4. Conclusions

The quartz capillary micro-reactor technique was further evaluated and previously obtained results with this specific experimental technique were re-examined under the light of these observations. The main conclusions of this work can be summarized as follows:

- H_2 diffusion can take place through the quartz reactor wall. The amount depends on temperature and reaction time
- No carbon-containing gases (CO,CO_2, CH_4) diffuse through the quartz
- Oxygen does not diffuse through the quartz wall
- The quartz material shows slight catalytic activity for both water-gas shift and methane reforming
- Flushing of the capillary with N_2 is necessary, especially for low organics concentrations, to avoid partial product combustion by atmospheric O_2
- The effect on previously obtained results with this experimental technique is negligible because combinations of low temperatures-long reaction times (T<350°C, t = 60 min) and high temperatures-short reaction times (T=400-800° C, t = 1-60 min) are utilized.

Notation

F_{H2}	=	hydrogen fraction; defined as the fraction of hydrogen initially present in the capillary. Initial hydrogen amount is at t=10 min at 800°C
ID	=	internal diameter, mm
OD	=	outside diameter, mm
P	=	pressure, bar
t	=	reaction time, min
T	=	temperature, °C
V	=	volume, ml
Y_{H2}	=	hydrogen yield; defined as the percentage of the maximum amount of hydrogen, which can be produced according to the following reaction:

$$C_xH_yO_z + (2x\text{-}z)H_2O \rightarrow xCO_2 + \left(\frac{y}{2} + 2x\text{-}z\right)H_2$$

Y_i	=	yield of product i; defined as :

$$Y_i = \frac{mol_{C_i}}{mol_{C_{feed}}} x100\%$$

where mol_{Ci} is the moles of carbon present in the gas product as component i and mol_{Cfeed} is the moles of carbon present in the feed

Abbreviations

EQ = Equilibrium

TCD = Thermal Conductivity Detector

Literature cited

1. Knežević D., Rep M., Kersten S.R.A., Prins W., van Swaaij W.P.M., Hydrothermal liquefaction and pyrolysis: A visualization study, In: Science in Thermal and Chemical Biomass Conversion; Bridgwater A.V., Boocock D.G.B., Eds.; CPL Press: UK, **2006**; Vol. 2, pp 1082-1090.

2. Knežević D., Schmiedl D., Meier D., Kersten S.R.A., van Swaaij W.P.M., High-throughput screening technique for conversion in hot compressed water: Quantification and characterization of liquid and solid products, *Ind. Eng. Chem. Res.* **2007**, 46, 1810-1817.

3. Knežević D., van Swaaij W.P.M., Kersten S.R.A., Hydrothermal conversion of biomass: Part I, Glucose conversion in hot compressed water, *Ind. Eng. Chem. Res.* **2009**, 48, 4731-4743.

4. Knežević D., van Swaaij W.P.M., Kersten S.R.A., Hydrothermal conversion of biomass: Part II, Wood and pyrolysis oil conversion in hot compressed water, *Ind. Eng. Chem. Res.* **2010**, 49, 104-112.

5. Potic B., Kersten S.R.A., Prins W., van Swaaij W.P.M., A high-throughput screening technique for conversion in hot compressed water, *Ind. Eng. Chem. Res.* **2004**, 43, 4580-4584.

6. Kersten S.R.A., Potic B., Prins W., van Swaaij W.P.M., Gasification of model compounds and wood in hot compressed water, *Ind. Eng. Chem. Res*. **2006**, 45, 4169-4177.

7. van Rossum G., Potic B., Kersten S.R.A., van Swaaij W.P.M., Catalytic gasification of dry and wet biomass, *Catal. Today* **2009**, 145, 10-18.

8. Yoshida K., Wakai C., Matubayasi N., Nakahara M., NMR spectroscopic evidence for an intermediate of formic acid in the water-gas-shift

reaction, *J. Phys. Chem. A* **2004**, 108, 7479-7482.

9. Soave G., Barolo M., Bertucco A., Estimation of high-pressure fugacity coefficients of pure gaseous fluids by a modified SRK equation of state, *Fluid Phase Equilib.* **1993**, 91, 87-100.

10. Johnson J.B., Burt R.C., The passage of hydrogen through quartz glass, *J. Opt. Soc. Am.* **1922**, 6, 734-738.

11. Lou V., Sato R., Tomozawa M., Hydrogen diffusion in fused silica at high temperatures, *J. Non-Cryst. Solids* **2003**, 315, 13-19.

12. Hörnlund E., Hultquist G., Experimental findings in support of atomic transport of hydrogen in silica, *J. Appl. Phys.* **2003**, 94, 4819-4823.

13. Schoderböck P., Lahaye J., The influence of impurities contained in quartz sand on the catalytic reduction of nitric oxide by carbon monoxide, *Appl. Surf. Sci.* **1996**, 93, 109-118.

14. Bongiorno A., Colombo L., Cargnoni F., Hydrogen diffusion in crystalline SiO_2, *Chem. Phys. Lett.* **1997**, 264, 435- 440.

15. Heraeus. www.heraeus.com. Material grades, quartz tubes. (Website accessed on 05-02-2011).

Chapter 4

Intrinsic Reactivity of Biomass-derived Char under Steam Gasification Conditions

The influence of ash on the steam gasification rate of pine wood derived char particles in the temperature range of 600-800°C is investigated. Ash derived from pine wood or specific ash components were added to the pine-wood (before pyrolysis) or to the produced char (after pyrolysis) via physical mixing or impregnation. The addition method and the amount and type of ash/ash component have been studied and the obtained gasification rates are compared.

Impregnation of ash/ash components by ~10 wt.% or more (in the original pine wood) always resulted in a significant increase in the (initial) gasification rate. At 700°C, e.g., impregnating 9.5 wt.% KOH in pine wood resulted in complete char conversion within 12 min, corresponding to an increase in (initial) gasification rate by a factor 30 compared to char without impregnation. SEM images of the chars showed that impregnating the wood with concentrations up to 14 wt.% resulted in unevenly distributed ash (components) in the particles. Based on this, the hypothesis is that besides the overall amount of ash also its distribution among and inside the char particles is important for enhancement of the reaction rate. A biomass gasification concept in which the steam gasification reaction of char is catalyzed by concentrating the ashes in the biomass is feasible.

4.1. Introduction

The most important heterogeneous gasification reactions taking place during the gasification process which involve solid carbon are: the water-gas reaction (4.1), the Boudouard reaction (4.2) and the carbon hydrogenation reaction (4.3).

$$C + H_2O \rightarrow CO + H_2 \quad (4.1)$$

$$C + CO_2 \leftrightarrow 2CO \quad (4.2)$$

$$C + 2H_2 \rightarrow CH_4 \quad (4.3)$$

In this chapter, reaction (4.1) is studied and in particular the effect of ash additives on the reaction (gasification) rates. Char steam gasification has been a research topic for many years, especially in the coal gasification research of the 1980's. A lot of work is available on the steam gasification of coal char with various mixed or impregnated alkali metals such as: K_2CO_3 [1-15], KOH [2-3, 11, 15], KCl [3, 6, 11, 15], $KHCO_3$ [15], KNO_3 [12, 15], K_3PO_4 [12], Na_2CO_3 [4, 6, 11], NaOH [8, 11], NaCl [3, 6, 11]. Calcium has also been studied for coal char steam gasification as a cheap alternative to alkali metals: CaO [6, 14], $Ca(OH)_2$ [10], $CaCl_2$ [6], as well as iron in the forms of Fe_2O_3 [7] or $Fe(NO_3)_3$ [9, 14]. Studies also exist dealing with steam gasification of demineralized coal char [9, 16] or catalysis by impregnated composites [9, 11, 14] or eutectic mixtures [13] of the abovementioned additives. Inhibition effects by H_2 [1, 14, 17, 18], CO [4, 16] and CO_2 [10, 14] during coal char steam gasification have also been studied. The main conclusions concerning the catalytic coal char steam gasification research can be summarized as follows:

- mineral matter in the coal works catalytically for steam gasification,
- impregnated alkali metals seem to be active gasification catalysts only when they can interact with the carbon substrate and form carbonate(s),
- part of added metal components to the coal is deactivated because of interaction with the indigenous mineral matter of the coal (illite $[(K,H_3O)(Al,Mg,Fe)_2(Si,Al)_4O_{10}[(OH)_2, (H_2O)]$ and kaolinite $[Al_2Si_2O_5(OH)_4]$),
- decreasing catalytic activity is in the order: $KNO_3 > K_2CO_3 \approx KOH > KHCO_3 > Na_2CO_3 > KCl > NaCl > CaO$. In the case of KOH, conversion rates of up to a factor 85 higher than the original coal char can be achieved,
- an increase of the M/C ratio for potassium leads to higher conversion rates until a "saturation" point, the level of which depends on the addition or coal

pretreatment method,

- impregnated eutectic salts can increase conversion rates in steam by an order of magnitude compared to impregnated K_2CO_3, probably because of the better contact between the additive and the carbon surface when a liquid eutectic is present,
- the presence of chloride in coal inhibits the catalytic effect of Na_2CO_3. The inhibition increases with higher Cl/Na ratio,
- many types of active intermediates have been proposed for potassium catalysis, such as metallic K [19], metal clusters or particles [20-22], K_2CO_3 [3, 19], K_2O [3, 12, 19], K_2O_2 [23] and K-O-C [2, 15, 20]. There is still discussion and ongoing research to clarify the mechanism and active intermediates/sites of catalysis by alkali metals under steam gasification conditions.

There is, though, considerably less research dealing with the effects of (alkali) metals on the gasification of biomass-derived char [24-30]. Results obtained by Barrio et al. [30] point out that not large differences occur in the reactivity of different wood-derived chars. However, there are differences in gasification reactivity between wood chars and chars produced from agricultural residues, possibly because of the higher ash content of the latter [31]. Studies dealing with gasification of chars obtained from varying biomass/coal blends demonstrate that increasing alkali metal content in the char because of higher biomass/coal ratio causes an increase in overall char reactivity [32-34]. There are also experimental results on the catalytic effect of ash by demineralization of the biomass [24-26]. Other studies investigate the catalytic effects of biomass-derived char impregnated with alkali chlorides [27] or alkali carbonates [28, 29]. Inhibition effects by H_2 have been studied as well [26, 30, 35, 36]. The observations and conclusions from these investigations with wood are in general agreement with those for coal.

In this chapter we investigate the steam gasification of pine wood-derived char, with the interest mainly on the catalytic potential of wood ash as cheap and plentifully available catalyst. Also straw was tested as an ash-rich biomass source. To the best of our knowledge, only the research by Hauserman [37] showed that mixing wood with wood ash increased the gasification rate. Hauserman mixed wood ash (10 wt.%) and wood and observed that the overall gasification rate (starting from wood) increased by a factor 32 at 700°C. In our work, we first produced char from the wood and then studied solely the

steam gasification of the char. Ash derived from pine wood or specific ash components were added to the pine wood (before pyrolysis) or to the produced chars (after pyrolysis) via (dry) mixing or (wet) impregnation. Inhibition by CO and H_2 was also studied, because these compounds are always present in any industrial gasifier.

4.2. Experimental Section

4.2.1. Materials and Methods

The wood used for all the measurements was pinewood, purchased from Rettenmaier & Söhne GMBH, Germany. Wheat straw was purchased from Puik, The Netherlands. Wood and straw were dried at 105°C for 24 h prior to all tests realized. The following salts were tested as model components for biomass ash: K_2CO_3, $KHCO_3$, K_2HPO_4, NaOH, CaO and KBr (Sigma-Aldrich), KOH (Merck), KNO_3 (Alfa Aesar), KCl (Sigma) and Fe_2O_3 (87.9 wt.% Fe_2O_3, 9.2 wt.% Cr_2O_3, 2.7 wt.% CuO, 0.03 wt.% Al_2O_3, 0.27 wt.% MnO).

The impregnated samples were prepared by adding distilled water to the desired amount of salt to obtain 10 ml of aqueous solution. This solution was stirred until all salt was dissolved (in case of wood ash only partial dissolution occurred) and the solution was poured onto 1 g of wood/char sample on a watch glass. The wood/char solution was mixed well until it formed a slurry. This slurry was directly dried in the oven at 105°C for 24 hr. Also some samples were dried after 24 hours at room temperature. This had no effect on the TGA results. After drying, the sample was cooled down and weighed. The impregnated sample was stored in a sample vial and the empty watch glass was weighed again to calculate the exact amount of salt loading. Mass balances of the impregnated samples were satisfactory meaning that more than 94% of the added salt/ash was recovered in the biomass. The homogeneity of the impregnated wood batches of 1 g was checked by measuring the ash content of samples of 1 to 10 mg (for the TGA typically 7 mg was used). The standard deviation of these small samples was rather large. For instance, for the wood with 1.6 wt.% KOH (based on 1 g sample), the KOH content of the smaller samples was 2.2 +/- 1.3 wt.% (based on four measurements). Hence, there were differences in the ash/ash-component loadings of the individual particles in the TGA samples. Loading of individual particles here refers to the spatially averaged loading of a particle.

Ash and ash-component loadings are reported as wt.% of the 1-g sample or as

M/C (metal/carbon) mole ratio. Initial loadings refer to the loading of the biomass before pyrolysis.

For the reader's convenience: an initial loading of 9.5 wt.% (M/C = 0.046) KOH in wood corresponds to 39.6 wt.% KOH (M/C = 0.149) in the corresponding char.

For the case of ash-impregnated wood, the ash was dissolved in distilled water and the solution was added to the wood. The same impregnation procedure was followed as described previously. Some of the ash components (denoted in Table 4.2 with an asterisk) reacted with water and their reaction product was water-soluble. After oven-drying at 105°C for 24h, the impregnated wood contained both the water-soluble and water-insoluble fractions of the wood ash. These samples are referred to in the text as "impregnated" samples, although they are actually partially impregnated (at least 56 wt.% on initial ash basis is water-soluble).

Some samples were prepared by mixing of the additives with the wood. These samples were: (1) wood with Fe_2O_3, because the metal is water-insoluble and therefore not possible to impregnate in the wood and (2) a wood with KOH (9.5 wt.% in wood) in order to study the effect of the ash (component) addition method.

A washed char sample was also used in this study. This char was made from KOH-impregnated wood (9.5 wt.%) by heating to 700°C in a N_2 atmosphere. The char was then washed by stirring in 250 ml of distilled water for 24 h. Salt removal of about 99 wt.% was achieved.

In a standard test, the char was produced in-situ as described further in section 4.2.3. However, for some tests, the char was made *externally* in an electrical oven prior to pretreatment and reaction in the TGA system. The char was produced this way because larger char quantities were necessary for realization of the specific tests. These tests were: (1) tests for exclusion of mass transfer limitations (see section 4.2.5) and (2) tests for investigation of the addition method of KOH to either wood or char (see section 4.3.4).

The biomass pretreatment methodology is schematically summarized in Figure 4.1.

4.2.2. Analyses

Elemental compositions (analyzed with a Flash 2000, Thermo Scientific, column temperature: 900°C) and ash contents of the tested feeds are presented in

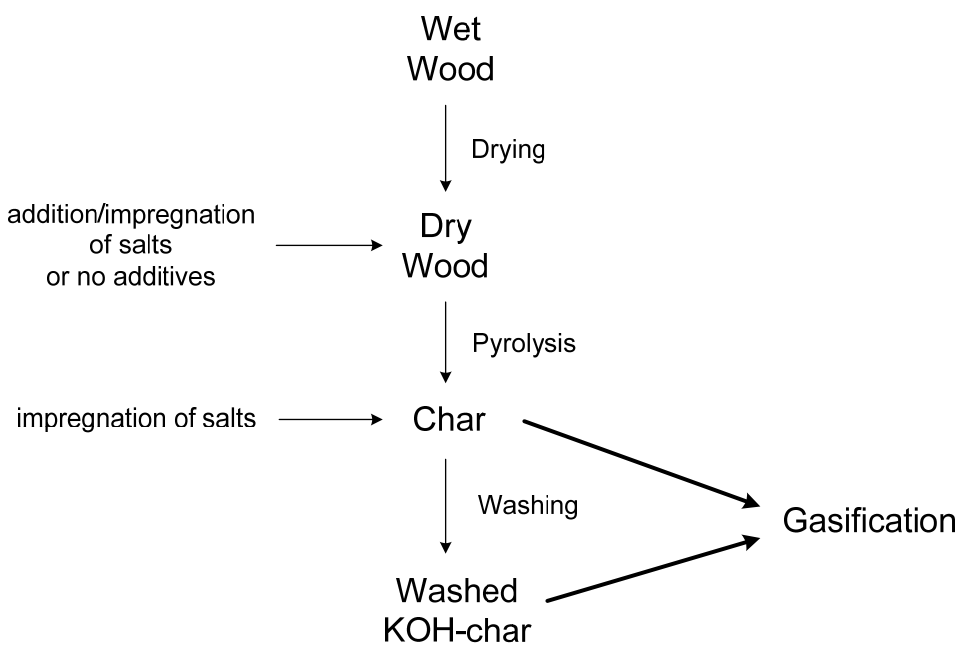

Figure 4.1. Schematic representation of biomass pretreatment methodology.

Table 4.1. The ash content was determined by combustion of the sample in air at 550°C for 24 h, according to the procedure developed by Fernández Llorente and Carrasco García [38]. The ash necessary for the ash-impregnated samples was produced by the same procedure.

The ash compositions of wood and straw were determined by X-ray fluorescence spectrometry (XRF) and are presented in Table 4.2.

The morphology of the chars was characterized by Scanning Electron Microscopy (SEM; JEOL TSM 5600) after drying in a vacuum oven at 80°C.

Table 4.1. Elemental composition (C, H) of the tested materials on "dry, ash-free" basis[a].

	wood	**straw**
compound	**wt.%**	**wt.%**
C	49.1	48.0
H	5.4	6.3
Difference (100-C-H)	45.5	45.7
Ash	0.4	5.3

[a]The difference is mainly oxygen (O) in case of wood. The ash contents are expressed on a dry basis.

Table 4.2. Ash compositions of wood and straw. The "rest" are volatile components that could not be analysed (Cl and/or S).

	wood ash	**straw ash**
component	**wt.%**	**wt.%**
K_2O*	5.08	18.38
Na_2O*	0.00	5.16
CaO*	34.41	7.60
MgO*	10.28	2.66
Fe_2O_3	6.97	0.46
TiO_2	0.49	0.05
SO_3*	3.16	2.91
P_2O_5*	2.16	5.56
Al_2O_3	1.68	0.77
SiO_2	7.33	45.49
MnO	3.90	0.00
SrO*	0.18	0.00
NiO	0.16	0.00
ZnO	0.17	0.00
BaO*	0.40	0.00
Rest	23.63	10.96

*Components that can react with water and their reaction product is water-soluble.

4.2.3. Experimental set-up

The set-up used was a modification of the thermogravimetric analyzer (Sartorius) used by Noorman et al. [39]. A schematic overview is shown in Figure 4.2. The wood or impregnated/mixed wood or straw sample (typically about 7 mg) was weighed in an external balance and placed (ca. 200 particles) in the sample basket (nr.8 in Figure 4.2), which was hung on a platinum wire connected to a balance (nr.10 in Figure 4.2). The sample basket was made of quartz glass (H=6 mm, OD=6 mm) and the bottom part of it was a quartz filter (H=1 mm). A N_2 purge stream was used to prevent exposure of the sensitive electronics in the balance to reactive gases. The quartz tube (nr.7 in Figure 4.2) was attached to the cylindrical oven (nr.9 in Figure 4.2) and could be moved vertically. After placing the loaded sample basket on the platinum wire, the oven could be lifted so that the sample basket would be located inside the quartz tube as depicted in Figure 4.2. The sample temperature was measured just below the sample basket and this was used to control the temperature of the oven.

The wood sample was heated at an average heating rate of 10 K/min in a N_2 flow (10 Nml/s) regulated by a mass flow controller (Brooks Instruments) and at atmospheric pressure to the desired temperature. While heating up in an inert atmosphere, the wood transformed into char via pyrolysis (produced char amounts varied between 1 to 4 mg). When the desired temperature was reached, then the flow was switched to steam or to a N_2/steam(/CO/H_2) mixture to initiate reaction of the char at isothermal conditions.

The temperature and voltage (balance output) were logged onto a computer every 1 s. The balance was calibrated by linear correlation of the voltage output to different standard weights. At the end of the test, the reactants flow was switched back to N_2. Then the oven was switched off and the system was cooled down. The oven was lowered to its initial position and the sample basket containing the remaining sample was weighed in an external balance.

4.2.4. Data analysis

Figure 4.3A shows an example of the raw mass and temperature data obtained during a test. The voltage readout of the balance was translated via a calibrated linear relation to mass. The data was obtained for a sample of wood impregnated with KOH at 9.5 wt.%. At time t=0 s the wood sample was heated in a N_2 flow of 10 Nml/s at an average heating rate of 10 K/min. When the tem-

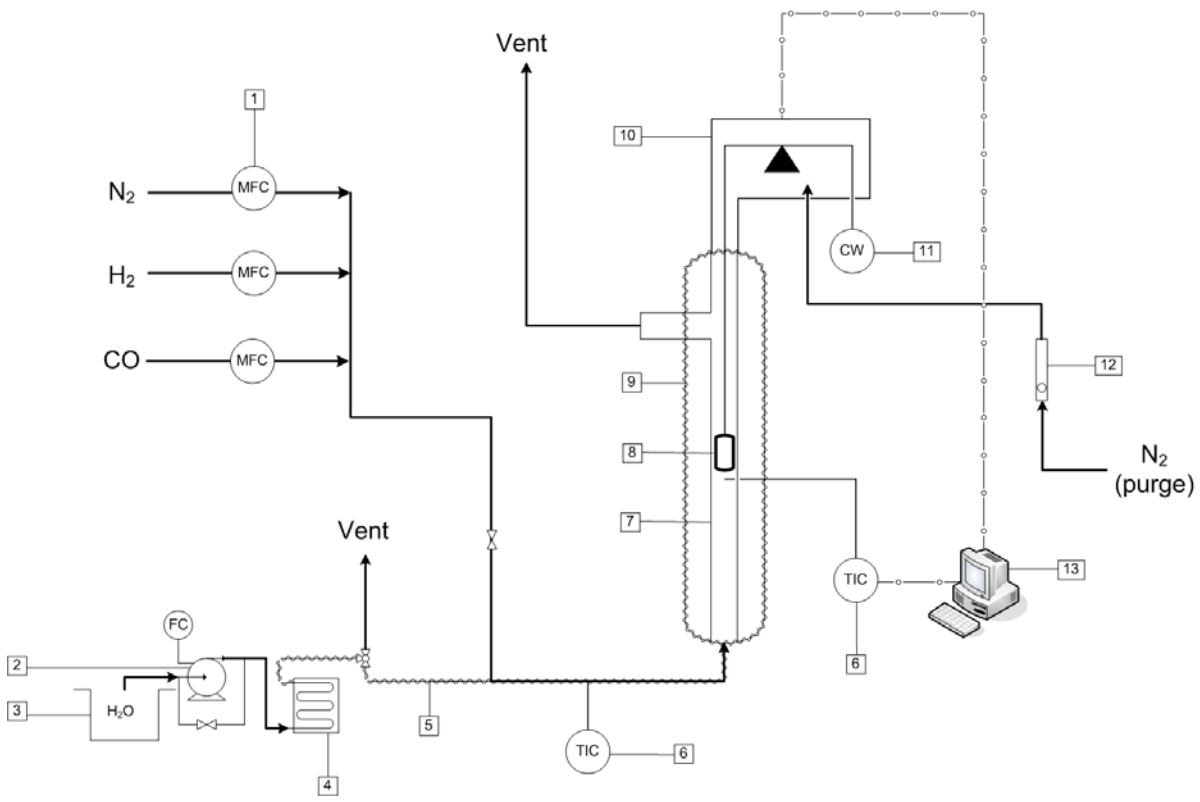

Figure 4.2. Char steam gasification set-up. 1.Mass flow controller (MFC), 2.HPLC pump with flow control (FC), 3.Water supply, 4.Water evaporator, 5.Heating element/Tracing, 6.Temperature Indicator/Controller (TIC), 7.Quartz tube, 8.Sample basket, 9.Oven, 10.Balance, 11.Counter weight (CW), 12.Rotameter, 13.Data logging.

perature of the sample reached the desired set point of 700°C (at t_{start}=4128 s for 700°C), the flow was switched to 10 Nml/s of steam. The char sample was then gasified isothermally at 700°C. Conversion was calculated by the following equation:

$$X = \frac{m_0 - m_t}{m_0 - m_{ash}} \qquad \text{(eq.4.1)}$$

where m_0 is the sample weight at time t_{start}=4128 s (time at which steam flow was switched on), m_t is the sample weight at time t and m_{ash} is the amount of ash remaining.

The calculated conversion of the char sample in steam is illustrated in Figure 4.3B (solid data points). For the tests with incomplete conversion, the experiment was stopped after 1300-1450 s. In this case, since the solid residue contained both carbon and ashes, m_{ash} used in eq.4.1 is the calculated amount of ash in the sample, based on the impregnated/mixed amount of additive and

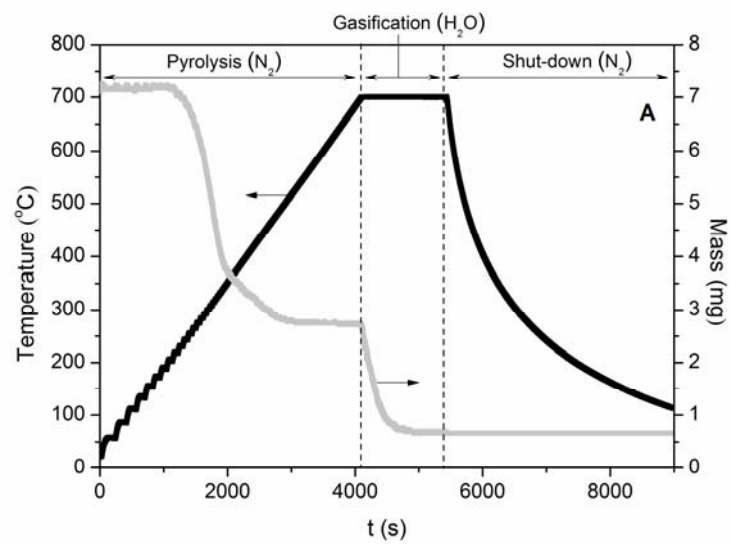

Figure 4.3. (A) Raw data output obtained during a char gasification experiment (wood+KOH, 9.5 wt.%- impregnated), **(B)** Conversion vs. time obtained from raw data (A) and fitted curves, **(C)** Conversion vs. time; example of incomplete conversion (wood+KOH, 9.5 wt.%-mixed).

the ash content of the wood itself. Figure 4.3C shows the calculated conversion (according to eq.4.1) in time (solid data points) as an example of an incompletely converted sample (wood mixed with KOH at 9.5 wt.%).
As can be seen from Figures 4.3B and 4.3C, the balance gave inaccurate weight changes at high(er) conversions (because of low conversion rates) which resulted in the occurrence of horizontal regions in the conversion versus time curve. In order to present the data more elegantly, fitted polynomial trendlines (6^{th} order) are shown instead of the "raw" conversion data (grey line in Figure 4.3B) to improve readability of the figures. Some data sets could not be described accurately enough with a polynomial. In those cases, a manual fit is chosen to represent the "raw" conversion data. (see Figure 4.3C).
In order to compare the measured conversions versus time curves, on the basis of a single number, the first order rate constant was determined. This was done by fitting the "raw" conversion data to a first-order reaction equation (see Figure 4.3B for an example):

$$X = 1 - e^{-kt} \qquad \text{(eq.4.2)}$$

In case of incomplete conversion, only the initial slope of the data curve (conversion range X= 0.2-0.7) was taken into account for the exponential fit (see Figure 4.3C). Hence, we are comparing initial (low conversion) first order rate constants. These rate constants are shown in the legend of the conversion versus time plots.
Because ca. 200 particles were used in each TGA test, the measured conversion is an averaged value over all the particles. Hence, if overall first order conversion behavior was observed, this could mean that indeed every individual particle reacted according to a first order or that we e.g. observed the average of a distribution of particles reaction according to different zero order rates.

4.2.5. Kinetics measurements

Some tests were done in order to exclude external and internal mass transfer limitations from our system and thus to verify that measurements were in the kinetically controlled regime. In these tests, the steam flow was varied (1, 5 and 10 Nml/s) to check for external mass transfer limitations from the steam flow to the bed, the bed height was varied (5 and 10 mg) to check for interparticle mass transfer limitations and the char particle size was varied (80 and

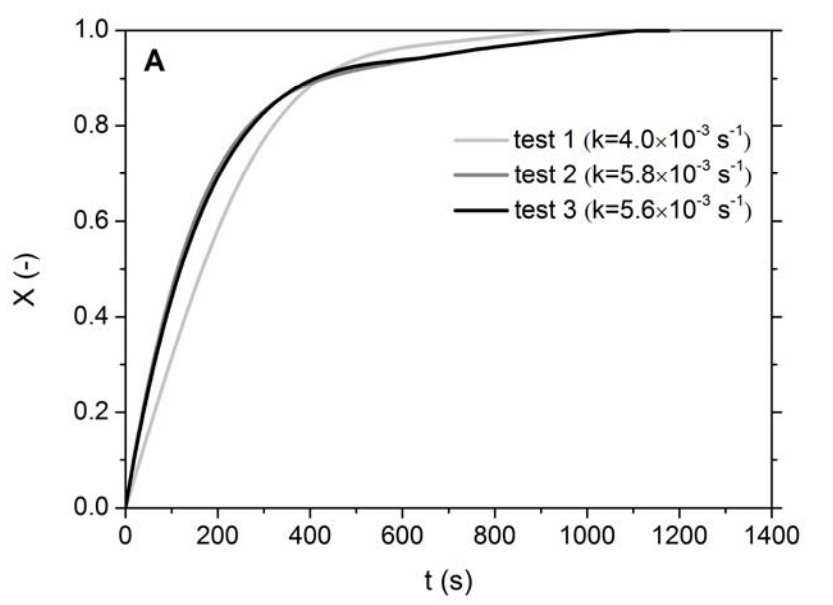
A
test 1 (k=4.0×10-3 s-1)
test 2 (k=5.8×10-3 s-1)
test 3 (k=5.6×10-3 s-1)
X (-)
t (s)
0.0
0.2
0.4
0.6
0.8
1.0
0
200
400
600
800
1000
1200
1400

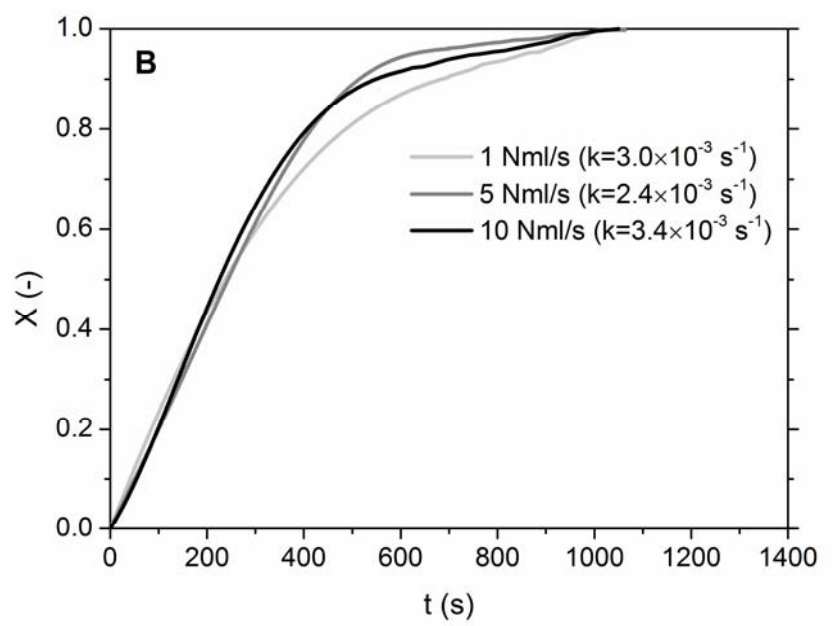
B
1 Nml/s (k=3.0×10-3 s-1)
5 Nml/s (k=2.4×10-3 s-1)
10 Nml/s (k=3.4×10-3 s-1)
X (-)
t (s)
0.0
0.2
0.4
0.6
0.8
1.0
0
200
400
600
800
1000
1200
1400

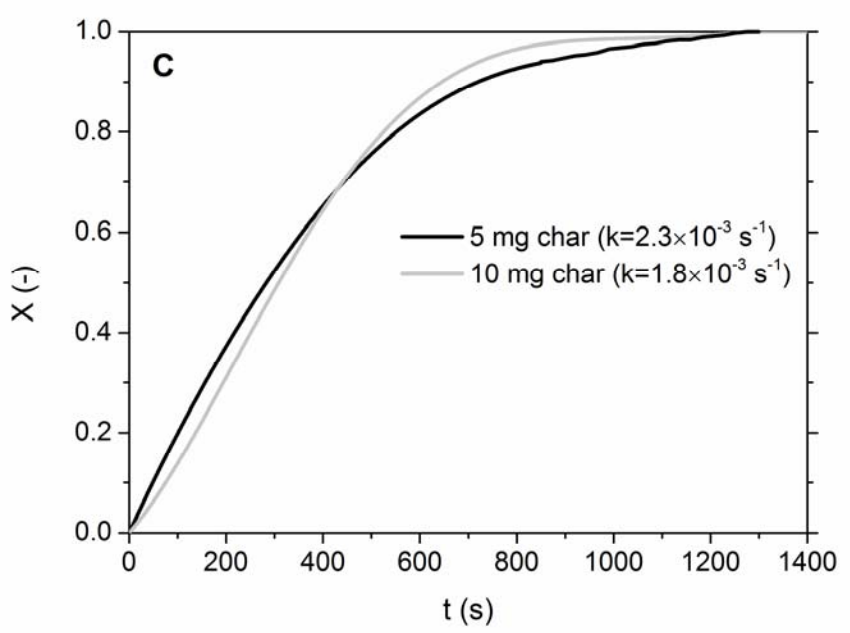
C
5 mg char (k=2.3×10-3 s-1)
10 mg char (k=1.8×10-3 s-1)
X (-)
t (s)
0.0
0.2
0.4
0.6
0.8
1.0
0
200
400
600
800
1000
1200
1400

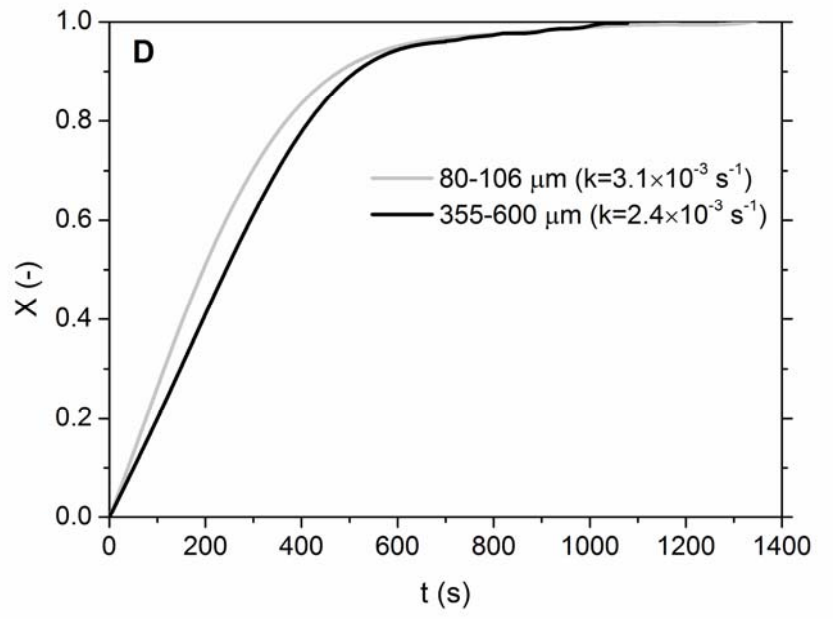

Figure 4.4. (A) Reproducibility of experiments for char conversion. The repeated sample is wood impregnated with 9.5 wt.% KOH, gasified in 10 Nml/s steam flow at 700° C. The chars were made by heating up the sample in N_2 at a heating rate of 10 K/min up to 700°C, **(B)** Effect of steam flow variation on char conversion. Particle size range = 355-600μm, **(C)** Effect of initial char sample weight on char conversion. Steam flow = 10 Nml/s, **(D)** Effect of char particle size range on char conversion. Steam flow = 5 Nml/s. The chars in (B), (C) and (D) were made *externally* by heating up wood+KOH (9.5 wt.%-impregnated) in N_2 to 700°C.

355 μm) to check for intra-particle mass transfer limitations. In order to interpret these tests, first the reproducibility was checked. Figure 4.4A shows a typical example of a triple test. Analysis of such triple test led to an estimate of accuracy for the first order rate constant of +/- 25% (on standard deviation).
Figure 4.4B shows the conversion versus time curve of char (d_p=355-600μm) from wood impregnated with 9.5 wt.% KOH with varying steam flow. The values obtained in this case for the first order reaction constant k according to eq.4.2 was within the experimental accuracy as determined previously. Therefore, from these results we excluded external mass transfer limitations (steam flow to fixed bed).
Figure 4.4C shows the conversion versus time plot of char from wood impregnated with 9.5 wt.% KOH with varying initial char sample weight, i.e. bed height. Also these results were within the deviation calculated for repeated experiments and therefore we concluded that our experimental results are free of inter-particle mass transfer limitations. Calculation of the bed's Thiele modulus (φ) and the effectiveness factor (η) for typical experimentally observed

overall rates showed that φ=0.18 and η=0.99. In this calculation, it was assumed that there were no external mass transfer limitations from the steam flow to the fixed bed and that the steam diffused into the bed from both the top and bottom at equal rates. These calculations are given in Appendix C at the end of this Chapter. Even if the reaction becomes a factor 4 faster, then the effectiveness factor is still η>0.95.

Figure 4.4D presents the conversion versus time curve of char from wood impregnated with 9.5 wt.% KOH with varying char particle size range. The 355-600 μm particle size range is more relevant to the rest of our obtained data because about 40 wt.% of the char consists of this range of particle size. The smaller particle size range (80-106 μm) corresponds to less than 2.5 wt.% of the char. There is no significant difference between the two measured conversions and therefore we can exclude intra-particle mass transfer limitations.

Overall, we concluded that the measurements do not suffer from mass transfer limitations.

4.3. Results and Discussion

4.3.1.Effect of ash component type

We tested ten different additives for their steam gasification reactivity at 700° C. The ash components were impregnated before pyrolysis and all the samples had an initial metal/carbon (mol) ratio of ~0.05 (in wood). Conversion versus time curves are shown in Figures 4.5A and 4.5B for the various samples. According to our results, the catalytic activities are ranked as (in decreasing order): KNO_3 > $KHCO_3$ ≈ K_2CO_3 ≈ KOH > NaOH > CaO > K_2HPO_4 > KBr > KCl > no additive > Fe_2O_3. This is in agreement with earlier reported results on coal and biomass derived char [6, 7 ,12, 15].

According to Yuh et. al [40] the limited catalytic effect of KCl is low due to the strength of the potassium-chloride bond. Lang [11] discusses that the catalytic activity of any salt is the result of a competition between its cation and its anion to form the initial salt or to form an active gasification site on the char's surface. The presence of strong-acid anions such as chloride does not favor the cation-char surface interaction, but rather the formation of the initial salt [11]. Yuh et al. [15] proposed that the active gasification site is a carbonate, which they could detect by FT-IR spectroscopy. Calculations of the Gibbs free energy of the involved reactions indeed revealed that carbonate salt is the favored state for: KNO_3, $KHCO_3$, K_2CO_3, KOH, NaOH and CaO. The rest of the addi-

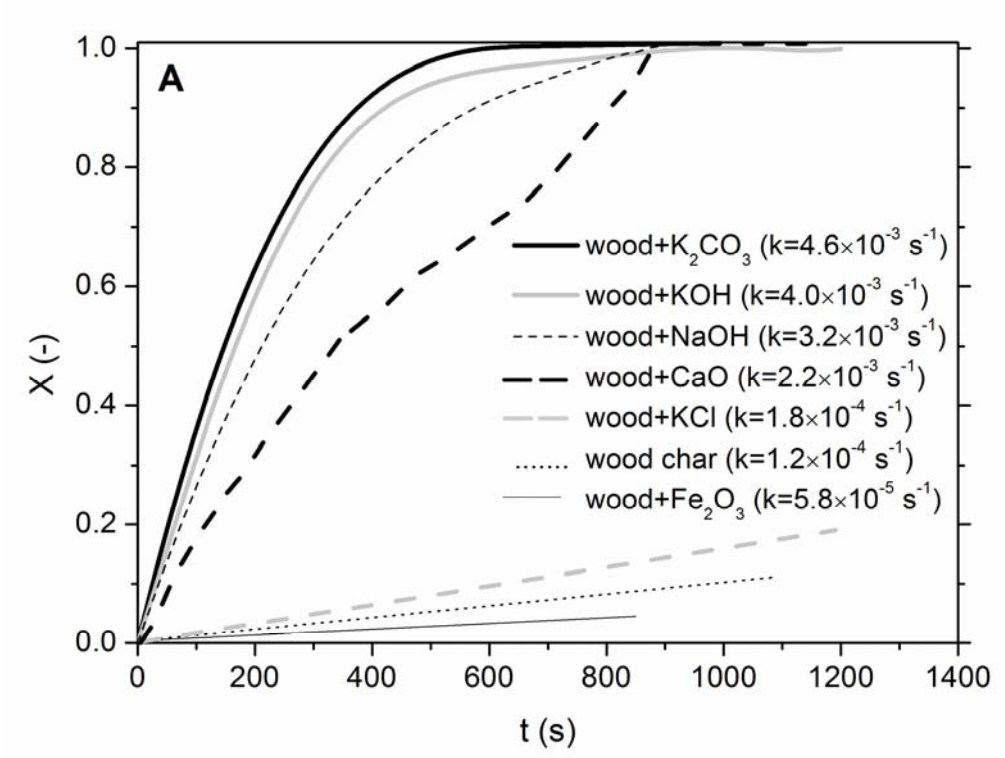

Figure 4.5. Effect of different inorganics on wood char conversion at T=700°C and P_{H2O}=1 bar. **(A)** Potassium, sodium, calcium and iron additives and **(B)** Other potassium additives. The chars were made by heating up the sample in N_2 at a heating rate of 10 K/min up to 700°C. M/C (in wood) (mol/mol) = 0.05.

tives (K_2HPO_4, KBr, KCl, Fe_2O_3) remain essentially in their original form according to thermodynamics. Wood ash contains K and Ca (see Table 4.2), mostly as carbonate among other oxide forms [41], which should indicate that wood ash enhances the steam gasification reaction like the tested K and Ca hydroxides and carbonates. KNO_3 seems to result in the highest initial conversion rate, although it can form the same stable carbonate salt as KOH, K_2CO_3 and $KHCO_3$. This component, though, also contains nitrogen which could transform to gaseous/volatile nitrogen compounds during reaction and, thus, could be demonstrated as higher weight loss rate in the TGA.

4.3.2. Effect of temperature

Among K_2CO_3, $KHCO_3$ and KOH, which had similar conversion rates, KOH was chosen. The effect of pyrolysis and subsequent gasification temperature was studied in the range of 600-800°C for char samples from wood+KOH (9.5 wt.%-impregnated). The first order rate constants (k) were calculated from eq.4.2 in section 4.2.4 and the obtained Arrhenius plot is shown in Figure 4.6. The activation energy was calculated by the slope of the obtained linear fit and was equal to E_a=137 kJ/mol. This value is in the lower range of literature values (94 and 198 kJ/mol) reported for catalytic gasification of wood char with K_2CO_3 [28, 29], which are comparable since the conversion rates of K_2CO_3 and KOH are similar. At 800°C, 95% conversion is achieved within 4.1 min compared to 8.8 min at 700°C. At 600°C, 40% conversion is reached within 17.5 min.

4.3.3. Catalytic potential of wood and straw ash

Figure 4.7 presents the conversion vs. time plot for wood- and straw-derived char and char from wood impregnated (before pyrolysis) with two different concentrations of wood ash. The concentration of (wood) ash in the wood sample is defined as the whole ash present in the wood. This includes water-reactive/soluble and water-insoluble components (see Table 4.2).

Clearly, impregnation of ash increases the steam gasification rate of pine wood char. Impregnated wood ash increased char reactivity by a factor 15. This is in agreement with results by Timpe et al. [5] for coal who showed that coal char reactivity increased by a factor 20 by mixing it with the aqueous extract of wood ash. Results by Hauserman [37] are comparable and showed that a load-

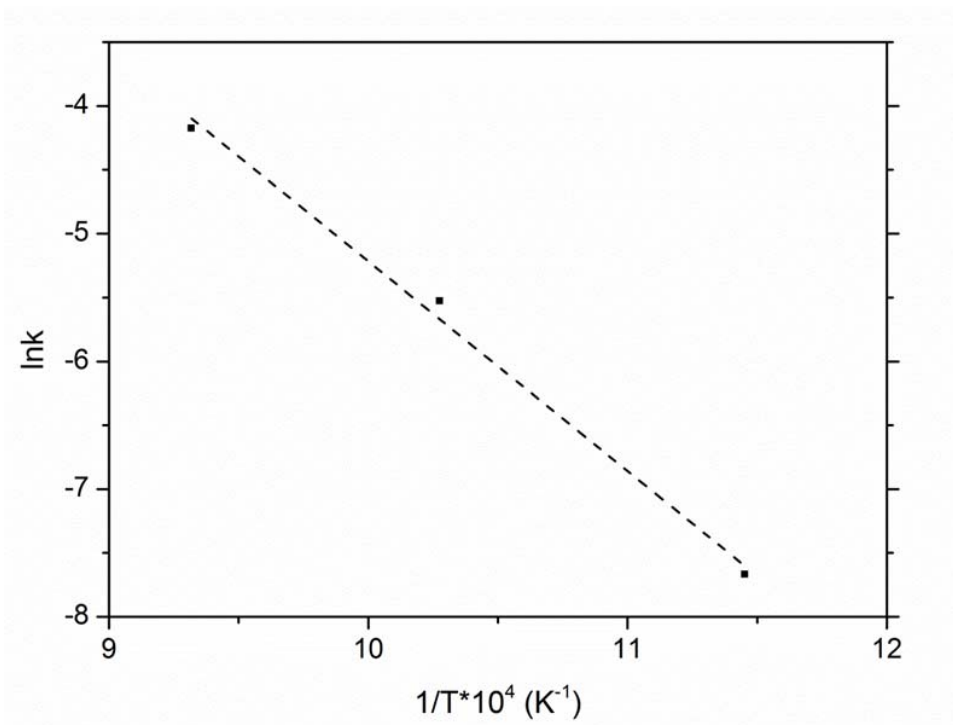

Figure 4.6. Arrhenius plot for gasification of char from wood+KOH (9.5 wt.%-impregnated) at P_{H2O}=1 bar. The chars were made by pyrolysis of the sample in N_2 at a heating rate of 10 K/min up to the desired gasification temperature (600-800°C).

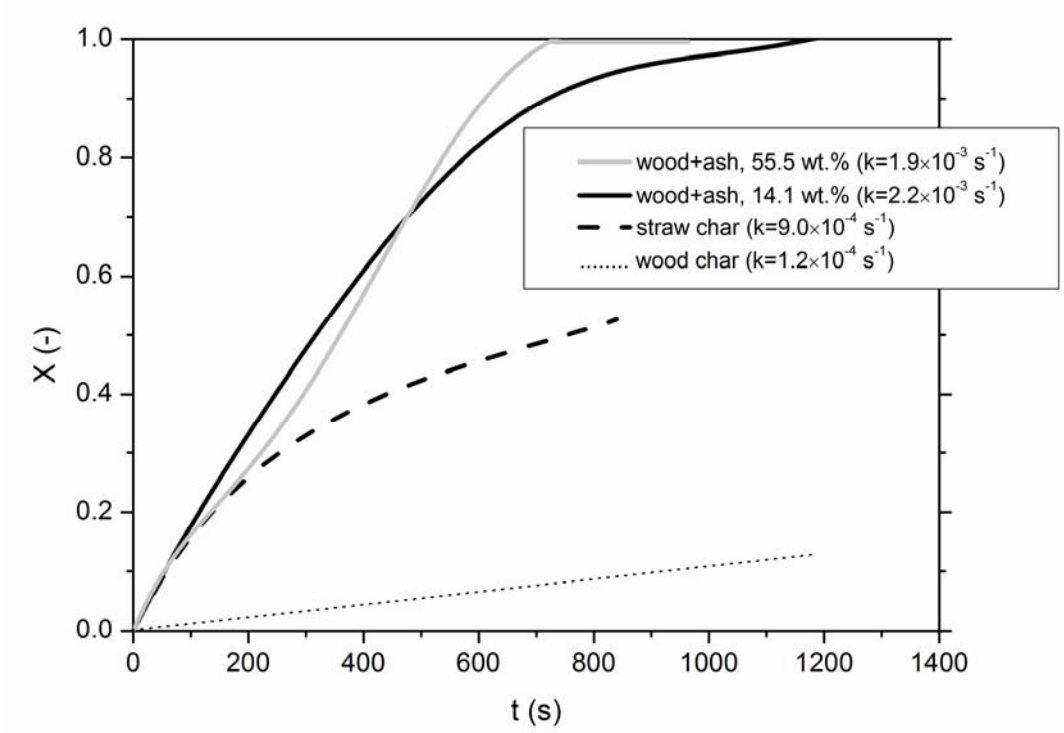

Figure 4.7. Effect of ash concentration/composition on char conversion at T=700°C and P_{H2O}=1 bar. The chars were made by heating up the sample in N_2 at a heating rate of 10 K/min up to 700°C.

ing of 10 wt.% wood ash on wood increased its reactivity in steam by a factor 32 at 700°C. Wood ash demonstrates a similar conversion path to that of CaO (see Figure 4.5A) and this can be explained by the fact that Ca is the most abundant component in wood ash (see Table 4.2).

Also ash that occurs naturally in the biomass seems to have an effect on char reactivity. Straw with an ash content of 5.3 wt.% has a clearly higher initial steam gasification rate compared to pine wood with 0.4 wt.% ash. However, in the case of straw char the gasification rate decreases above 20% conversion. It is known that ashes in biomass are not uniformly distributed. Especially concerning K and Ca distribution, Frömm [42] has shown that these two elements occur in different concentrations depending on the type of tissue of the developing biomass. K concentrations are highest in the developing cells whereas Ca occurs mostly in the bark of the plant.

Superposition of regions (in the straw ash) with high(er) ash content and thus high(er) rate with regions of low(er) ash content and thus low(er) rate could result in the observed conversion profile of straw char. It is plausible, that next to the amount of ash, also the distribution of ash (components) in the char (distribution of active sites) is important. This will be investigated further in the next sections.

For coal char it was found that chlorine inhibits the catalytic effect of Na_2CO_3 [40]. We did experiments with a mixture of wood ash and KCl impregnated in wood and did not observe this inhibition.

4.3.4. KOH addition method

Figure 4.8 shows the effect of the initial KOH loading on the steam gasification reactivity of wood-derived char. Please remember that the reported loadings were measured from samples of 1 g and that the loading of individual particles or the averaged loadings of TGA batches may have differed considerably, up to 50% of the 1-g samples.

Clearly, KOH impregnation of wood has a substantial effect on the reactivity of the produced char. A 1.6 wt.% KOH loading already increases the initial rate considerably; the initial first order rate constant increases by more than a factor 10 compared to char only. However, beyond a conversion of ca. 30% the gasification rate drops considerably to a value close to the one of char. Increasing the KOH loading to 9.5 wt.% increases char reactivity further (~30 fold increase of the first order rate constant compared to char only). For the highest

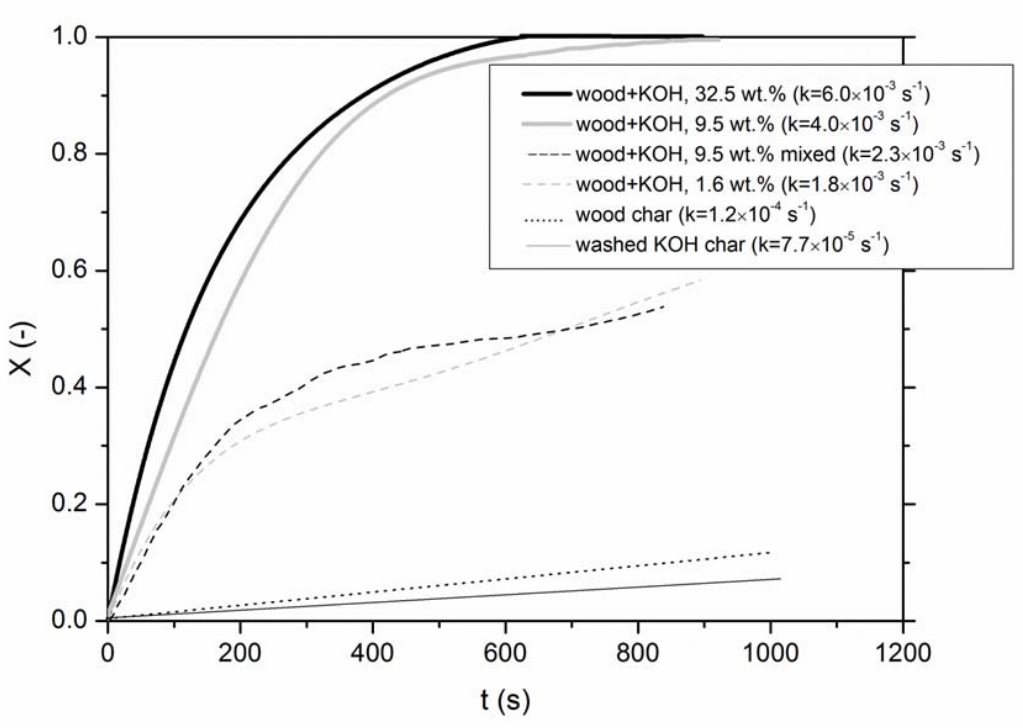

Figure 4.8. Effect of initial KOH loading on char reactivity at T=700°C and P_{H2O}=1 bar. The "washed KOH char" is a char that was produced from KOH-impregnated wood (9.5 wt.%) and was then washed in distilled water to remove the salts. Potassium loadings refer to the initial wood sample (1-g sample average). The chars were made by heating up the sample in N_2 at a heating rate of 10 K/min up to 700°C.

loadings (9.5 and 32.5 wt.%) the increased reactivity is maintained over the whole conversion regime and complete conversion is reached in about 12 minutes at 700°C. There is no significant difference between the samples of 9.5 and 32.5 wt.% KOH. From these experiments it may appear that the (initial) metal loading is the most important parameter, as suggested by Hauserman [37], in determining the conversion rate. Hauserman showed that the reactivity of wood increases with increasing K/C ratio with a level-off occurring at a ratio of about 0.1. However, in the research of Hauserman it is not clearly stated which salt addition method was used.

Below it is reasoned why the loading is not the only important parameter. In the trajectory towards complete conversion, the KOH loading of the char sample increases. For instance, the sample with an initial loading of 1.6 wt.% in wood (M/C in char = 0.023) has a loading of M/C = 0.149 in the char (corresponding to 9.5 wt.% in the wood) at a conversion of 0.84.

If the actual KOH loading is the only parameter that determines the conversion rate, the conversion rate should increase as the conversion increases. We

have not observed this, on the contrary, the rate decreases as the loading increases which is most clearly seen from the 1.6 wt.% KOH test. Our hypothesis is that next to the loading, also the distribution in and/or over (amongst) the char particles is important. A poor potassium distribution would lead to a poor distribution/availability of potassium activated gasification sites.

Because of the complexity of the multiple particle system studied and the impregnation method it is not (yet) possible to say whether intra or inter particle KOH loading distributions are more important. In Figure 4.8 results of tests designed to study the effect of metal loading distribution are reported.

One char (9.5 wt.% KOH in wood) was prepared by impregnating the KOH into the wood and the other char is prepared by dry mixing the same amount of KOH with the wood prior to pyrolysis. It is assumed that in the case of dry mixing the KOH, this is less well distributed in and over the particles [see Figure 4.10]. The impregnated char reaches 100% conversion at 900 s, while the mixed char conversion at that time is only 50%. Though, the initial first order rates of the chars do not differ that much; 4.0×10^{-3} vs. 2.3×10^{-3} s^{-1} for impregnated and mixed KOH, respectively. The activity of potassium, even when physically mixed, has been ascribed to its mobility on the char surface [10]. Potassium has a positive effect in the initial stages of gasification ($X<0.25$), but this is not the case at higher conversions. Assuming that potassium is mobile on the char surface, this does not seem to have the same result after a certain conversion level.

Figure 4.9 shows the difference obtained in reactivity when impregnating with the same concentration of KOH (on basis of C in char) before and after pyrolysis of the sample. Also in this case, it is obvious that not only the potassium loading determines the conversion rate because at high conversion the conversion rates clearly differ. Adding the potassium before pyrolysis results in higher conversion rates above 40% conversion. When wood is impregnated with KOH and then pyrolyzed, higher char yields are obtained and the char produced is more reactive than char from wood only, as was observed in Chapter 3. Increased char yield when impregnating wood with KOH before pyrolysis has also been demonstrated by others [43]. However, the actual mechanism and effect of K on pyrolysis is still debatable. The increase of char is at the expense of vapor formation and will likely result in an overall lower (heavy) tar

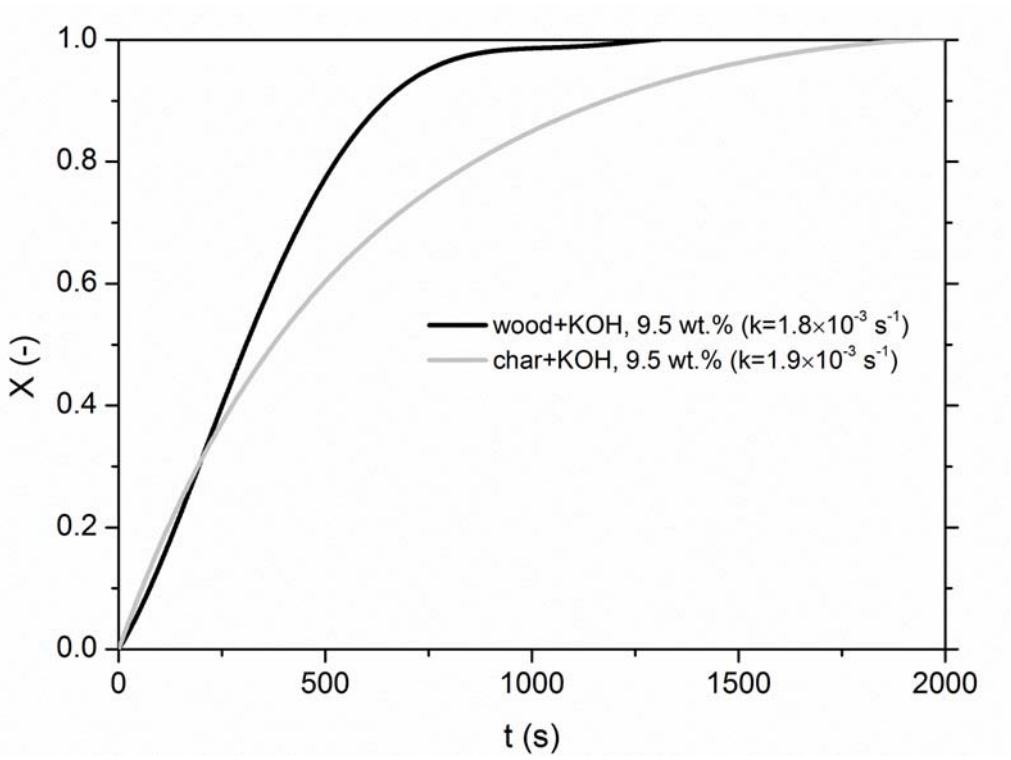

Figure 4.9. Effect of KOH impregnation (9.5 wt.%) before and after pyrolysis. The chars were made *externally* by heating up wood(+KOH) in N_2 to 700°C.

formation [43-45] which is an advantage for tar conversion and/or down-stream gas cleaning.

4.3.5. Char morphology (SEM)

Figure 4.10 presents the SEM images of six char samples produced from wood with different KOH loading and from wood impregnated with (wood) ash prior to their reaction in steam. All images on the right in Figure 4.10 are magnifications of the images on the left.

Figure 4.10A shows an image of wood char where it can be noted that the structure of the original wood is preserved. The same is valid for the char sample from wood impregnated with 1.6 wt.% KOH (Figure 4.10B). However, impregnating (Figure 4.10C) or mixing (Figure 4.10D) 9.5 wt.% KOH in wood, causes a drastic change in char structure and volume, creating a swollen, sponge-like matrix. Researchers have shown that KOH works as an activating agent for producing activated carbons with high surface areas both when mixing and impregnating the KOH into the carbon-containing substrate [46, 47] creating similar structures as observed in Figure 4.10 [48, 49]. The general mechanism of this chemical activation is not well understood and various

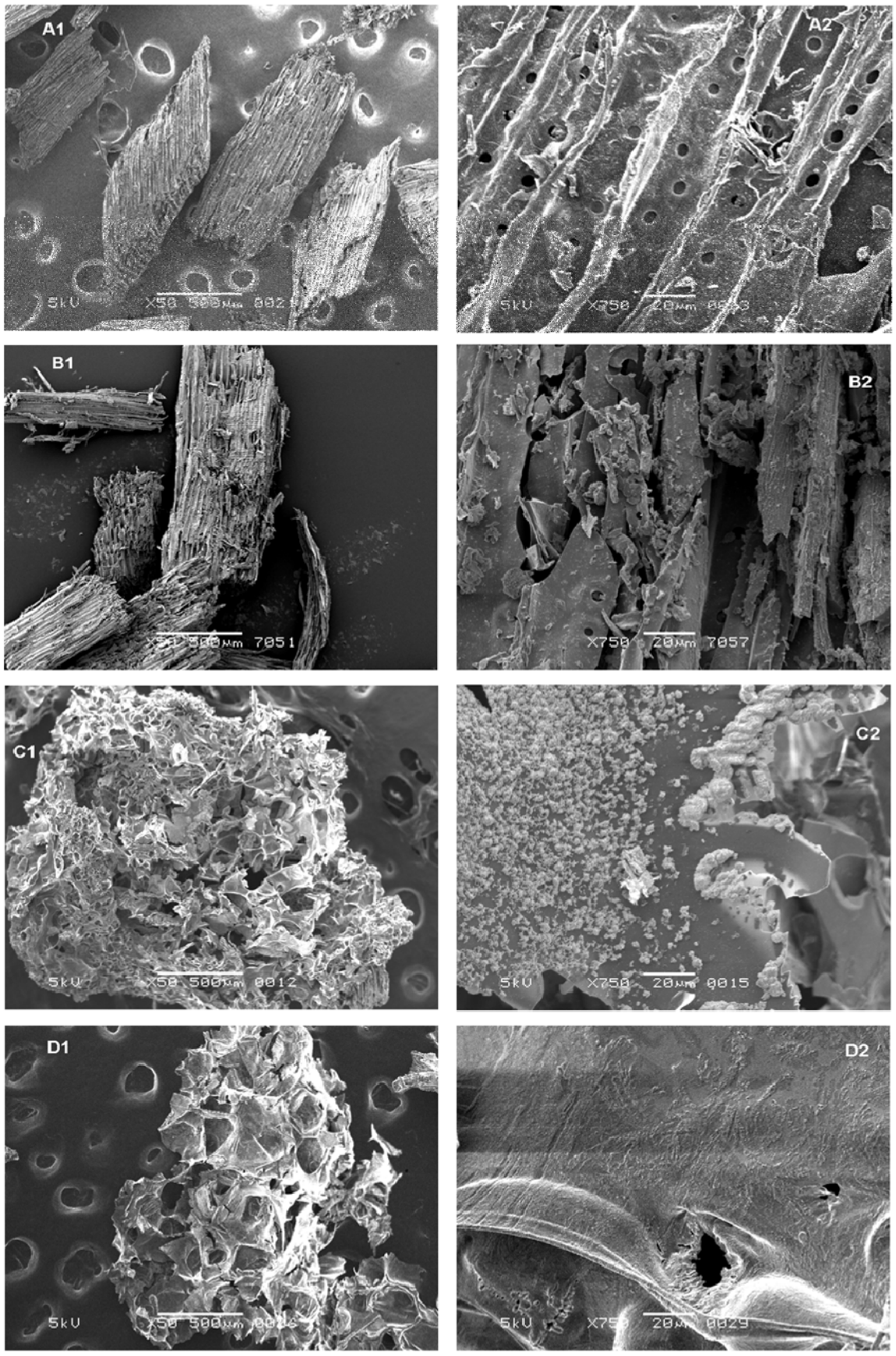
A1
5kU X50 500µm 0021
A2
5kU X750 20µm 0023
B1
X50 500µm 7051
B2
X750 20µm 7057
C1
5kU X50 500µm 0012
C2
5kU X750 20µm 0015
D1
5kU X50 500µm 0018
D2
5kU X750 20µm 0029

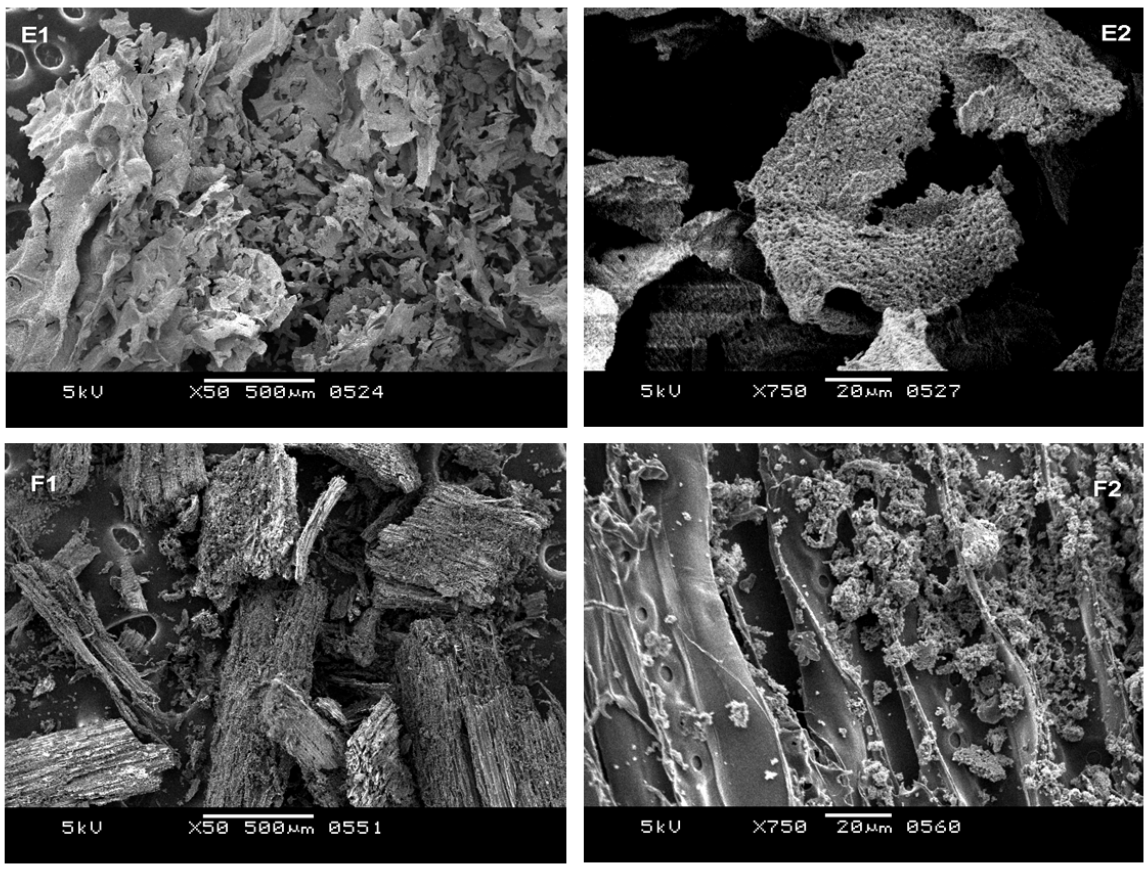

Figure 4.10. SEM images of char from wood and KOH-impregnated wood, made at 700°C with a heating rate of 10 K/min in N_2 flow: **(A)** wood-derived char, **(B)** wood+KOH, 1.6 wt.% (impregnated), **(C)** wood+KOH, 9.5 wt.% (impregnated), **(D)** wood+KOH, 9.5 wt.% (mixed), **(E)** wood+KOH, 32.5 wt.% (impregnated) and **(F)** wood+(wood) ash, 14.1 wt.% (impregnated). Images on the right (A2 to F2) are magnifications of the corresponding images on the left (A1 to F1). Background interference appearing as dark spots is caused by thermal degradation of the adhesive tape used during drying in a vacuum oven prior to analysis.

studies available demonstrate the complexity of this process [46, 50]. BET surface area measurements of wood char (Figure 4.10A) and char from 9.5 wt.% KOH-impregnated wood (Figure 4.10C) revealed that the surface area is 400 m^2/g for the first and 11 m^2/g for the latter. This lower measured surface area for char from impregnated wood could be caused by pore blockage due to incomplete carbon activation. The KOH-impregnated char was also washed in order to remove the salts and the structure remained intact, but the gasification rate dropped to values equal to the original wood char (see Figure 4.8). Therefore, the change in structure of the char does not influence the obtained gasification rates, which are only related to an effect of the added KOH.

In Figure 4.10, the lighter regions or spots in the magnified images (on the right) are assumed to be the salt under investigation. From the magnified images (A,B,C and E) of the samples with increasing KOH loading it can be observed that the salt distribution differs per sample. The distribution of salt visible in these SEM images is the surface distribution, whereas there is probably also a salt distribution inside the particle. The surface loading of KOH (salt) changes from single spots at 1.6 wt.% to a fully covered surface at 32.5 wt.%.
In the case of Figure 4.10D where KOH is added to the wood (at 9.5 wt.%) there is no salt identified in the magnified image (Figure 4.10D2). Probably in this case, a uniform layer of potassium exists on the char surface rather than a salt surplus identified as crystals.
Figure 4.10F2 indicates that also for impregnated wood ash a clear distribution of the salt occurs in the char particle. In this case, no swelling of the char particles occurred, something which appears to be a property of KOH in this concentration range.
Overall, we can conclude that next to the ash loading also the ash distribution is important. Impregnation of the wood before pyrolysis results in a better distribution/availability of active sites than mixing with the wood or impregnation of the char (after pyrolysis).
For impregnation, a minimum amount of ash is needed (corresponding to a loading between 1.6 [M/C=0.023] and 9.5 wt.% KOH [M/C=0.149]). Above this amount, there is locally always sufficient ash (active sites) to achieve high conversion rates throughout the whole conversion range. Below this amount, regions exist with (too) low ash loading resulting in low conversion rates. This is also demonstrated in the results obtained by Hauserman [37].
Wood contains a very low amount of ash (0.4 wt.%) and this indicates that a large ash recycle would have to be used in the process to reach the desired ash loading in the feed. If ash-rich biomass is used as feedstock (e.g. straw) then a smaller ash recycle will be needed.

4.3.6. Effect of steam pressure and inhibition by CO and H_2

During the steam gasification of char in a large-scale gasifier also CH_4, CO_2, CO and H_2 are present. There is evidence from coal and biomass research that the latter two compounds (CO+H_2) can strongly inhibit char steam gasification. These gases probably interact with active gasification sites on the substrate surface blocking them from steam gasification [17, 36]. Inhibition of CO

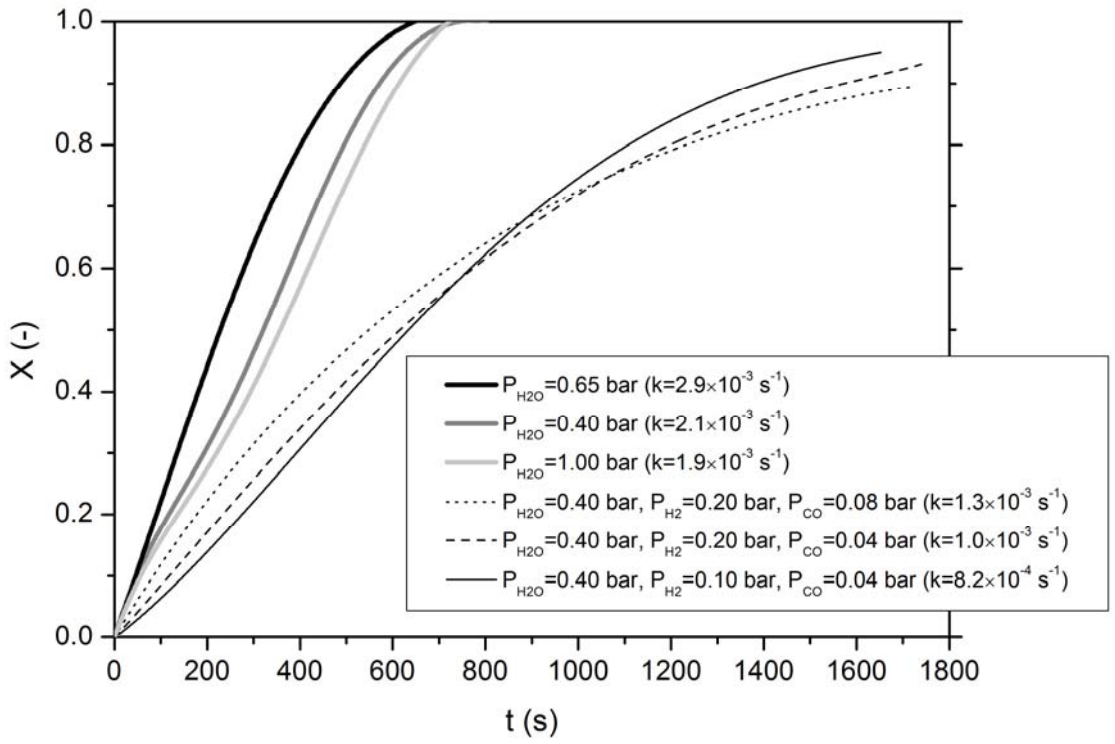

Figure 4.11. Effect of steam pressure and syngas concentration on conversion of char made from wood impregnated with 55.5 wt.% (wood) ash. P_{tot}=1 bar, the rest is N_2. The chars were made by heating up wood+ash (impregnated) to 700°C with a heating rate of 10 K/min in N_2 flow.

and H_2 was investigated in steam gasification of char made from ash-impregnated wood (55.5 wt.%).

Figure 4.11 shows that variation of steam pressure in the range 0.4-1.0 bar does not provide a clear trend. Therefore, we conclude that there is no essential effect of steam pressure in this pressure range.

It is evident that syngas strongly inhibits char steam gasification; the initial gasification rate is lowered by about a factor 2 in the presence of syngas. Additionally, variation of either CO or H_2 partial pressures of the syngas mixture had a negligible effect on char reactivity and therefore, inhibition seems already saturated at low CO/H_2 concentrations. Our result on hydrogen inhibition is not in agreement with results obtained by other authors for similar hydrogen partial pressures who showed that hydrogen inhibition on biomass char steam gasification increases with increasing hydrogen partial pressure (P_{H2} = 0 - 0.20 bar [26], P_{H2} = 0 - 0.30 bar [30], P_{H2} = 0 - 0.25 bar [36]). These results are for inhibition under noncatalytic steam gasification conditions and are also realized at higher temperatures (800-850°C).

Findings by Walker et al. [16] on effects of hydrogen and carbon monoxide on catalytic coal char steam gasification at 850°C show that carbon monoxide inhibits catalysis by Ca^{+2}, K^{+} and Na^{+}, whereas hydrogen inhibits only catalysis by calcium (P_{H2} = 0.73-0.97 bar, P_{CO} = 0.24-0.97 bar).

4.4. Conclusions

The steam gasification of wood-derived char was studied in a vertical thermogravimetric analyzer. Investigated parameters include: presence of ash components, their concentration and addition method as well as type of ash components. Inhibition by syngas ($CO+H_2$) was also studied. The main conclusions can be summarized as follows:

- Biomass gasification can be catalytically enhanced by its own ash
- The use of biomass feedstock with high ash content seems promising
- Char can be completely gasified within 12 min at 700°C
- Except for ash loading, also ash distribution inside and among biomass char particles proves to be important for obtaining enhanced gasification rates
- Impregnation of the ash before pyrolysis results in the highest overall conversion rates; a minimum loading is needed corresponding to a KOH amount between 1.6 and 9.5 wt.%
- The presence of low concentrations of CO and H_2 in the gasifier can inhibit char gasification by a factor 2, but the effect seems constant.

Notation

E_a	=	activation energy, kJ/mol
H	=	height, mm
k	=	reaction rate constant, s^{-1}
m_0	=	initial sample weight, mg
m_{ash}	=	amount of ash in sample, mg
m_t	=	sample weight at time t, mg
OD	=	outside diameter, mm
P	=	pressure, bar
t	=	reaction time, s
t_{start}	=	time at which steam flow is switched on and reaction is initiated, s
X	=	conversion of char; raw conversion data by eq.4.1 and exponential fit by eq.4.2

Greek symbols

η	=	effectiveness factor
φ	=	Thiele modulus

Abbreviations

CW	=	Counter Weight
FC	=	Flow Control
FT-IR	=	Fourier Transform Infrared
HPLC	=	High-Pressure Liquid Chromatography
M/C	=	metal over carbon molar ratio; defined as the moles of metal (M^+) mixed with or impregnated in the biomass, divided by the moles of carbon present in the biomass and the metal
MFC	=	Mass Flow Controller
SEM	=	Scanning Electron Microscopy
TGA	=	Thermogravimetric Analyzer/Analysis
TIC	=	Temperature Indicator/Controller
XRF	=	X-Ray Fluorescence spectrometry

Literature cited

1. Exxon Catalytic Coal Gasification-Process Development Program. Final Project Report; Technical Report, Nov. 1, **1981**.

2. Mims C.A., Pabst J.K., Alkali catalyzed carbon gasification. I. Nature of the catalytic sites, *Prepr. Am. Chem. Soc. Div. Fuel Chem.* **1980**, 25, 258–262.

3. Veraa M.J., Bell A.T., Effect of alkali metal catalysts on gasification of coal char, *Fuel* **1978**, 57, 194-200.

4. McKee D.W., Spiro C.L., Kosky P.G., Lamby E.J., Catalysis of coal char gasification by alkali metal salts, *Fuel* **1983**, 62, 217-220.

5. Timpe R.C., Kulas R.W., Hauserman W.B., Catalytic effect on the gasification of a bituminous Argonne premium coal sample using wood ash or tarconite as additive, *Prepr. Am. Chem. Soc. Div. Fuel Chem.* **1991**, 36, 892-897.

6. Liu Z.-liang, Zhu H.-hui, Steam gasification of coal char using alkali and alkaline-earth metal catalysts, *Fuel* **1986**, 65, 1334-1338.

7. Kayembe N., Pulsifer A.H., Kinetics and catalysis of the reaction of coal char and steam, *Fuel* **1976**, 55, 211-216.

8. McKee D.W., Chatterji D., The catalyzed reaction of graphite with water vapor, *Carbon* **1978**, 16, 53-57.

9. Köpsel R., Zabawski H., Catalytic effects of ash components in low rank coal gasification. 2. Gasification with steam, *Fuel* **1990**, 69, 282-288.

10. Lang R.J., Neavel R.C., Behaviour of calcium as a steam gasification catalyst, *Fuel* **1982**, 61, 620-626.

11. Lang R.J., Anion effects in alkali-catalysed steam gasification, *Fuel* **1986**, 65, 1324-1329.

12. McKee D.W., Gasification of graphite in carbon dioxide and water vapor-The catalytic effects of alkali metal salts, *Carbon* **1982**, 20, 59-66.

13. McKee D.W., Spiro C.L., Kosky P.G., Eutectic salt catalysts for graphite and coal char gasification, *Fuel* **1985**, 64, 805-809.

14. Guo C.-tao, Zhang L.-ming, Kinetics of coal char gasification at elevated pressures, *Fuel* **1986**, 65, 1364-1367.

15. Yuh S.J., Wolf E.E., FTIR studies of potassium catalyst-treated gasified coal chars and carbons, *Fuel* **1983**, 62, 252-255.

16. Walker Jr., P.L., Matsumoto S., Hanzawa T., Muira T., Ismail I.M.K., Catalysis of gasification of coal-derived cokes and chars, *Fuel* **1983**, 62, 140-149.

17. Hüttinger K., Minges R., The influence of the catalyst precursor anion in catalysis of water vapour gasification of carbon by potassium. 2. Catalytic

activity as influenced by activation and deactivation reactions, *Fuel* **1986**, 65, 1122-1128.

18. Schumacher W., Mühlen H.-J., van Heek K.-H., Jüntgen H., Kinetics of K-catalysed steam and CO_2 gasification in the presence of product gases, *Fuel* **1986**, 65, 1360-1363.

19. McKee D.W., Mechanisms of the alkali metal catalysed gasification of carbon, *Fuel* **1983**, 62, 170-175.

20. Mims C.A., Pabst J.K., Role of surface salt complexes in alkali-catalysed carbon gasification, *Fuel* **1983**, 62, 176-179.

21. Cerfontain M.B., Kapteijn F., Moulijn J.A., Characterization of alkali carbonate catalysts for carbon gasification with ^{18}O labeled CO_2, *Carbon* **1988**, 26, 41-48.

22. Chen S.G., Yang R.T., The active surface species in alkali-catalyzed carbon gasification: Phenolate (C-O-M) groups vs clusters (particles), *J. Catal.* **1993**, 141, 102-113.

23. Saber J.M., Falconer J.L., Brown L.F., Interaction of potassium carbonate with surface oxides of carbon, *Fuel* **1986**, 65, 1356-1359.

24. Yip K., Tian F., Hayashi J.-i., Wu H., Effect of alkali and alkaline earth metallic species on biochar reactivity and syngas compositions during steam gasification, *Energy Fuels* **2010**, 24, 173-181.

25. Marquez-Montesinos F., Cordero T., Rodríguez-Mirasol J., Rodríguez J.J., CO_2 and steam gasification of a grapefruit skin char, *Fuel* **2002**, 81, 423-429.

26. Kajita M., Kimura T., Norinaga K., Li C.-Z., Hayashi J.-i., Catalytic and noncatalytic mechanisms in steam gasification of char from the pyrolysis of biomass, *Energy Fuels* **2010**, 24, 108-116.

27. Encinar J.M., González J.F., Rodríguez J.J., Ramiro M.J., Catalysed and uncatalysed steam gasification of eucalyptus char: influence of variables and kinetic study, *Fuel* **2001**, 80, 2025-2036.

28. DeGroot W.F., Shafizadeh F., Kinetics of wood gasification by carbon dioxide and steam, Fundamentals of Thermochemical Biomass Conversion, International Conference Proceedings, Estes Park, CO, Oct 18-22, **1982**.

29. Hawley M.C., Boyd M., Anderson C., DeVera A., Gasification of wood char and effects of intraparticle transport, *Fuel* **1983**, 62, 213-216.

30. Barrio M., Gøbel B., Risnes H., Henriksen U., Hustad J.E., Sørensen L.H., Steam gasification of wood char and the effect of hydrogen inhibition on the chemical kinetics, Progress in Thermochemical Biomass Conversion; IEA Bioenergy, Cornwall, U.K., **2001**; Vol. 1, pp 32-46.

31. Ollero P., Serrera A., Arjona R., Alcantarilla S., The CO_2 gasification kinetics of olive residue, *Biomass Bioenergy* **2003**, 24, 151-161.

32. Xu Q., Pang S., Levi T., Reaction kinetics and producer gas compositions of steam gasification of coal and biomass blend chars, part 1: Experimental investigation, *Chem. Eng. Sci.* **2011**, 66, 2141-2148.

33. Kumabe K., Hanaoka T., Fujimoto S., Minowa T., Sakanishi K., Co-gasification of woody biomass and coal with air and steam, *Fuel* **2007**, 86, 684-689.

34. Zhu W., Song W., Lin W., Catalytic gasification of char from co-pyrolysis of coal and biomass, *Fuel Process. Technol.* **2008**, 89, 890-896.

35. Nandi S.P., Onischak M., Gasification of chars from maple and jack pine woods, Fundamentals of Thermochemical Biomass Conversion, International Conference Proceedings, Estes Park, CO, Oct 18-22, **1982**.

36. Fushimi C., Wada T., Tsutsumi A., Inhibition of steam gasification of bio-

mass char by hydrogen and tar, *Biomass Bioenergy* **2011**, 35, 179-185.

37. Hauserman W.B., High-yield hydrogen production by catalytic gasification of coal or biomass, *Int. J. Hydrogen Energy* **1994**, 19, 413-419.

38. Fernández Llorente M.J., Carrasco García J.E., Concentration of elements in woody and herbaceous biomass as a function of the dry ashing temperature, *Fuel* **2006**, 85, 1273-1279.

39. Noorman S., Gallucci F., van Sint Annaland M., Kuipers J.A.M., Experimental investigation of a CuO/Al_2O_3 oxygen carrier for chemical-looping combustion, *Ind. Eng. Chem. Res.* **2010**, 49, 9720-9728.

40. Yuh S.J., Wolf E.E., FTIR studies of the effect of alkali metal salts and the use of alkali metal chlorides in the catalytic gasification of coal chars, *ACS division of fuel Chemistry* **1984**, 29, 206-211.

41. Sjöström E., Alén R., *Analytical methods in wood chemistry, pulping and papermaking*; Springer-Verlag Berlin Heidelberg, Germany, **1999**.

42. Frömm J., Wood formation of trees in relation to potassium and calcium nutrition, *Tree Physiol.* **2010**, 30, 1140-1147.

43. Di Blasi C., Galgano A., Branca C., Effects of potassium hydroxide impregnation on wood pyrolysis, *Energy Fuels* **2009**, 23, 1045-1054.

44. Ahmadpour A., Do D.D., The preparation of active carbons from coal by chemical and physical activation, *Carbon* **1996**, 34, 471-479.

45. Sueyasu T., Oike T., Mori A., Kudo S., Norinaga K., Hayashi J.-i., Simultaneous steam reforming of tar and steam gasification of char from the pyrolysis of potassium-loaded woody biomass, *Energy Fuels* **2012**, 26, 199 -208.

46. Lillo-Ródenas M.A., Ros A., Fuente E., Montes-Morán M.A., Martin M.J., Linares-Solano A., Further insights into the activation process of sewage

sludge-based precursors by alkaline hydroxides, *Chem. Eng. J.* **2008**, 142, 168-174.

47. Lozano-Castelló D., Lillo-Ródenas M.A., Cazorla-Amorós D., Linares-Solano A., Preparation of activated carbons from Spanish anthracite: I. Activation by KOH, *Carbon* **2001**, 39, 741-749.

48. Sricharoenchaikul V., Pechyen C., Ath-ong D., Preparation and characterization of activated carbon from the pyrolysis of physic nut (Jatropha curcas L.) waste, *Energy Fuels* **2008**, 22, 31-37.

49. Jibril B., Houache O., Al-Maamari R., Al-Rashidi B., Effects of H_3PO_4 and KOH in carbonization of lignocellulosic material, *J. Anal. Appl. Pyrolysis* **2008**, 83, 151-156.

50. Raymundo-Piñero E., Azaïs P., Cacciaguerra T., Cazorla-Amorós D., Linares-Solano A., Béguin F., KOH and NaOH activation mechanisms of multiwalled carbon nanotubes with different structural organization, *Carbon* **2005**, 43, 786-795.

Chapter 4

Appendix C

Calculation of the Thiele Modulus (φ) and the Effectiveness Factor (η)

In this appendix the calculations of the Thiele modulus (φ) and effectiveness factor (η) are presented for the reaction of steam with char in the TGA system used in this chapter.

Steam diffuses to the char sample as shown in Figure C.1. The diffusion process can be described by Fick's Law and the overall mass balance can be expressed as:

$$D_e \frac{d^2C}{dz^2} - k = 0 \qquad \text{(eq.C.1)}$$

If we substitute:

$$\psi = \frac{C}{C_0} \quad \text{and} \quad \zeta = \frac{z}{L} \qquad \text{(eq.C.2)}$$

Then eq.C.1 becomes:

$$\frac{D_e C_0}{L^2} \frac{d^2\psi}{d\zeta^2} - k = 0 \qquad \text{(eq.C.3)}$$

The general expression of the Thiele modulus for an nth order reaction is:

$$\varphi = \frac{V}{A} \sqrt{\frac{(n+1)kC_0^{n-1}}{2D_e}} \qquad \text{(eq.C.4)}$$

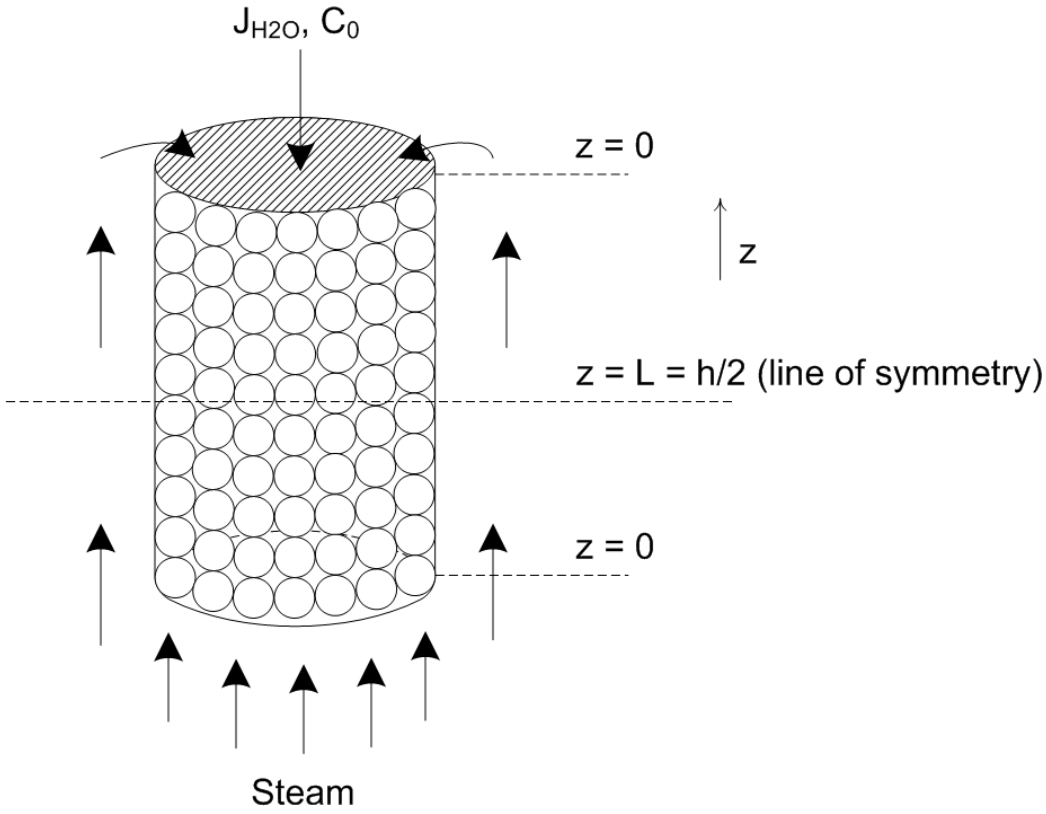

Figure C.1. Schematic representation of steam diffusion to the char bed situated inside the quartz basket.

Since the reaction order in steam appears to be zero from our experimental results (see Figure 4.11 of this chapter), then for n=0, eq.C.4 becomes:

$$\varphi = L\sqrt{\frac{k}{2C_0 D_e}} \qquad \text{(eq.C.5)}$$

Solving for k gives:

$$k = \frac{2\varphi^2 C_0 D_e}{L^2} \qquad \text{(eq.C.6)}$$

Substituting eq.C.6 in eq.C.3 we get:

$$\frac{d^2\psi}{d\zeta^2} = 2\varphi^2 \qquad \text{(eq.C.7)}$$

In order to solve this second order differential equation, we substitute:

$$\frac{d\psi}{d\zeta} = u \qquad \text{(eq.C.8)}$$

Then, eq.C.7 becomes:

$$\frac{du}{d\zeta} = 2\varphi^2 \qquad \text{(eq.C.9)}$$

Integrating this gives:

$$u = 2\varphi^2\zeta + C_1 \qquad \text{(eq.C.10)}$$

for $\zeta = 1$: $\frac{du}{d\zeta} = 0$ (line of symmetry)

substituting the boundary condition in eq.C.10 we get:

$$C_1 = -2\varphi^2 \qquad \text{(eq.C.11)}$$

Then, eq.C.8 becomes:

$$\frac{d\psi}{d\zeta} = u = 2\varphi^2\zeta - 2\varphi^2 = 2\varphi^2(\zeta - 1) \qquad \text{(eq.C.12)}$$

For $\zeta = 0$, eq.C.12 becomes:

$$\frac{d\psi}{d\zeta} = -2\varphi^2 \qquad \text{(eq.C.13)}$$

The expression for the flux of steam to the reactive char surface is:

$$J = -D_e \frac{dC}{dz} \qquad \text{(eq.C.14)}$$

Substitution of eq.C.2 in C.14 gives:

$$J = \frac{-D_e C_0}{L} \frac{d\psi}{d\zeta} \qquad \text{(eq.C.15)}$$

By substituting eq.C.13 in eq.C.15 we get:

$$J = \frac{D_e C_0 2\varphi^2}{L} \qquad \text{(eq.C.16)}$$

Solving for φ gives:

$$\varphi = \sqrt{\frac{JL}{2C_0 D_e}} \qquad \text{(eq.C.17)}$$

The steam flux *J* in eq.C.17 is calculated by the raw data obtained for typical test conditions. The sample used for this calculation is char from impregnated wood with KOH (9.5 wt.%), reacted at 700°C (data shown in Figure 4.5A of this chapter). For a char conversion of X=0-0.5, about $t_{0.5}$=170 s are needed according to the data obtained for this sample (initial rate). So, the reacted/ diffused amount of steam can be calculated from the steam-char reaction (char is assumed to contain mostly carbon):

$$C + H_2O \rightarrow CO + H_2 \qquad \text{(C.1)}$$

Therefore, the steam flux is:

$$J = \frac{N}{A} = \frac{N}{\pi r^2} \qquad \text{(eq.C.18)}$$

where N (mol/s) is the amount of diffused steam and A (m^2) is the reactive surface area of the char sample, denoted in Figure C.1 by the shaded surface.

$$N = \frac{0.5(m_0/2)}{MW_C t_{0.5}} \qquad \text{(eq.C.19)}$$

where m_0 (g) is the initial mass of char (just before initiation of char reaction with steam) and MW_C (g/mol) is the molecular weight of carbon. By substituting the known values in eq. C.19:

$$N = \frac{0.5(0.00257/2)}{12 \times 170} = 3.15 \times 10^{-7}\ mol\ H_2O/s$$

From eq.C.18 we obtain:

$$J = \frac{3.15 \times 10^{-7}}{\pi \times 0.003^2} = 1.11 \times 10^{-2}\ mol\ H_2O/m^2 s$$

The steam concentration C_0 in eq.C.17 can be calculated from the ideal gas law:

$$P = C_0 RT \qquad \text{(eq.C.20)}$$

By solving for C_0 and substituting we get:

$$C_0 = \frac{P}{RT} = \frac{101325}{8.314 \times (700 + 273.15)} = 12.52\ mol/m^3$$

By substituting all known values in eq.C.17 we finally obtain:

$$\varphi = \sqrt{\frac{JL}{2C_0 D_e}} = \sqrt{\frac{1.11 \times 10^{-2} \times (1.5/2)}{2 \times 12.52 \times 10^{-5}}} = 0.18$$

The effectiveness factor can be estimated by:

$$\eta = \frac{tanh\varphi}{\varphi} = \frac{\tanh(0.18)}{0.18} = 0.99 \qquad \text{(eq.C.21)}$$

Chapter 5

Methane Production over and Gasification of Char from Potassium-impregnated Wood

Methane production and char gasification were investigated at 25 bar and 700°C in a pressurized packed bed. Different tests were realized where CO and/or H_2 were led over a char bed, with or without added K_2CO_3, to investigate methane formation. A methane steam reforming test was also realized to study methane consumption. The gasification tests were done by using steam and/or CO_2 as gasification agents.

The results obtained point out that K_2CO_3, a model component for wood ash, does enhance the formation of methane (by a factor 3 to 8 compared to char without added K_2CO_3), but only when solid carbon (char) is present in the (reaction) system. The results made clear that methane is formed by hydrogenation of the carbon present in the char. When feeding CO and H_2 simultaneously over char with added K_2CO_3 the overall stoichiometry is described by $2CO+2H_2 \rightarrow CH_4+CO_2$. This may suggest that the dominant reactions are $2CO \rightarrow C+CO_2$ and $C+2H_2 \rightarrow CH_4$, although the exact mechanism could not be deduced from our experimental data. Steam gasification rate of char at high pressure is increased in the presence of K_2CO_3. Possible inhibition effect by produced H_2 and CO results in lower gasification rates than in experiments previously performed at atmospheric pressure.

5.1. Introduction

Methane formation by CO and H_2 has been the research subject of many publications in the past and especially over Ni, Ru, Pt or Rh catalysts. Several researchers have dealt also with catalysis by alkali-metals impregnated in carbon, coal and char from coal. Some of them [1-6] claim that alkali metals catalyze the direct formation of methane via the methanation reaction (5.1), while others claim [7-8] that alkali metals catalyze the formation of methane via carbon deposition (5.2) and subsequent hydrogenation (5.3).

$CO + 3H_2 \leftrightarrow CH_4 + H_2O$ $\quad \Delta H_R^0 = -206.3$ kJ/mol (5.1)

$2CO \leftrightarrow C + CO_2$ $\quad \Delta H_R^0 = -172.5$ kJ/mol (5.2)

$C + 2H_2 \rightarrow CH_4$ $\quad \Delta H_R^0 = -75.0$ kJ/mol (5.3)

The formation of methane plays an important role in the concept of biomass self-gasification. Methane formation is not only important for the desired final product, but the reactions that lead to methane can also provide the reactor with the necessary heat for the gasification reactions to proceed, resulting in an autothermal process ideally without any addition of O_2/air (see also Chapter 2).

The aim of this current study is to investigate methane production/consumption at high pressures and the role of alkali metals. CO and/or H_2 were led over packed beds of catalyst or wood char (with/without K_2CO_3) and methane production was measured. Also, methane consumption was studied as the reverse of the methanation reaction (5.1). The effect of gasifying medium (H_2O and/or CO_2) and presence of alkali in the char were studied for high-pressure gasification as well.

5.2. Experimental Section

5.2.1. Materials

The wood used for all the measurements was pinewood sawdust, purchased from Rettenmaier & Söhne GMBH, Germany. K_2CO_3 (Sigma Aldrich) was used as a pure catalyst bed and for preparation of the salt-impregnated wood samples. K_2CO_3 was used because it has similar gasification activity to ash from wood itself (as was seen in Chapter 4) and it was used in earlier literature for methanation experiments [1-8]. The impregnation procedure has been described in Chapter 4. The Ni/Al_2O_3 catalyst that was used (18 wt.% NiO) was a

commercial natural gas steam reforming catalyst.

Elemental compositions (analysed with a Flash 2000, Thermo Scientific, column temperature: 900°C) and ash contents of the initial wood and char from K_2CO_3-impregnated wood are presented in Table 5.1. The ash was determined by combustion of the sample in air at 550°C for 24 h, according to the procedure developed by Llorente and García [9]. According to their experimental data, most of the ash produced under these conditions exists in oxides form (about 85 wt.%). Most of the ash measured in the K_2CO_3-char sample (Table 5.1) is then in the form of K_2O. For interpretation of our experimental results and for comparison on the same char basis, the char amount present in the bed was in all cases recalculated to a K_2CO_3-free char. Char samples were made by heating up wood impregnated with 14 wt.% K_2CO_3 in N_2 up to 700°C in an electrical oven.

5.2.2. Experimental set-up and methodology

A schematic overview of the high-pressure set-up used for experimentation is shown in Figure 5.1. The char/salt sample (typically about 0.5 g for wood char) was weighed and loaded into the quartz reactor (nr.17 in Figure 5.1) to form a fixed bed of around 20 cm in length. The fixed bed was held in place by quartz wool packing. The quartz tube (L=68 cm, ID=3mm, OD=5mm) was inserted and fixed onto the bottom of a metal tube (nr.12 in Figure 5.1, L=70 cm, ID=6mm, OD=20mm), which was surrounded by two consecutive, cylindrical

Table 5.1. Elemental composition (C, H) of the tested materials on "dry, ash-free" basis[a].

	wood	**char from wood impregnated with K_2CO_3**
compound	**wt.%**	**wt.%**
C	49.1	78.2
H	5.4	0.7
Difference (100-C-H)	45.5	21.1
Ash	0.4	28.2

[a] The difference is mainly oxygen (O), with some traces of nitrogen (N) and sulphur (S). The ash contents are expressed on a dry basis.

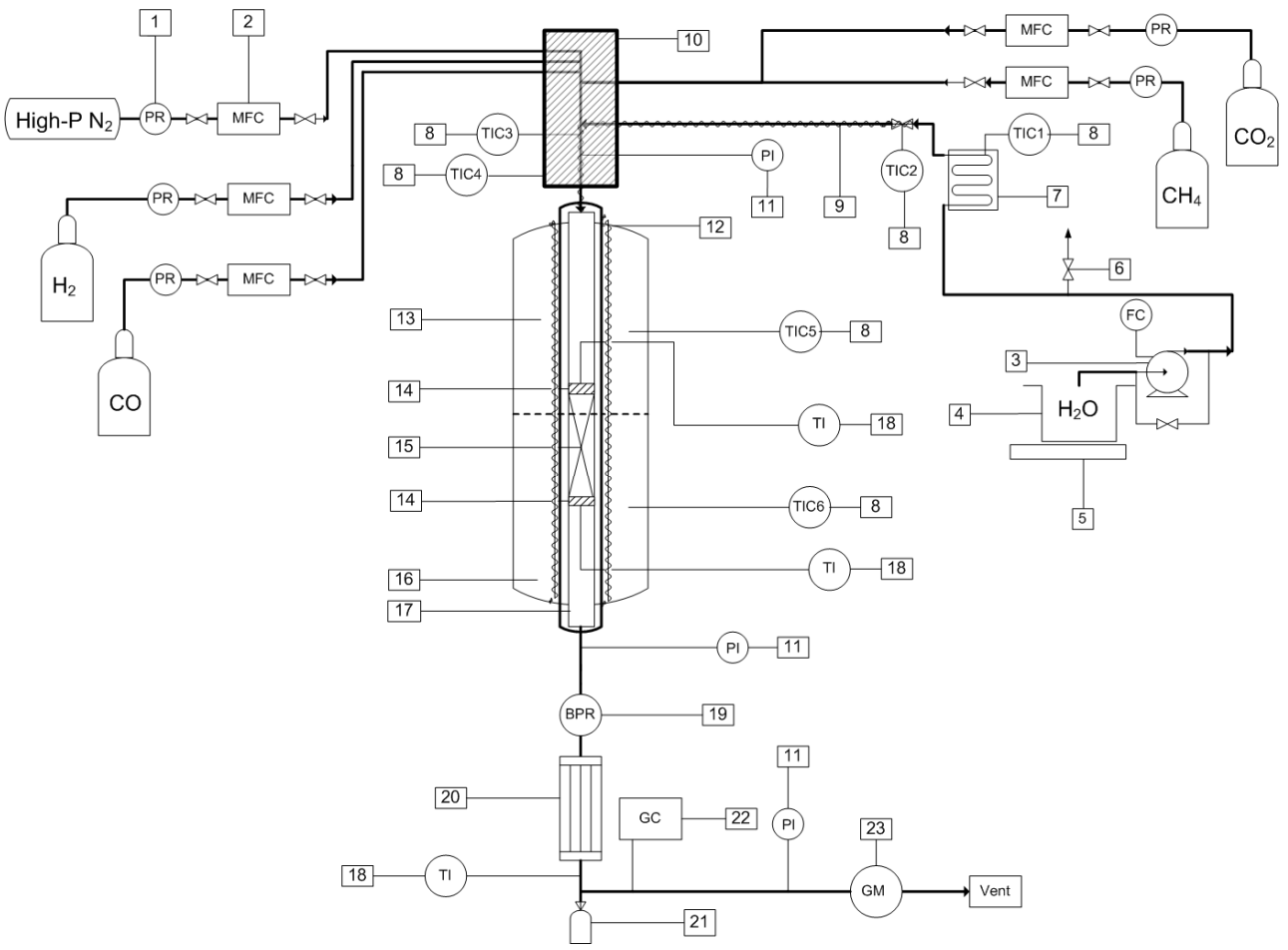

Figure 5.1. High-pressure set-up for the investigation of methane formation/steam reforming and char gasification. 1.Pressure regulator, 2.Mass flow controller (MFC), 3.HPLC pump with flow controller (FC), 4.Water tank, 5.Balance, 6.Safety vent, 7.Water vaporizer, 8.Temperature Indicator/Controller (TIC), 9.Heating element/ Tracing, 10.Preheater, 11.Digital pressure indicator (PI), 12.Metal tube, 13.Oven I, 14.Quartz wool packing, 15.Packed bed, 16.Oven II, 17.Quartz tube reactor, 18.Temperature indicator (TI), 19.Back-pressure regulator (BPR), 20.Condenser, 21.Water collection vessel, 22.Gas chromatograph (GC), 23.Gas meter (GM).

ovens (nr.13 and nr.16 in Figure 5.1). The metal tube was used for pressurization of the reactor and for its ease of connection to the rest of the set-up, while the quartz tube was used for its inert properties as a reactor.

The two ovens could be individually controlled and isothermal conditions could be achieved in the fixed bed. The gas flows were regulated by mass flow controllers (Brooks Instruments), which were calibrated at a ΔP= 5 bar for all pressures. The design pressure of the set-up was 40 bar.

After the quartz reactor and all parts were in place, the N_2 flow was switched on and the system was brought to operating pressure for leakage testing. When the system was leakage-free, the pressure was released and the char/catalyst sample was heated at 36-58 K/min in a N_2 flow at atmospheric pressure to the desired temperature (700°C). The temperature was measured every 1s just above and just below the fixed bed (nr. 18 in Figure 5.1). During heating up of the char some CO and H_2 were detected in the outgoing gas stream. When the desired temperature was reached, then the system was pressurized and the flow was switched to a desired gas mixture (N_2 and CO, CO_2, CH_4, H_2 and/or steam) to initiate reaction. Typical reaction times varied between 1 and 1.5 h. When Ni/Al_2O_3 catalyst was used it was reduced in a H_2 atmosphere (7.2 bar) at 600°C for 1.5 h prior to reaction.

The pressure of the reactor was controlled by a back-pressure regulator (nr. 19 in Figure 5.1), after which product gases expanded to atmospheric pressure and were cooled to ~15°C. Any moisture present in the gas condensed and could be collected in a vessel (nr. 21 in Figure 5.1). An on-line Varian microGC CP-4900 with TCD detectors (10m MS5, Ar, 70°C, 120 kPa/10m MS5, He, 70°C, 120 kPa/10m PPQ, He, 80°C, 120 kPa) was used (nr. 22 in Figure 5.1) to take samples of the product gas every ~3 min. N_2 was used in each test because it served as an internal standard for determining the volumetric flows of the produced gases.

At the end of the test, the pressure was released and the gas mixture was switched back to N_2. The ovens, water vaporizer, tracing and preheater are turned off and the system is cooled down. Gas measurements continued until reactive gases reached concentrations <1 vol.%. Afterwards, the quartz tube was removed from the set-up and weighed.

Figure 5.2 shows a typical run according to the previously described procedure. This run corresponds to test nr. 4 presented in Table 5.2. At time t=0 h, heating up of the char started at atmospheric pressure until t=0.8 h when it reached the desired temperature of 700°C. At t=0.8 h the reactor was pressurized and feed gases (in this case CO and H_2) were switched on to initialize the reaction. The run lasted until t=2.6 h, where the inlet gases and ovens were switched off and the set-up was flushed with N_2.

When the reactive gases were switched on (at t=0.8 h), the quantities of produced gases slowly reached a constant value in time. Typically, the first two data points in this lag are caused by the change in the flow after switching on the inlet gases and pressurizing the reactor (from P≈1 bar to P≈25 bar). This effect is not noted at the end of the run at t=2.6 h, because the reactive gases are switched to N_2 and the pressure is released back to P≈1 bar (from P≈25 bar). Therefore, residence time is very short resulting in a flushing effect of the system.

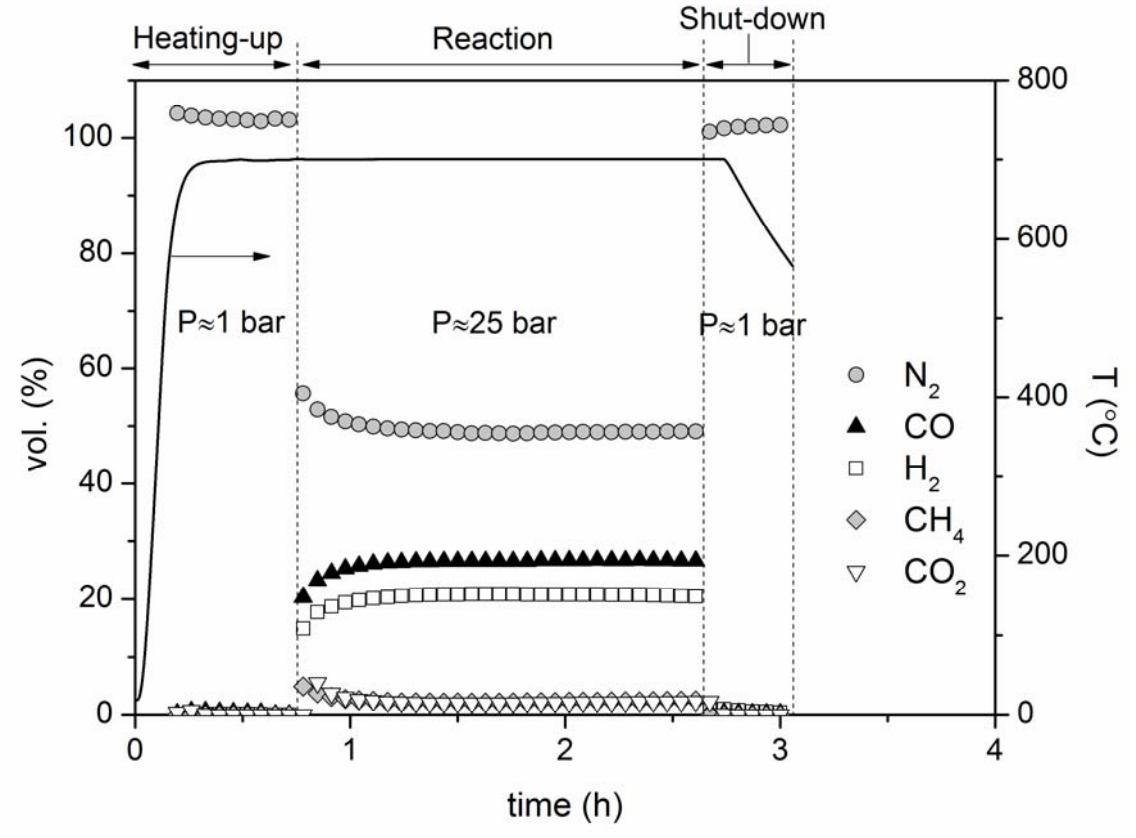

Figure 5.2. Gas composition data obtained from a typical run. Char bed: wood char+K_2CO_3. P_{tot}=25 bar, T=700°C, P_{CO}^{IN}=7.8 bar, P_{H2}^{IN}=5.9 bar, τ=2.7 s.

5.3. Results and Discussion

5.3.1. Methane production

A number of tests were realized and compared on basis of methane production. Table 5.2 presents the packed bed used in each test, the (total) gas residence time in the packed bed, as well as the partial pressures of used feed gases. The (total) gas residence time is defined as the residence time of the gas (including N_2) in the volume of the empty bed. The production of methane and carbon dioxide measured in each test are expressed in mole flow per amount of catalyst bed or char (kg) initially present in the packed bed. The weight of the char considered in this expression is excluding any K_2CO_3 present. The packed bed in all tests had the same volume, but it differed in weight due to variation in density. The actual initial weights of the various packed beds used were: Ni/Al_2O_3=3.56 g, K_2CO_3=1.97 g, wood char=0.25±0.04 g, wood char+K_2CO_3=0.50±0.05 g. Methane production is also given in absolute mass flow for comparison to calculated (heterogeneous) equilibrium values which are also included in Table 5.2. In these calculations, it was assumed that solid carbon was present in excess.

CH_4 and CO_2 production rates are referred to the total amount of methane or carbon dioxide, respectively, produced during reaction time (time that feed gases are flowing through the packed bed) divided by that reaction time and represent the average production rate. The column with the packed bed includes the sample weight conversion on char basis (excluding K_2CO_3), denoted between brackets, determined by weighing the quartz reactor tube before and after the test. The minus sign in front of the char bed conversion in test nr. 4 signifies a weight increase.

The specific CO/H_2 feed ratios were chosen for tests nr. 2 to 8 as an average of CO/H_2 ratio that can exist in producer gases from biomass gasifiers (see Chapter 3, section 3.4). In tests 7 and 8 the feed gases (H_2 and CO) were led individually over the packed bed of char. In these tests, first CO was fed to the reactor for about 45 min, then the CO flow was switched off and immediately after, the H_2 flow was switched on.

The results in Table 5.2 show that when a CO/H_2 mixture was led over a Ni/Al_2O_3 catalyst bed (Test nr. 1), there was methane production close to equilibrium. When a K_2CO_3 packed bed was used instead, there was no methane production noted (Test nr. 2). Carbon dioxide production during the test is a measure of carbon deposition via the Boudouard reaction (5.2). It is noted

Table 5.2. Overview of test parameters, methane production results and equilibrium amounts. T=700°C, P_{tot}=25 bar.

Test Nr.	Packed bed[a] (X,-)	τ (s)[b]	P_{CO} (bar)	P_{H2} (bar)	$\Phi_N CH_4$ (mol/kg bed/s)	$\Phi_N CO_2$ (mol/kg bed/s)	$\Phi_M CH_4$ (g/h)	Equilibrium $\Phi_M CH_4$ (g/h)
1	Ni/Al_2O_3	4.4	2.0	6.6	2.2×10^{-3}	5.6×10^{-4}	4.5×10^{-1}	5.1×10^{-1}
2	K_2CO_3 (0.03)	2.4	7.3	5.4	0.0	8.7×10^{-5}	0.0	2.8×10^{-1}
3	wood char (0.00)	2.7	7.8	6.3	1.9×10^{-3}	2.2×10^{-3}	2.8×10^{-2}	3.1×10^{-1}
4	wood char + K_2CO_3 (-0.22)	2.7	7.8	5.9	1.4×10^{-2}	1.3×10^{-2}	2.2×10^{-1}	2.9×10^{-1}
5	wood char (0.17)	2.8	-	6.3	8.9×10^{-4}	0.0	1.5×10^{-2}	5.4×10^{-1}
6	wood char + K_2CO_3 (0.62)	2.8	-	6.9	4.3×10^{-3}	0.0	6.8×10^{-2}	6.2×10^{-1}
7A	wood char[c]	2.6	7.6	-	0.0	1.0×10^{-3}	0.0	0.0
7B	(0.13)	2.8	-	6.4	8.9×10^{-4}	1.1×10^{-4}	1.2×10^{-2}	4.3×10^{-1}
8A	wood char + K_2CO_3[c]	2.6	7.6	-	0.0	5.5×10^{-3}	0.0	0.0
8B	(0.16)	2.8	-	6.2	1.9×10^{-3}	1.0×10^{-4}	3.6×10^{-2}	3.8×10^{-1}

[a] Volume of packed bed is similar for all tests, but weight load varies: Ni/Al_2O_3=3.56 g, K_2CO_3=1.97 g, wood char=0.25±0.04 g, wood char+K_2CO_3 (excluding K_2CO_3)=0.29±0.03 g.

[b] Gas residence time refers to the total feed gas, including N_2.

[c] In tests nr. 7 and 8, CO and H_2 were led over the char bed separately, i.e. first CO was led over the packed bed and when the CO flow was switched off, then H_2 was led over the char. Results for both parts of the tests are presented on separate rows in the table.

from Table 5.2 that by using a packed bed of K_2CO_3 there was CO_2 production and the carbon deposition on the salt observed at the end of the test, was the verification that reaction (5.2) took place.

A bed of wood char resulted in some methane production (Test nr 3.) and when the char also contained K_2CO_3, methane produced was close to equilibrium amounts (Test nr. 4) as was the case with the bed of Ni/Al_2O_3 catalyst (Test nr. 1). Otake et al. [6] also demonstrated that coal char with K_2CO_3 as bed material had an activity similar to a conventional nickel catalyst for methane production. Methane production rates presented by Otake et al. [6] are in agreement with our results. These tests (nr. 2-4) indicate that K_2CO_3 does not catalyze methane formation on its own, but when it exists in contact with carbon, methane production approaches equilibrium.

Gas production and consumption during test nr. 4 indicated that not only the

produced CH_4/CO_2 (mol) ratio, which was about 1 throughout the test (see Table 5.2), but also the consumption rates of ingoing CO and H_2 were according to the stoichiometry of the following (overall) reaction:

$$2CO + 2H_2 \rightarrow CH_4 + CO_2 \qquad (5.4)$$

In this test, the amount of carbon in the total ingoing gas (as CO) was a factor 11 higher than the amount of carbon present in the (initial) char bed.
When only H_2 was led through the char bed (Tests nr. 5 and 6) methane was produced and it was the only product gas obtained which means that its formation could only be the result of hydrogenation of the carbon present in the char:

$$C(har) + 2H_2 \rightarrow CH_4 \qquad (5.5)$$

The results also showed that there was more methane formed by this reaction when K_2CO_3 was present in the char and thereby catalyzing the char hydrogenation reaction.
Tests nr. 7 and 8 give more insight on the role of carbon deposition via the Boudouard reaction (5.2). When only H_2 flowed through the char+K_2CO_3 bed (Test nr. 6) the amount of produced methane was almost double than when the char had been in contact with CO gas prior to H_2 (Test nr. 8B). This difference was not noted when no K_2CO_3 was present in the char (Tests nr. 5 and 7B). When leading only CO through the char bed, the Boudouard reaction (5.2) takes place producing CO_2 (which we measured during the test) and forming carbon inside and outside the fixed bed (which we observed after the test). Therefore, in the case of Test nr. 8B there was more carbon available for reaction with the H_2, so the amount of methane formed should be at least equal to Test nr. 6 where only H_2 was fed to the char bed. This suggests that the carbon deposits could have blocked active alkali-carbon sites for methane formation, which has also been claimed in the literature [8, 10, 11]. Also, this shows that the carbon deposits by the Boudouard reaction (5.2) are probably inactive for reaction with H_2 which is in agreement with the literature [8, 11]. This is also supported by Test nr. 2 where carbon deposition takes place on the K_2CO_3 packed bed, but no methane formation occurs. It is also known from the literature that at temperatures of 700°C rather inactive forms of carbon can occur by

CO decomposition [12].

Overall, methane was formed when no K_2CO_3 was present in the char (Tests nr. 3, 5 and 7B), but always in lower amounts by factors 3 to 8 (on absolute mass flow basis) compared to tests where K_2CO_3 was present in the char (Tests nr. 4, 6 and 8B). This means that K_2CO_3 does promote the formation of methane.

When CO and H_2 were led simultaneously through the char bed (Tests nr. 4 and 3) the amount of produced methane was higher than the respective tests where only H_2 was used (Tests nr. 6 and 5) or when CO and H_2 were led separately through the fixed bed (Tests nr. 8 and 7). This indicates that CO plays an important role in the methane formation by increasing methane production by about a factor 3.6 (on absolute mass flow basis) in the case of char+K_2CO_3 (Test nr. 4), compared to only hydrogenation (Test nr. 6). This implies that besides carbon hydrogenation, a reaction involving CO is also responsible for the formation of methane.

It has been suggested in the literature that active carbon intermediates are formed by CO [6, 8, 11]. Due to the occurrence of the Boudouard reaction (5.2) it is likely that hydrogenation of these active carbon intermediates can take place by simultaneous carbon deposition and hydrogenation, both catalyzed by K_2CO_3. There is apparently a combined effect needed, with simultaneous carbon deposition and hydrogenation of these carbon deposits to avoid blockage of the active sites. From our tests, however, no conclusion can be drawn about the possible existence of active carbon intermediates and the overall mechanism involved in methane formation remains inconclusive.

In the literature, essentially two different mechanisms are discussed for the methanation reaction of CO and H_2. In the first mechanism, adsorbed carbon is proposed as active intermediate via CO dissociation. This carbon then reacts stepwise with hydrogen to form methane [13-16]. The second mechanism involves the formation of a CH_xO surface complex by reaction of H_2 and CO which is further hydrogenated to methane [17-19].

The reverse of reaction (5.1), which is methane steam reforming was tested as well. This test is presented and discussed in the following section.

5.3.2. Gasification and Steam Reforming

Some tests involving gasification of char were realized in order to study high-pressure gasification in CO_2 and/or H_2O of char with or without K_2CO_3. The

steam reforming of methane over char with K_2CO_3 was investigated as well in order to examine whether the reverse of the methanation reaction (5.1) can take place under the conditions tested.

The carbon conversion of char in time is presented in Figure 5.3, where the effects of K_2CO_3 and gasification medium are shown. Carbon conversion was determined by measuring the carbon-containing gases in time (CO, CO_2 and CH_4). The conversion of pure potassium carbonate was measured in a separate test and is included in Figure 5.3.

The k constants included within the brackets in the legend of Figure 5.3, refer to the first-order reaction constant obtained from fitting the data curve to the following equation:

$$X = 1 - e^{-kt} \qquad \text{(eq.5.1)}$$

The data curve fitting procedure has been explained in Chapter 4 and in this

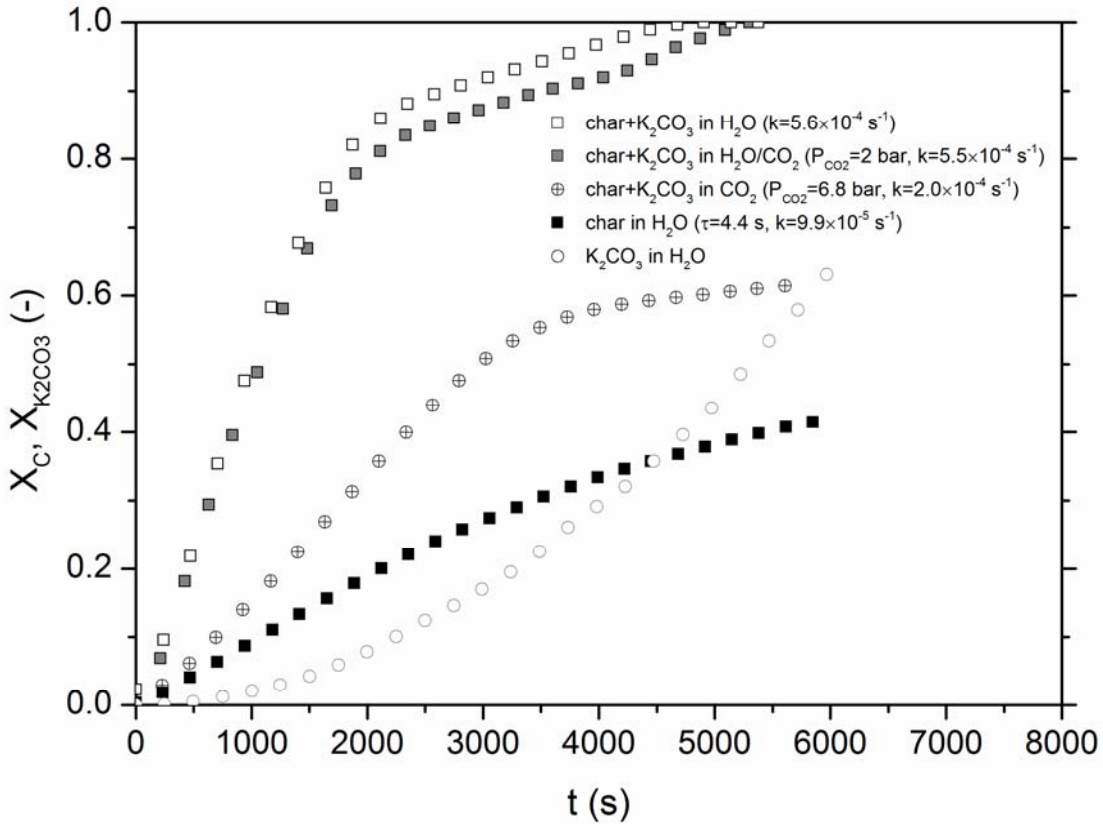

Figure 5.3. Char and carbonate conversion in time. Effect of K_2CO_3 and gasification medium on char conversion, T=700°C, P_{tot}=25 bar, P_{H2O}=12.4±0.1 bar, τ=2.6±0.1 s (unless otherwise stated). The rest is N_2.

case it was applied in the conversion range of X=0-0.4 for all tests.

When K_2CO_3 was present in the char, it increased its reaction rate by at least a factor 6, considering that gasification of char only was realized under a higher steam residence time (τ=2.6 for the first and τ=4.4 s for the latter). Steam conversion was below 15% for both tests. Gasification by only CO_2 was about a factor 3 lower compared to gasification only by steam which was expected [20]. During CO_2 gasification of the char, the only gaseous product was CO and was produced in stoichiometric amounts according to the reverse of reaction (5.2). The conversion increased up to about X=0.5, after which it seemed to have reached a constant value where neither CO_2 was consumed nor CO was produced anymore. At the end of this experiment the packed bed still contained carbon. This points out to a loss in activity of the char bed after this conversion level.

When a mixture of CO_2 and steam was used as gasification medium, there was no significant difference in the initial conversion rate of the char compared to steam only. However, in the high conversion regime (X>0.8) the added CO_2 caused a somewhat lower conversion rate. During steam gasification, the potassium carbonate in the char is being transformed into hydroxide while releasing CO_2 according to the reaction:

$$K_2CO_3 + H_2O \leftrightarrow 2KOH + CO_2 \qquad (5.6)$$

The conversion of pure potassium carbonate in time is also depicted in Figure 5.3. Therefore, it seems possible that in the high conversion range where most of the residue in the packed bed is K_2CO_3/KOH, that the slightly higher conversion measured in steam is due to the extra CO_2 release of the carbonate. This is a slow reaction compared to catalyzed steam and CO_2 gasification of char.

Steam gasification rate of char at this pressure (P=25 bar) is similar to the steam gasification rate of char obtained at atmospheric pressure in a TGA system studied in Chapter 4. However, the gasification rate of char with K_2CO_3 is an order of magnitude lower at this pressure than obtained in Chapter 4. Produced H_2 and CO during steam gasification resulted in partial pressures of about P_{H2}=3 bar and P_{CO}=0.5 bar at reaction conditions in the packed bed. This points out to a possible inhibition effect by H_2 and CO.

A steam reforming test of methane over a char+K_2CO_3 packed bed was also realized in order to verify whether the reverse of the methanation reaction can take place. Since steam was used for reaction with methane, gasification of the char also occurred simultaneously. Therefore, the methane steam reforming test is compared to a steam gasification test (char+K_2CO_3 steam gasification test in Figure 5.3) on basis of the produced amounts of H_2 and CO. The results are presented in Figure 5.4 as gas production curves obtained during reaction time. Gas production rates are expressed on initial char basis, excluding K_2CO_3.

What can be seen in Figure 5.4 is that gas production is initiated as soon as steam (and CH_4) are switched on (at t=0 s). The trends are similar for both tests and for both CO and H_2. The gas production increases until a maximum around 1000 s, where also CO_2 production goes through a maximum, indicating water-gas shift activity. In time, their amounts steadily decrease until a reaction time of 3000 s is reached. Further reaction gives very low gas produc-

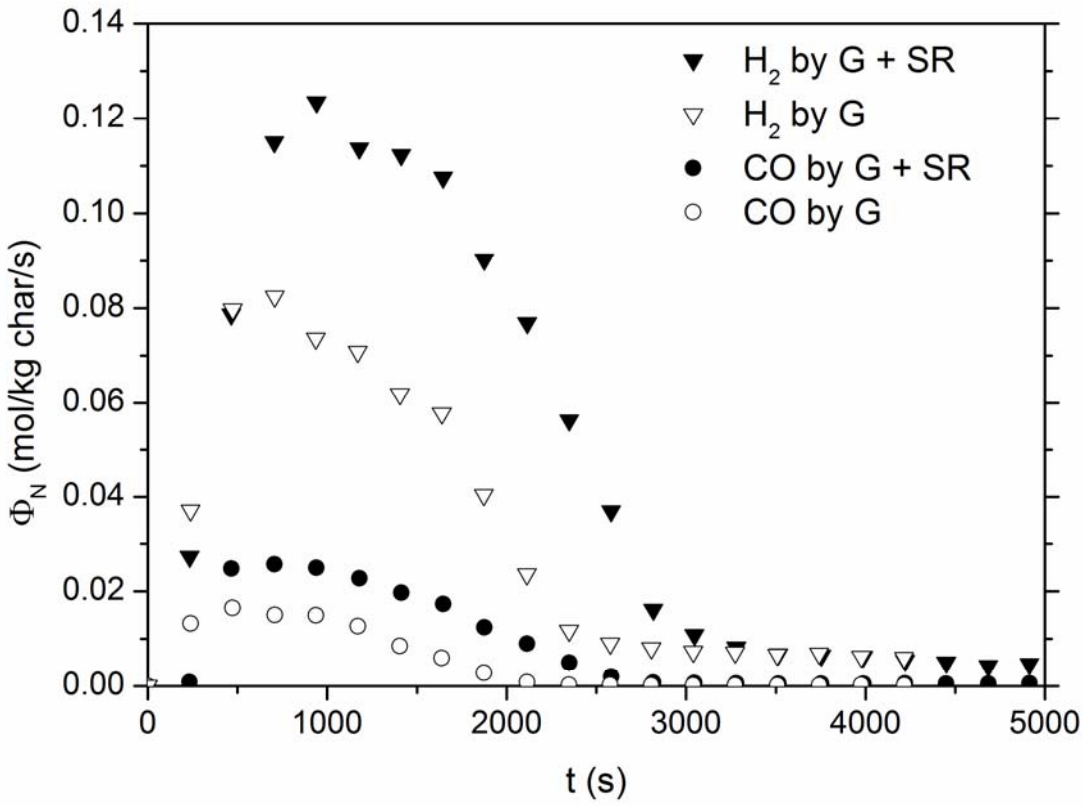

Figure 5.4. H_2 and CO gas production rates during methane steam reforming over char and steam gasification of char. Packed bed: wood char+K_2CO_3. T=700°C, P_{tot}=25 bar, P_{H2O}(G)=12.5 bar, P_{H2O}(G+SR)=9.6 bar, P_{CH4}=4.6 bar, τ=2.5 s. G: Gasification, SR: Steam Reforming.

tion until 4500-5000 s, where char conversion is complete for both tests. In this high char conversion regime there is still CO, H_2 and CO_2 production noted in the same rates for both tests. CO and H_2 are probably generated by gasification of the remaining char and CO_2 is formed by reaction of the potassium carbonate in the bed to hydroxide according to reaction (5.6) and/or by the water-gas shift reaction (5.8).

A good reforming activity is noted until 2000 s. This time corresponds to ~85% conversion of the char (see Figure 5.3). H_2 and CO production during steam reforming are constantly higher than the corresponding gases produced by steam gasification only.

The char conversion profile obtained from the steam reforming test is identical to the steam gasification test shown in Figure 5.3 (open squares). Also, the steam residence time is similar in both cases (6.6 s for gasification vs. 5.0 s for reforming). This indicates that both tests exhibit similar steam gasification activity. Therefore, the additional H_2 and CO produced during steam reforming can only originate from the extra CH_4 added in the feed gas.

The differences in amounts of H_2 and CO between t=700s and t=2120s result in a produced ratio of H_2/CO=3-6.5, which is probably caused by the combined effect of the methane steam reforming (5.7) and water-gas-shift (5.8) reactions:

$$CH_4 + H_2O \leftrightarrow CO + 3H_2 \quad (5.7)$$

$$CO + H_2O \leftrightarrow CO_2 + H_2 \quad (5.8)$$

Reactions proceed under (overall) non-carbon deposition conditions, but the mechanism still remains debatable. In the literature, two proposed mechanisms exist on the steam reforming of methane using conventional catalysts, which are the reverse reactions of the corresponding methanation mechanisms that were mentioned previously in section 5.3.1. So, one mechanism proposes an active carbon intermediate [21, 22] and the other assumes a CH_xO complex as an intermediate [23, 24]. There are also specific mechanisms for methane reforming described in the literature involving a redox cycle of the oxide catalyst support [25]. The active carbon intermediate in the methanation mechanism is formed by CO adsorption and dissociation, whereas in the reforming mechanism it is formed via CH_4 adsorption and dissociation.

5.4. Conclusions

High-pressure methane production/consumption over wood char and gasification of wood char at 25 bar and 700°C were investigated in this chapter. Methane production was tested by passing CO and/or H_2 over a char bed with or without added K_2CO_3, which was studied as a typical model component for wood ash. Methane consumption was studied by methane steam reforming tests over a char bed with K_2CO_3. Char gasification tests were realized to examine the effect of gasification medium (CO_2 and/or H_2O) and existence of K_2CO_3 in the char. The conclusions can be summarized as follows:

- K_2CO_3 enhances the formation of methane both from carbon present in char and CO
- However, K_2CO_3 does not form methane from CO and H_2 on its own, only in the presence of reactive carbon
- Methane can be formed by direct hydrogenation of the carbon present in the char
- The mechanism of the methanation reaction is not clear yet. However, a mechanism involving an active carbon intermediate seems plausible
- At 25 bar gasification of char with K_2CO_3 is clearly slower than at 1 bar. This is most probably the result of enhanced inhibition due to higher CO and H_2 partial pressures
- Carbon deposits created by the Boudouard reaction (5.2) are less reactive than carbon present in the char and may hinder catalysis by K_2CO_3 under the conditions tested.

Notation

ID	=	internal diameter, mm
k	=	first-order reaction rate constant, s^{-1}
L	=	length, cm
OD	=	outer diameter, mm
P	=	pressure, bar
t	=	reaction time, h or s
T	=	temperature, °C
X	=	conversion

Greek symbols

ΔP	=	pressure drop/difference

τ	=	residence time, s
Φ_M	=	gas production, g/h
Φ_N	=	gas production, mol/kg (char) bed/s

Abbreviations

BPR	=	Back-Pressure Regulator
FC	=	Flow Control
G	=	Gasification
GC	=	Gas Chromatograph(y)
GM	=	Gas Meter
HPLC	=	High-Pressure Liquid Chromatography
MFC	=	Mass Flow Controller
PI	=	Pressure Indicator
SR	=	Steam Reforming
TI	=	Temperature Indicator
TIC	=	Temperature Indicator/Controller

Literature cited

1. Hirsch R.L., Gallagher Jr., J.E., Lessard R.R., Wesslhoft R.D., Catalytic coal gasification: An emerging technology, *Science* **1982**, 215, 121-127.

2. Gallagher Jr., J.E., Marshall H.A., SNG from coal by catalytic gasification, *Coal Proc. Tech.* **1979**, 5, 199-204.

3. Kaplan L.J., Methane from coal aided by use of potassium catalyst, *Chem. Eng.* **1982**, 89, 64-66.

4. Marshall H.A., Smits F.C.R.M., Exxon catalytic coal gasification process and large pilot plant development program, Proceedings of the 9th Annual International Conference on Coal Gasification, Liquefaction and Conversion to Electricity, Pittsburgh, PA, Aug 3-5, **1982**, 357-377.

5. Nahas N.C., Exxon catalytic coal gasification process: Fundamentals to flowsheets, *Fuel* **1983**, 62, 239-241.

6. Otake T., Tone S., Kimura S., Hino Y., Methane formation over potassium

carbonate catalyst loaded on coal char, *J. Chem. Eng. Jpn.* **1984**, 17, 503-508.

7. Cabrera A.L., Heinemann H., Somorjai G.A., Methane production from the catalyzed reaction of graphite and water vapor at low temperatures (500-600 K), *J. Catal.* **1982**, 75, 7-22.

8. Mims C.A., Krajewski J.J., Mechanism of methane formation in potassium catalyzed carbon gasification, *J. Catal.* **1986**, 102, 140-150.

9. Fernández Llorente M.J., Carrasco García J.E., Concentration of elements in woody and herbaceous biomass as a function of the dry ashing temperature, *Fuel* **2006**, 85, 1273-1279.

10. Walker Jr., P.L., Matsumoto S., Hanzawa T., Muira T., Ismail I.S.M., Catalysis of gasification of coal-derived cokes and chars, *Fuel* **1983**, 62, 140-149.

11. Meijer R., van Doorn R., Kapteijn F., Moulijn J.A., Methane formation in H_2, CO mixtures over carbon-supported potassium carbonate, *J. Catal.* **1992**, 134, 525-535.

12. Bartholomew C.H., Mechanisms of catalyst deactivation, *Appl. Catal., A* **2001**, 212, 17-60.

13. van Ho S., Harriott P, The kinetics of methanation on nickel catalysts, *J. Catal.* **1980**, 64, 272-283.

14. Inoue H., Funakoshi M., Kinetics of methanation of carbon monoxide and carbon dioxide, *J. Chem. Eng. Jpn.* **1984**, 17, 602-610.

15. Araki M., Ponec V., Methanation of carbon monoxide on nickel and nickel-copper alloys, *J. Catal.* **1976**, 44, 439-448.

16. Underwood R.P., Bennett C.O., The CO/H_2 reaction over nickel-alumina studied by the transient method, *J. Catal.* **1984**, 86, 245-253.

17. van Herwijnen T., van Doesburg H., De Jong W.A., Kinetics of the methanation of CO and CO_2 on a nickel catalyst, *J. Catal.* **1973**, 28, 391-402.

18. Andersson M., Abild-Pedersen F., Remediakis I., Bligaard T., Jones G., Engbaek J., Lytken O., Horch S., Nielsen J., Sehested J., Rostrup-Nielsen J., Norskov J., Chorkendorff I., Structure sensitivity of the methanation reaction: H_2-induced CO dissociation on nickel surfaces, *J. Catal.* **2008**, 255, 6-19.

19. Coenen J.W.E., van Nisselrooy P.F.M.T., De Croon M.H.J.M., van Dooren P.F.H.A., van Meerten R.Z.C., The dynamics of methanation of carbon monoxide on nickel catalysts, *Appl. Catal.* **1986**, 25, 1-8.

20. Figueiredo J.L., Moulijn J.A., Carbon and Coal Gasification: Science and Technology; Martinus Nijhoff, The Netherlands, **1986**.

21. Wei J., Iglesia E., Structural requirements and reaction pathways in methane activation and chemical conversion catalyzed by rhodium, *J. Catal.* **2004**, 255, 116-127.

22. Nielsen B. Ø., Luntz A.C., Holmblad P.M., Chorkendorff I., Activated dissociative chemisorption of methane on Ni(100): a direct mechanism under thermal conditions?, *Catal. Lett.* **1995**, 32, 15-30.

23. Xu J., Froment G. F., Methane steam reforming, methanation and water-gas shift: I. Intrinsic kinetics, *AIChE J.* **1989**, 35, 88-96.

24. Campbell R., Szanyi J., Lenz P., Goodman D.W., Methane activation on clean and oxidized Ni(100), *Catal. Lett.* **1993**, 17, 39-46.

25. Kurungot S., Yamaguchi T., Stability improvement of Rh/γ-Al_2O_3 catalyst layer by ceria doping for steam reforming in an integrated catalytic membrane reactor, *Catal. Lett.* **2004**, 92, 181-187.

Chapter 5

Main Conclusions

& Outlook

In this thesis, the work has been focused on the production of methane from biomass via gasification. The results obtained, though, are not restricted to targeting methane as a product, but give valuable information for biomass gasification processes in general (e.g. for syngas or fuel gas production). The market for natural gas (e.g. methane) itself has changed in the last couple of years, with decreasing prices mainly due to newly built LNG terminals allowing large scale transport of natural gas to remote markets, independent of pipelines and the utilization of shale gas resources which is expected to be a game-changer for the primary energy market in the coming decades. Therefore, from an economical point of view, it has become less attractive to produce methane from biomass. Nevertheless, from an ecological point of view, gasification of biomass offers the opportunity to produce synthetic natural gas (SNG) which is neutral with respect to net CO_2 emissions and its application could be attractive, especially on remote locations where LNG/pipeline infrastructure is too expensive.

The thermochemical conversion route of dry biomass to methane is conventionally envisaged in a two-step process: In the first step, fuel gas is produced by gasification, which requires heat at high temperature (700-900°C). In the second step, the produced gas is led to a methanation unit where methane is formed releasing heat at low temperature (350-500°C). In this configuration no heat integration is possible between the two process stages. To overcome this issue, a new gasification concept is investigated in this thesis, the direct methane formation via biomass gasification, termed *self-gasification* of biomass. The concept entails an intermediate temperature (600-800°C) and pressure (25-35 bar) steam gasifier (potentially with a gas recycle), where recycled alkali metal components contained in the biomass itself serve as potential "catalysts" for char gasification, methane formation and tar cracking. The focus of the present research lies on process evaluation and the role of ashes in the aforementioned reactions.

Below, the results are first discussed on basis of a reaction scheme on biomass particle level. Both biomass ash itself and model compounds (potassium and sodium salts) have been used in this study. In Figure 1 the paths toward gas are visualized schematically. It has been shown that char, ashes in combination

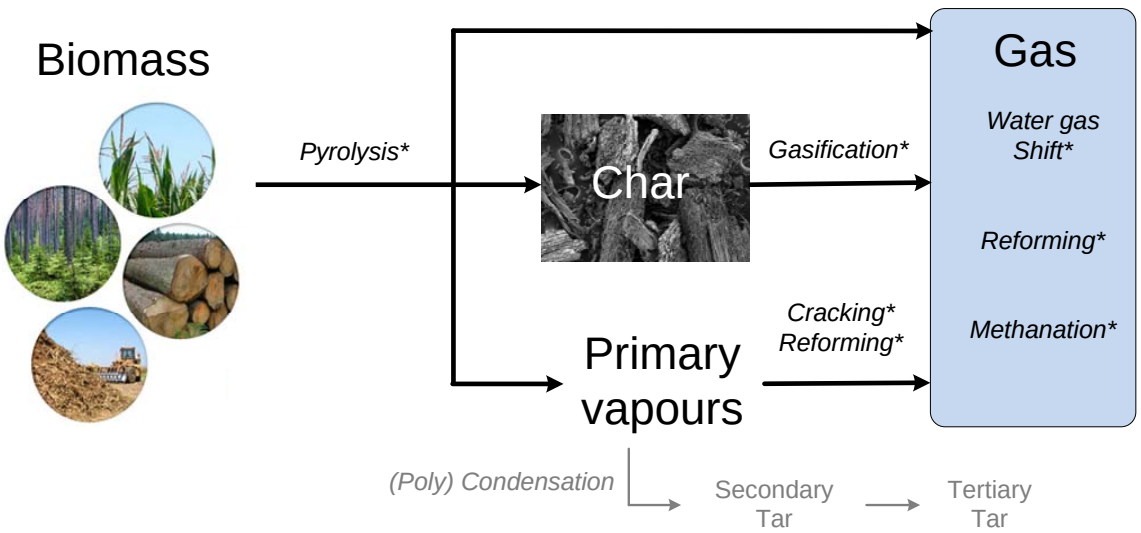

Figure 1. Reaction scheme for biomass gasification. (*) The ash in the char has an impact on this reaction.

with carbon, have interaction in all branches of the reaction network leading to product gas.

The temperature at which biomass pyrolysis (Chapter 3) starts to take place is lowered when potassium/sodium hydroxide/carbonate salts are applied. Steam and CO_2 gasification (Chapter 4 and 5) rates of char are significantly increased, up to ~30 times when ashes or ash model compounds are well distributed onto the char, while CO and H_2 showed inhibition effects. Methanation (and its reverse reaction of methane steam reforming) and the water-gas-shift reaction (Chapter 5) were all catalyzed at significant rates when using ash model compounds but only when they were in contact with carbon from the char. Only catalytic vapor conversion was not part of this study but this is expected to proceed leading to low tar levels. Other researchers have studied a similar process where char from wood or potassium-impregnated wood was used as a catalyst for tar cracking [1, 2]. Hosokai et al. report conversions of heavy tar (b.p.>336°C) of nearly 100% at temperatures of 750-850°C [1]. Heavy tar yields could be decreased by a factor 100, resulting in tar concentrations in the dry gas as low as 20 mg/Nm^3 even at lower temperatures (600-700°C) when char was used from potassium-impregnated wood [2].

Regarding the overall process, implementation of a wood/biomass impregnation step in the process is important. The original biomass ash content as well as the required ash loading for catalytic gasification will determine to a large extent the ash recycle ratio via biomass impregnation. The required (pine

wood) ash content lies in the order of up to 14 wt.% for the catalytically active components, which was studied in Chapter 4. In order to achieve this specific ash loading after impregnation, the ash recycle ratio (ash that has to be recycled over ash content of the biomass) for wood would be ~35. If straw would be used instead of wood, then the ash recycle ratio would be ~2.6 for the same required ash loading as straw has a high ash content which is also rich in K and Na. Therefore, the effective recycle ratio for ash would be reduced by more than a factor 10 if an active, ash-rich feed like straw would be used compared to wood. The ash-impregnated char maintains reasonable gasification rates even if a CO/H_2 recycle would be applied as was seen in Chapter 4. The reactor can be operated at e.g. 80% carbon conversion by gasification (Chapter 4 and 5) and the remaining char can be utilized for combustion providing the necessary hot utility to the process (Chapter 2).

The presence of K/Na during gasification is known to cause ash melting behavior issues. When sand is used as bed material, alkali metals and especially potassium tend to react with the sand (silica) and form low melting point silicates. So, there is a eutectic coating formed on the surface of the sand particles increasing their tendency to stick together and form clusters leading to agglomeration [3, 4]. However, no sand is used in this present concept, but the char itself is utilized as bed material and such issues are believed to be avoided. Hot spots are another common problem in gasifiers that make use of O_2/air as oxidizing agent. This can further lead to ash melting issues as well as evaporation of alkali metal components. Nevertheless, in the present concept hot spots are avoided since the gasifier is envisaged to run on steam instead of O_2/air. Although evaporation of alkali metals is expected to be minimal since low gasification temperatures are envisaged to be utilized in this concept, any evaporated K can be fully captured by a downstream wood char bed [2].

Different process configurations were also studied in this thesis by process modeling (Chapter 2). Here, the gasifier was modeled as a Gibbs reactor, which has been shown to be a good approximation since all gas phase reactions are significantly catalyzed and low tar levels are expected. This study indicated that gasifier operation at 700°C and at pressures higher than 20 bar is promising for obtaining high efficiencies toward methane (55-66%). For methane production, an operation mode of the gasifier at elevated pressure with a CO/H_2 recycle is most favorable. To make operation possible without an ex-

tra heat input (hot utility), CO_2 has to be separated utilizing a technology with low energy requirements (≤ 2 MJ/kg CO_2). If the desired product is syngas, then a more traditional configuration of the gasifier without a recycle is most suitable.

Catalytic biomass gasification using its own ash as a catalyst (with a possible recycle and impregnation step) has been studied in sufficient depth and can now be tested as an integrated bench-scale biomass gasification process. This can be done for the concept which was investigated in this thesis (high pressure gasification for the production of methane using a CO/H_2 recycle) as well as for a new steam gasification process for the production of syngas. To overcome the technical difficulty of pressurizing biomass for gasification, different pre-treatment strategies could be applied like feeding a liquid ash-enriched biomass slurry [5] as to impregnated solid bulky biomass.

Literature cited

1. Hosokai S., Norinaga K., Kimura T., Nakano M., Li C.-Z., Hayashi J.-i., Reforming of volatiles from the biomass pyrolysis over charcoal in a sequence of coke deposition and steam gasification of coke, *Energy Fuels* **2011**, 25, 5387-5393.

2. Sueyasu T., Oike T., Mori A., Kudo S., Norinaga K., Hayashi J.-i., Simultaneous steam reforming of tar and steam gasification of char from the pyrolysis of potassium-loaded woody biomass, *Energy Fuels* **2012**, 26, 199-208.

3. Arvelakis S., Gehrmann H., Beckmann M., Koukios E.G., Effect of leaching on the ash behavior of olive residue during fluidized bed gasification, *Biomass Bioenergy* **2002**, 22, 55-69.

4. Fryda L.E., Panopoulos K.D., Kakaras E., Agglomeration in fluidised bed gasification of biomass, *Powder Technol.* **2008**, 181, 307-320.

5. Henrich E., Dahmen N., Dinjus E., Cost estimate for biosynfuel production via biosyncrude gasification, *Biofuels Bioprod. Biorefin.* **2009**, 3, 28-41.

List of Publications

1. Nanou P., van Rossum G., van Swaaij W.P.M., Kersten S.R.A., Evaluation of catalytic effects in gasification of biomass at intermediate temperature and pressure, *Energy Fuels* **2011**, 25, 1242-1253.

2. Nanou P., van Swaaij W.P.M., Kersten S.R.A., van Rossum G., Evaluation of catalytic effects in gasification of biomass at intermediate temperature and pressure. II. Process performance analysis, *Energy Fuels* **2011**, 25, 4085-4094.

3. Nanou P., van Swaaij W.P.M., Kersten S.R.A., van Rossum G., High-throughput screening technique for biomass conversion in hot compressed water, *Ind. Eng. Chem. Res.* **2012**, 51, 2487-2491.

4. Nanou P., Gutiérrez Murillo H.E., van Swaaij W.P.M., van Rossum G., Kersten S.R.A., Intrinsic reactivity of biomass-derived char under steam gasification conditions-Potential of wood ash as catalyst, *Chem. Eng. J.* **2013**, 217, 289-299.

5. Nanou P., van Swaaij W.P.M., Kersten S.R.A., van Rossum G., Methane production over and gasification of char from potassium-impregnated wood at 700°C and 25 bar, *in preparation*.

Acknowledgments

Everyone and everything played a role, big or small, in completion of this thesis and I would like to dedicate these two pages to thank everyone that crossed my path during this journey.

Firstly, I want to thank my two promoters Sascha Kersten and Wim van Swaaij as well as the assistant promoter Guus van Rossum for their trust and confidence in me. I want to thank you all three for your guidance and support through the good and bad days. Secondly, I would like to thank the rest of the committee members for gladly accepting to be part of this very special day for me.

I want to thank the TCCB group for being my family far away from home for all of these years and especially: Ferran, Judith, Guus, Laura, Dragan, José, Mariken, Elly, Agnes, Roel, Prasad. Thank you for your friendship and all the good times not only at work, but also outside working hours.

My sincere gratitude goes to the technicians of the group: Benno, Robert, Karst and Johan. I appreciate all your help with the design, construction and repairing of the set-ups. Without your insightful advice, experiments would never have finished (well, also being a woman in the HDL helps getting advice faster ;-))

The newer people in TCCB, or correctly said the SPTers, with whom I mostly experienced my last, finishing-up-the-thesis days in the group and who saw the more relaxed version of me at work: Rens, Maria, Stijn, Diego, Xavi, Sam, Michal, Mireille, Cecilia, Xiaohua, Cindy. Thank you for the fun lunches and extra cold beers we shared.

I would also like to thank Yvonne for helping me out with all kinds of forms, paperwork, e-mails and for always being available for a pleasant discussion accompanied by cookies or drop (when Sascha had not finished them all!). Many thanks go to the rest of the group as well: Wim, Erna, Maarten, Louis, David, Annemarije, Boelo for the enthusiastic discussions and for allowing me to sit at their desk in the last period when I was leading my nomad life.

Special thanks go to the backstage technical support during my PhD, namely to Gea Jannink-Heuver for always sending me very fast all the literature I needed, Clement Nijkamp for all IT-related problems and all the technicians at the glass workshop for preparing endless quartz capillaries for my experi-

ments.
Many thanks go to Rik Akse, who was the first person I met at the university and with whom we later shared great trips to Greece for student recruitment, which finally paid off ;-)
Special thanks go to the bachelor and master students that helped me with the research described in this thesis: Paul, Roma (Alex), Hector, Petra and Chiel. Thank you for all your effort and the great results that you delivered!
I also want to mention, of course, Michael, Rebeca and Can who are linked to the greater TCCB family. Thank you for all the great fun we had and will still have no matter where everyone will be living!
I want to take this opportunity to also thank the Greek community of Enschede and especially: Vasilis, Pelagia, Dimitris R., Dimitris S., Tasos, Athena, Christos, John Kostakos, Giorgos, Filippos, Helias for making me miss the Greek sea and sun a bit less.
A special place in my acknowledgments is reserved for Helia and her dance school for giving me the balance I truly needed between body and mind during the thesis-writing period.
Also special thanks go to my "teacher" Dimitris Katevas from the Technical University of Kavala for encouraging me to go abroad for my further studies and future career.
My two paranymphs/models also deserve a special acknowledgment: Laura, thank you for being a good friend and for always being there for me. Dina, thank you for being the listening ear to all my complaints about everything. Thank you both for being here next to me on this very special day.
Last but not least, I want to express my sincere appreciation to my family and friends in Greece as well as to my partner, Dimitris, for all their love and support during these years.

Παυλίνα

About the Author

Pavlina Nanou was born in Groningen (The Netherlands) on the 7th of May, 1981. At the age of six she moved with her family to Preveza (Greece). After finishing high school in 1999 with a focus on the subjects of Mathematics, Physics, Chemistry and Composition (language) she studied Petroleum & Natural Gas Technology at the T.E.I. of Kavala (Greece). She obtained her B.Sc. degree in 2004 on completion of her Bachelor thesis entitled "Use of co-ferments in anaerobic microbial degradation process of biomass and removal of CO_2 from biogas with zeolites". The thesis was realized during the Erasmus-Socrates exchange program in Emden (Germany) at the University of Applied Sciences - Hochschule Emden under the supervision of Prof.Dr.rer.nat.habil. M. Schlaak. After obtaining her Bachelor degree, she followed a two-year Master Program on Chemical Engineering at the University of Twente. She did her internship at The Safety Lab at Akzo Nobel, Deventer (The Netherlands) and graduated in 2007 in the Thermo-Chemical Conversion of Biomass (TCCB) Group on the subject: "Biomass self-gasification: Proof of principle and screening techniques" under the supervision of Dr.ir. G. van Rossum. She worked as a researcher in the same group on the optimization of the energy usage of a commercial charcoal production facility by combined charcoal and electricity generation. The project was realized in cooperation with CleanFuels (Enschede, NL), Carbo B.V. (Almelo, NL) and Ekoblok (Almelo, NL). In 2007 she started her PhD in the TCCB research group on "Biomass Gasification for the Production of Methane" supervised by Prof.dr. S.R.A. Kersten, Prof.dr.ir. W.P.M. van Swaaij and Dr.ir. G. van Rossum as described in this thesis.

Notes

Notes

Notes